IN SITU INFARED STUDIES OF CATALYTIC PARTIAL OXIDATION


by


CHUNDI CAO


B.Sc., Beijing University of Chemical Technology, 1999

M.S., Research Institute of Petroleum Processing, SINOPEC, 2002


AN ABSTRACT OF A DISSERTATION


submitted in partial fulfillment of the requirements for the degree


DOCTOR OF PHILOSOPHY


Department Of Chemical Engineering
College of Engineering


KANSAS STATE UNIVERSITY
Manhattan, Kansas


2008

# Abstract

Catalytic partial oxidation (CPO) has received considerable interest recently both as a way to utilize remote natural gas resources and to provide $H_2$ for a fuel cell. Studies on the reactions at lower temperatures and transient conditions were performed, which can provide insights on the mechanism of CPO at high reactions, particularly on the role of the chemical and physical state of the noble metal catalyst. In this work, ignition of methane CPO on $Pt/Al_2O_3$ and $Rh/Al_2O_3$ catalysts and methanol CPO on $Pt/Al_2O_3$ catalysts were studied using in situ diffuse reflectance infrared Fourier transform spectroscopy (DRIFTS).

The ignition mechanism study of $CH_4$ on $Pt/Al_2O_3$ showed that oxygen mainly covers the surface until ignition. Competition between the two reactants is assumed. The heat of adsorption of oxygen is a key factor for ignition of the methane partial oxidation reaction on $Pt/Al_2O_3$. The ignition mechanism on $Rh/Al_2O_3$ was found to be different from $Pt/Al_2O_3$. The oxidation state of the catalyst changed significantly as the temperature was raised towards the ignition. An oxidized rhodium state, $Rh^{n+}$, progressively formed as the temperature was increased while $Rh^0$ decreased. In addition, a greater amount of $Rh^{n+}$ was found when the oxygen concentration in the feed was higher. From these results, it is hypothesized that ignition of methane CPO on $Rh/Al_2O_3$ is related to the accumulation of the $Rh^{n+}$ state.

Dissociation adsorption of methanol occurs on both $Al_2O_3$ and $Pt/Al_2O_3$. It is suggested that formate was one of the important intermediates in the reaction pathway. Oxygen species play a key role in the formation of formate on the catalysts, and it also affects the product composition.

Formate mainly decomposed into CO, which is the dominant source for $CO_2$ production in the reactions at higher temperatures.

IN-SITU INFARED STUDIES OF CATALYTIC PARTIAL OXIDATION


by


CHUNDI CAO


B.Sc., Beijing University of Chemical Technology, 1999

M.S., Research Institute of Petroleum Processing, SINOPEC, 2002


A DISSERTATION


submitted in partial fulfillment of the requirements for the degree


DOCTOR OF PHILOSOPHY


Department of Chemical Engineering
College of Engineering


KANSAS STATE UNIVERSITY
Manhattan, Kansas


2008

Approved by:

Major Professor
Dr. Keith L. Hohn

# Copyright

CHUNDI CAO

2008

# Abstract

Catalytic partial oxidation (CPO) has received considerable interest recently both as a way to utilize remote natural gas resources and to provide $H_2$ for a fuel cell. Studies on the reactions at lower temperatures and transient conditions were performed, which can provide insights on the mechanism of CPO at high reactions, particularly on the role of the chemical and physical state of the noble metal catalyst. In this work, ignition of methane CPO on $Pt/Al_2O_3$ and $Rh/Al_2O_3$ catalysts and methanol CPO on $Pt/Al_2O_3$ catalysts were studied using in situ diffuse reflectance infrared Fourier transform spectroscopy (DRIFTS).

The ignition mechanism study of $CH_4$ on $Pt/Al_2O_3$ showed that oxygen mainly covers the surface until ignition. Competition between the two reactants is assumed. The heat of adsorption of oxygen is a key factor for ignition of the methane partial oxidation reaction on $Pt/Al_2O_3$. The ignition mechanism on $Rh/Al_2O_3$ was found to be different from $Pt/Al_2O_3$. The oxidation state of the catalyst changed significantly as the temperature was raised towards the ignition. An oxidized rhodium state, $Rh^{n+}$, progressively formed as the temperature was increased while $Rh^0$ decreased. In addition, a greater amount of $Rh^{n+}$ was found when the oxygen concentration in the feed was higher. From these results, it is hypothesized that ignition of methane CPO on $Rh/Al_2O_3$ is related to the accumulation of the $Rh^{n+}$ state.

Dissociation adsorption of methanol occurs on both $Al_2O_3$ and $Pt/Al_2O_3$. It is suggested that formate was one of the important intermediates in the reaction pathway. Oxygen species play a key role in the formation of formate on the catalysts, and it also affects the product composition.

Formate mainly decomposed into CO, which is the dominant source for $CO_2$ production in the reactions at higher temperatures.

# Table of Contents

# List of Figures

# List of Tables

# Acknowledgements

Many people have helped me in the course of my research, and any merit in it is in large measure due to them. First and foremost, I would like to thank my advisor Dr. Keith L. Hohn for providing me with the opportunity to complete my Ph.D thesis at Kansas State University. I especially want to thank him for his support and guidance, which made my thesis work possible. He has been actively interested in my work and has always been available to advise me. I am very grateful for his patience, motivation, enthusiasm, and immense knowledge in reaction engineering and catalysis field that, taken together, make him a great mentor.

I gratefully thank to Dr. John Schlup for his valuable comments on my papers and his great influence to my work. I also want to thank the committee members: Dr. Daniel Higgins, Dr. Jennifer Anthony, and Dr. Chris Sorensen for their contribution to this work and the time they put in.

Many thanks go to Dr. Chongmin Wang for his help during use of the TEM facility. Many thanks to Dr. Eric Doskocil in the Department of Chemical Engineering at the University of Missouri for running the microcalorimetry.

I want to thank Abdennour Bourane for sharing his knowledge. I have learned a lot from him from technical skills to ways of thinking. I also want to thank present and past members in my

research group: Chienchang Huang, Yuchuan Lin and Juan Salazar for the wonderful time spent together.

I want to express gratitude to the staff members in the Department of Chemical Engineering: Florence Sperman, Cindy Barnhart, Alison Hodges and David Threewit for their activities related to this research.

Special thanks to my husband Xiangxin Yang, Love and thanks! Without his enormous support, this research would never have been possible.

Finally, I thank my parents Zhisheng Cao and Yunlan Xue for their selfless love and sacrifice. My brother Chunshe(James) Cao and my sister Chunlin Cao as well as their families for their faith and support.

# Dedication

To my greatest love

Xiangxin Yang

To my parents

Zhisheng Cao and Yunlan Xue

To my brother and sister-in law

Chunshe (James) Cao and Haosheng Wang

To my sister and brother in-law

Chunlin Cao and Aimin Chen

To my nephews

Dong Chen

David Cao

Michael Cao

To my friends

David and Carol Pope

# Chapter 1 Introduction

## 1.1    Catalytic partial oxidation

Catalytic partial oxidation (CPO) is a reaction that occurs when an oxygen-lean mixture of fuel and oxygen is reacted at the presence of a catalyst. Catalytic partial oxidation can be used with any hydrocarbon or alcohol. The reactions usually occur at much lower temperature than homogeneous partial oxidation. In the 1990's, Dr. Schmidt and coworkers performed pioneering research on catalytic partial oxidation at millisecond contact times [1]. The reactor used operated adiabatically and autothermally. Due to high reactant flow rates, residence time is very low, typically 5-10 milliseconds. The catalysts used are highly active noble metals (Pt, Rh, Pd) in the form of metal foils or supported on powders and monolith.

Catalytic partial oxidations in millisecond contact time reactors have shown promise in many applications. For example, converting natural gas into syngas was successful with high conversion and $H_2$ selectivity.  Supplying $H_2$ for use in fuel cells on-board a vehicle by methanol partial oxidation has also shown promise in recent years.

### 1.1.1  *Utilization of natural gas to generate syngas*

The reserves of natural gas in the world are estimated to be 6359.172 trillion cubic feet [2] and new gas fields are discovered every year. $CH_4$ is the major component of natural gas, which is valuable by virtue of its heating value. Natural gas also contains small amount of other alkanes, such as $C_2H_6$, $C_3H_8$ and n-$C_4H_{10}$. Natural gas has clear environmental advantages over other

fossil fuels. For example natural gas combustion produces virtually no sulfur dioxide and particulate emissions and less emission of $CO_2$.

Despite the advantages of natural gas, the use of it as feedstock has been limited because of its physical property (a gas at atmosphere pressure and temperature), which increased the storage and transportation cost from the remote reservoirs. Thus, converting natural gas into more easily transportable chemicals on site becomes extremely important. At this time, the only economically available route for the conversion of natural gas into more valuable chemicals is via synthesis gas, a mixture of hydrogen and carbon monoxide. Synthesis gas is a feed stock for many processes, such as methanol synthesis and Fischer-Tropsch production of synthetic diesel fuel. Catalytic partial oxidation is one of the important processes for the conversion.

### 1.1.2 *On-board $H_2$ production from liquid fuels for fuel cells*

Fuel cells have been of interest in recent years due to their high energy efficiency. The most promising fuel cell technology for transportation appears to be the Polymer Electrolyte Membrane Fuel Cell (PEMFC) fueled by $H_2$. Hydrogen is ionized to protons and electrons at the anode of cell. Protons migrate through a membrane to the cathode where reaction to produce water occurs. Because fuel is oxidized electrochemically at low temperatures, around 353K, the efficiency is increased and nitrogen oxides usually generated at high temperatures are avoided.

A major roadblock in implementing PEMFC is the storage and distribution of $H_2$. At ambient conditions (300 K, 1 atm), the energy content of 1 liter of $H_2$ is only 10.7 kJ: three orders of magnitude too low for practical applications [3]. Even at ambient temperature with a high pressure of 3600 psi, energy content of is only 2.0 MJ/L. If the pressure is increased to 5000 psi,

the increase of the energy content is not significant, 2.75 MJ/L. In addition, pressurized vessels or metal hydrides in a vehicle increase weight and decrease fuel efficiency. It is unlikely that $H_2$ will be stored in pressurized tanks in practical fuel cell vehicles considering the space it will take, not to mention the safety issues. Thus, on board $H_2$ generation is a key to the success of compact and efficient fuel cell systems. Catalytic partial oxidation is a potential reaction for this purpose. Methanol is one of the promising fuels because methanol has very low emission of ozone-forming hydrocarbons and toxins and can be made from a variety of feedstock, including renewable ones.

### 1.1.3 *The role of catalytic partial oxidation and in situ IR*

Steam reforming reactions, as shown in following equations, can be used for converting natural gas or liquid fuels.

$$CH_4 + H_2O = CO + 3H_2 \ (\Delta H_{298} = 206 kJ/mol) \qquad \textbf{Equation 1.1}$$

$$CH_3OH + H_2O = CO_2 + 3H_2 \ (\Delta H_{298} = 49.6 kJ/mol) \qquad \textbf{Equation 1.2}$$
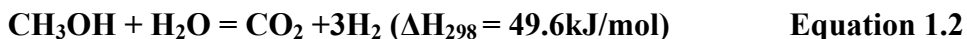
However, this method has its drawbacks. It is energy intensive and produces syngas with an unsuitable hydrogen to CO ratio for many subsequent processes. Thus, catalytic partial oxidation (CPO) has attracted interest as a potential replacement.

There are several advantages for catalytic partial oxidation compared to steam reforming. For example: partial oxidation is mildly exothermic, therefore, the reaction can run autothermally without extra heating. This makes the process more energy efficient than steam reforming. The $H_2$ to CO ratio produced in methane partial oxidation is around two, which makes the mixture suitable as a feedstock for either Fischer-Tropsch chemistry or methanol synthesis. The size of a

catalytic partial oxidation reactor would be much smaller than a steam reformer because of the short contact times. For instance, a laboratory scale reactor with a flow rate of 4SLPM produces around 6 lbs/day syngas and the GSHV can be increase up to $1.8 \times 10^6$ $hr^{-1}$ without loss in selectivity or conversion [4]. The production rate at this space velocity is 50 lbs/day. In addition, coking problems are generally avoided. Furthermore, the reaction is very fast, which results in very short response times to changes in fuel supply. All of these advantages make catalytic partial oxidation a great process to produce syngas from natural gas or to convert liquid fuels such as methanol into hydrogen for use in a fuel cell.

While the potential of catalytic partial oxidation for syngas and $H_2$ generation is considerable, the reaction mechanism, which is critical to development of millisecond contact time reactors and catalysts for $H_2$ production, is not well understood. For example, the conversion of methane to syngas has been attributed by some to direct partial oxidation, while others propose methane combustion followed by reforming and water-gas shift reactions. In particular, there is a lack of understanding of the surface species involved. As for the catalytic partial oxidation of methanol, many reactions may be occurring simultaneously and many reaction intermediates may be involved. Thus, study of the surface intermediates of the catalytic partial oxidation under conditions similar to those in a millisecond time reactor would be important to elucidate the reaction mechanism.

Infrared spectroscopy is capable of detecting surface intermediates at conditions characteristic of CPO (high temperature, near atmospheric pressure). It is also sensitive to many of the species that would be expected as surface intermediates in CPO reaction. Thus, in this work, in situ

4

infrared spectroscopy has been used to study CPO reactions. More specifically, in situ diffuse reflectance infrared Fourier transform spectroscopy (DRIFTS) was employed to detect the intermediate species present during catalytic partial oxidation. Mass spectroscopy was also used to detect reaction products while infrared spectra were being obtained.

Due to the experimental conditions of catalytic partial oxidation at short contact times, in situ characterization with the exact same conditions is extremely difficult. Thus, studies on catalytic partial oxidation of methane and methanol at lower temperatures and transient conditions, such as the ignition process of methane, were performed on supported catalysts.

## 1.2    Aim, scope, and outline of this thesis

The objective of the thesis is to study CPO reactions mainly using in situ diffuse reflectance infrared spectroscopy and mass spectroscopy. The catalysts used were supported platinum and rhodium. Special attention was given to the ignition process studies of methane catalytic partial oxidation.   Furthermore, methanol partial oxidation was investigated. This thesis can be divided in three main parts, as detailed below.

The first part deals with catalytic ignition of methane partial oxidation on supported Pt catalysts. The ignition process has been investigated at atmospheric pressure on different states of catalysts. Methane adsorption on these catalysts was also conducted under elevated temperature.

In the second part, ignition of methane CPO and methane activation on $Rh/Al_2O_3$ catalysts was studied on supported Rh catalysts. Different catalysts were studied: fresh, aged, sintered and oxidized catalysts. The ignition process was investigated with a focus on the effect of catalyst

5

type, catalyst states and oxygen-to-fuel ratio. Methane activation on different catalysts was also studied and the oxidation state of rhodium was characterized by using CO as a probe molecule.

In the final part, the reaction path way study of methanol partial oxidation was conducted. Methanol decomposition on $Al_2O_3$ and different state of $Pt/Al_2O_3$ was studied using in situ IR and MS. Methanol catalytic partial oxidation was studied at different temperatures from 723 K to 973 K, and for different methanol to oxygen mole ratios.

Final conclusions and recommendations for future work are discussed in Chapter 7.

## 1.3    References

1 D.A. Hickman, E. A. Haupfear, L. D. Schmidt, Catal. Lett. 17 (1993) 223

2 BP p.l.c., *BP Statistical Review of World Energy,* June 2006

3 G. Thomas, US DOE Hydrogen Program 2000 Annual Review, May 9-11, 2000 San Ramon,

California

4 K.L. Hohn, L. D. Schmidt, Appl. Catal. A: general 211 (2001) 53

# Chapter 2 Literature review

## 2.1 Catalytic partial oxidation of methane to syngas

### 2.1.1 *Methane catalytic partial oxidation on different catalysts*

There are many ways to convert natural gas. The dominant commercial process used to produce syngas and $H_2$ is steam reforming.

$$CH_4 + H_2O = CO + 3H_2 \ (\Delta H_{298} = 206kJ/mol) \hspace{2cm} \textbf{Equation 2.1}$$

This process has dominated syngas and $H_2$ production for about 80 years [1]. Although steam reforming is enhanced by improving the catalysts, operation conditions and heat transfer to achieve better performance, an unavoidable drawback of this process is its intensive energy requirement. Furthermore, the product $H_2/CO$ ratio of methane steam reforming is too high for many downstream reactions, such as Fischer-Tropsch chemistry or methanol synthesis.

Catalytic partial oxidation offers the potential to convert natural gas through exothermic reactions:

$$CH_4 + 1/2O_2 = CO + 2H_2 \ (\Delta H_{298} = -36kJ/mol) \hspace{2cm} \textbf{Equation 2.2}$$
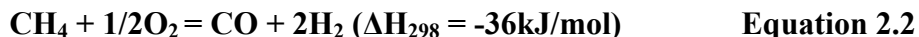
This process, like steam reforming, has a long history. Liander [2] first reported methane catalytic partial oxidation to syngas in 1929. But the process did not attracted much attention until the late 1980s, when Green and coworkers [3] revealed a lanthanide oxide-supported ruthenium catalyst that had excellent activity for methane partial oxidation. Schmidt and

coworkers [4] performed pioneering research in this field in the 1990s. Unlike other researchers, this research group operated CPO in an autothernal mode where no external heat was required. Catalytic partial oxidation of various hydrocarbons including methane, ethane, propane and butane [5] were studied in this mode.

Transition metal catalysts for methane catalytic partial oxidation have been of interest for a long time. In 1946, the reactions were conducted on supported Ni catalysts [6]. It was found that syngas with the product ratio of $H_2/CO = 2$ could be produced at 1000-1200 K and 1 atm. Dissanayake et al. [7] reported high syngas selectivities over $Ni/Al_2O_3$ at temperatures above 973 K, but found that nickel would deactivate by oxidation to inactive $NiAl_2O_4$ if the space velocity was increased beyond $10^5$ $hr^{-1}$. The reaction proceeded by complete oxidation on oxidized nickel at the start of the bed followed by reforming and water-gas shift reactions downstream on reduced nickel. Choudhary et al. [8] reported high syngas yields at residence times of only milliseconds on supported Ni at temperatures below 973 K. It is now generally agreed that Ni metal instead of Ni oxide is the active component for syngas production via methane partial oxidation. However, carbon deposition and loss of nickel surface area are still unavoidable, which causes catalyst deactivation.

Noble metal catalysts are also active in methane catalytic partial oxidation. Much higher activity for noble metal catalysts has been observed than Ni based catalysts [9]. Even a ruthenium catalyst with very low metal loading, 0.015% $Ru/Al_2O_3$, was found to be more active and selective than 5% $Ni/Al_2O_3$ [10]. Ashcroft and coworkers [11] have reported methane conversion of 90% with selectivity above 94% for alumina-supported ruthenium. Schmidt and coworkers

have run catalytic partial oxidation reactions over noble metal-coated monoliths and spheres [9]. The metals were mostly platinum and rhodium. At a $CH_4/O_2$ ratio of two, methane conversion was 85% with 93% CO selectivity and 94% $H_2$ selectivity on $Rh/Al_2O_3$ sphere. No carbon deposition was observed on these noble metal catalysts, which was a big improvement over the Ni based catalysts.

Other metal catalysts have been studied for methane partial oxidation to syngas. For example, Co based catalysts have been found to give a good performance [12] for the reaction when promoted with other elements. However, Co catalysts are very easy to oxidize which may affect the catalyst activity by losing the active component, metallic Co.

### 2.1.2 *Mechanism of CH$_4$ catalytic partial oxidation*

A unified mechanism for methane partial oxidation has not been reached so far. **Figure 2.1** shows the two possible reaction pathways for syngas production from methane over metal catalysts. The production of syngas from methane partial oxidation has been attributed by some to a direct catalytic partial oxidation [9]. Others have proposed an indirect process [13]; i. e. two-step reaction: combustion of methane followed by reforming reactions and water-gas shift to produce CO and $H_2$.

This question is critical to catalyst design for syngas production. The first model suggests that suitable catalysts allow direct formation of syngas while preventing non-selective oxidation to $CO_2$ and $H_2O$. If the second model is correct, catalysts would be desired with high combustion activity and high activity for water-gas shift and reforming reactions.

**CH$_4$**

CH$_4$+ ½ O$_2$; partial oxidation
$\Delta H$ = -36 kJ/mol

**CO + H$_2$**

$$CH_4 + H_2O \longrightarrow CO + 3H_2$$
$$\Delta H = 206 \text{ kJ/mol}$$
$$CH_4 + CO_2 \longrightarrow 2CO + 2H_2$$
$$\Delta H = 247 \text{ kJ/mol}$$
$$CO + H_2O \longrightarrow CO_2 + H_2$$
$$\Delta H = -41.2 \text{ kJ/mol}$$

Total oxidation
$\Delta H$ = -803 kJ/mol

**CH$_4$ +CO$_2$+H$_2$O**

Reforming and water gas shift

**CO + H$_2$**
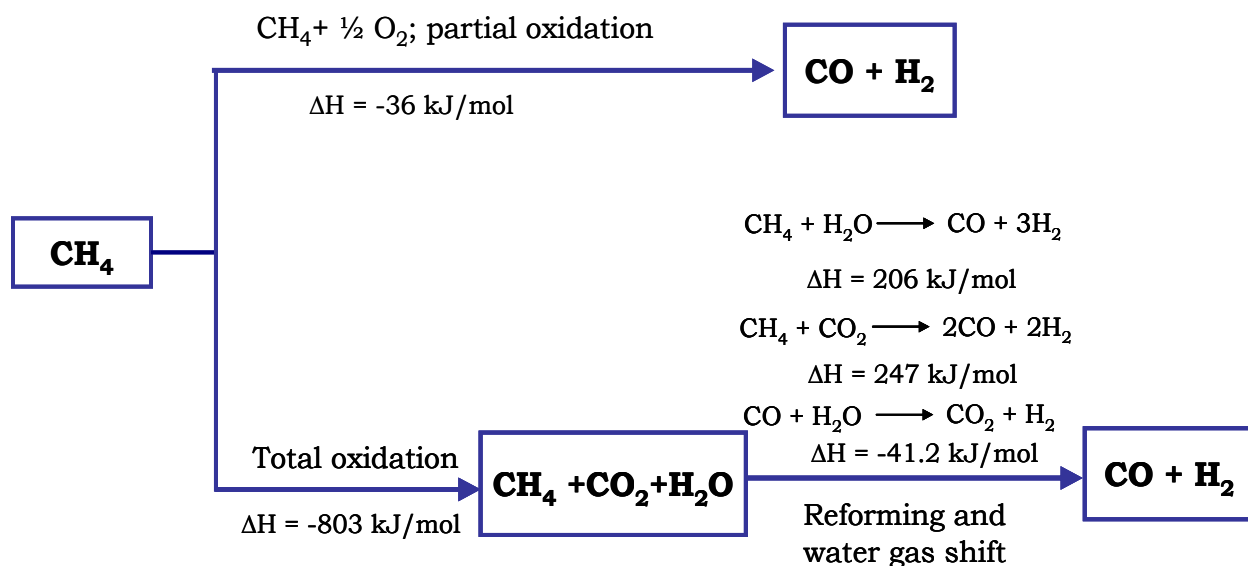
**Figure 2.1 Proposed mechanisms of catalytic partial oxidation of methane to syngas**

The indirect mechanism was proposed mostly due to the observations of the temperature profile of catalysts bed. It was found that the catalyst temperature was significantly higher in the front of catalyst bed than the latter part of catalyst bed, i. e. a hot spot existed in the front of the catalyst bed. This phenomenon was present on different catalyst and under different reaction conditions. As shown in **Figure 2.2**, the higher temperature in the front of Ni catalyst bed was assigned to the initial exothermic combustion reaction [14]. The subsequent lower temperature was explained on the basis of endothermic reforming reactions of the remaining methane with H$_2$O and CO$_2$, which were produced in the combustion reaction. A photograph of the actual Ni/MgO catalysts bed during operation is shown in **Figure 2.3** [15,16]. This photograph clearly shows the hot spot in the catalyst bed.

Many researchers favor this idea. The results from the mechanism study of methane partial oxidation to syngas on Pd [17] confirmed that the reaction starts off with the complete oxidation

11

of methane, irrespective of the palladium particles. Buyevskaya et al [13,18] suggested that CO is formed via a fast reaction of surface carbon species with $CO_2$. OH groups on the support were also considered to be involved in the $CH_X$ conversion to CO via a reforming reaction.
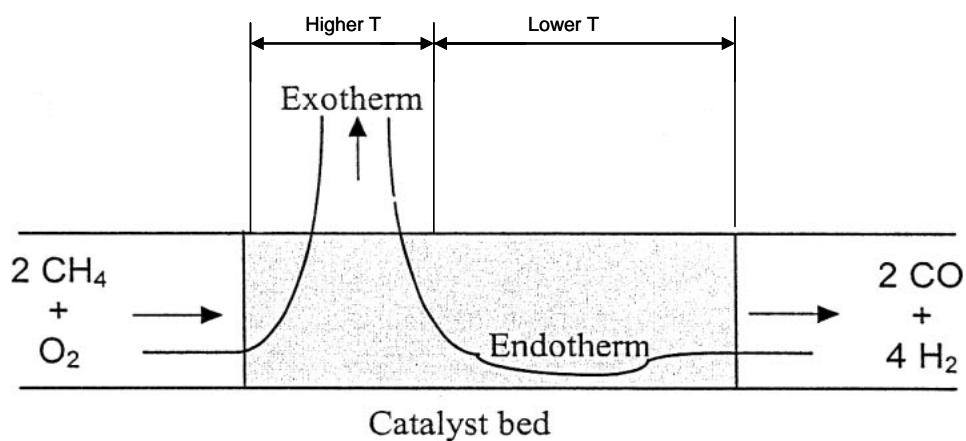


**Figure 2.2 Heat distribution**
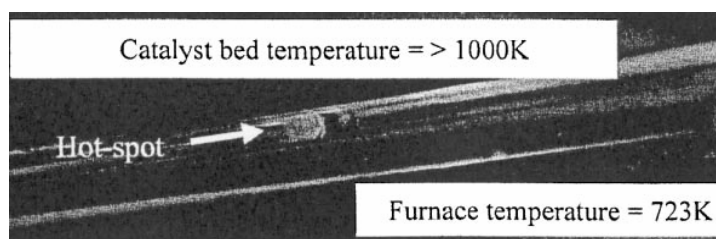


**Figure 2.3 Image of the Ni/MgO catalyst bed at high reactant flow rate ($5.2 \times 10^5 mL.g^{-1}.h^{-1}$)**

The direct mechanism has been proposed mainly based on results from methane catalytic partial oxidation reaction at short contact time on rhodium and platinum coated monolith catalysts [19,20,21]. As shown in the following equations, $CH_4$ pyrolysis on the catalysts and H atoms are abstracted from the $CH_4$ molecules. Adsorbed carbon species were oxidized into CO afterwards.

C-H bonds in methane had to be broken before CO formation in this case. Thus, syngas instead of $CO_2$ and $H_2O$ is produced as primary products.

$$CH_4 \rightarrow CH_{x,s} + H_s \rightarrow C_s + 4H_s \qquad \textbf{Equation 2.3}$$

$$C_s + O_s \rightarrow CO_s \rightarrow CO \qquad \textbf{Equation 2.4}$$

$$CO_s + O_s \rightarrow CO_{2,s} \rightarrow CO_2 \qquad \textbf{Equation 2.5}$$

$$2H_s \rightarrow H_2 \qquad \textbf{Equation 2.6}$$

Choudhary and coworkers [22,23] also advocated the direct oxidation of methane to syngas. Hu and Ruckenstein [24] have observed delayed $CO_2$ generation compared to CO generation in the transient response curves of products in a $CH_4/O_2$ pulse at 773 K over the reduced 20% $Ni/La_2O_3$ catalyst. They concluded, therefore, that CO is the primary product and $CO_2$ is only subsequently generated from CO. Au and Wang [25] agreed with the direct oxidation mechanism through deuterium isotope study. They found that methane dissociation is a key step for CO and $CO_2$ formation. Methane decomposition originated the intermediates from which CO and $CO_2$ were produced.

While the different opinions exist about the two different mechanisms, it was found that reaction path ways were different on different catalysts. Studies by Weng et al. [26, 49] on the supported Rh and Ru catalysts using in situ time-resolved FTIR suggested that CO is the primary product of methane partial oxidation over reduced and "working state" $Rh/SiO_2$ catalyst. However, $CO_2$ is the primary product over $Ru/Al_2O_3$ and $Ru/SiO_2$ catalysts. The two different mechanisms exist due to the different affinity of $O_2$ with different metals and $O_2$ concentration in the feedstock.

The recent study by Liu and Veser [27] studied the reaction at different positions along the reactor axis. Their results give evidence that the reaction proceeds in two stages: initial direct oxidation to CO and $H_2O$ at $\tau < 2$ ms, followed by steam reforming of methane. Water gas shift reaction plays only a minor role in all experimental conditions. It was suggested that different reaction path ways are applied to formation of syngas components, CO and $H_2$. $H_2$ is produced predominantly via indirect route, while CO is produced predominantly via direct mechanism. Thus the argument between the direct and indirect mechanism is meaningless.

The active sites for methane partial oxidation have also been studied. Buyevskaya [13] suggested that reduced rhodium were active sites for methane decomposition to surface carbon and oxidized rhodium were the active sites for methane complete oxidation to $CO_2$. Au et al proposed [28] that metallic nickel in $Ni/SiO_2$ were active for methane decomposition and syngas formation. Lunsford and co-workers [7] found that the unreduced $NiO/Al_2O_3$ were the active sites for the initial complete oxidation of methane. The reduced $Ni/Al_2O_3$ was said to be the active sites for the methane reforming reactions.

## 2.2 Methanol catalytic partial oxidation to $H_2$

### 2.2.1 Methanol catalytic partial oxidation on different catalysts

The most studied methanol conversion to $H_2$ method is steam reforming (**Equation 2.7**). The disadvantage of this reaction is that external heating is required due to a positive reaction enthalpy of 49.6 kJ/mol. Catalytic partial oxidation of methanol (**Equation 2.8**) offers the potential of producing hydrogen through an exothermic reaction and can be run in an

14

autothermal mode, where the heat necessary for the reaction comes from the reaction itself. The high reaction rates of catalytic partial oxidation lead to smaller reactors. Another advantage of methanol partial oxidation is its rapid response to change during the reaction. Most importantly, methanol partial oxidation produces only a small amount of CO, which is a poison for Pt electrode of PEMFC.

$$CH_3OH + H_2O = CO_2 + 3H_2 \ (\Delta H_{298} = 49.6kJ/mol) \qquad \textbf{Equation 2.7}$$

$$CH_3OH + 1/2O_2 = CO_2 + 2H_2 \ (\Delta H_{298} = -192.2kJ/mol) \qquad \textbf{Equation 2.8}$$
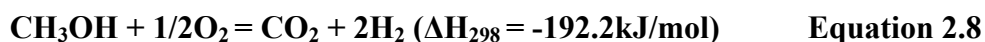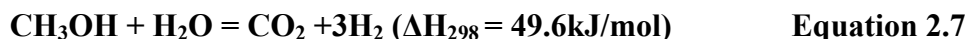
The popular catalysts for methanol partial oxidation are copper-based. Velu et al. [29] have studied methanol partial oxidation over catalysts derived from CuZnAl-layered double hydroxides. They found that a methanol conversion of 40-60% could be obtained over these catalysts with high selectivity to $H_2$ (more than 90%) and to $CO_2$ selectivity (more than 95%) at 473K. The undesired product, CO (a poison to catalyst anode of fuel cells), was not produced at a methanol space velocity of 0.3 $mol \cdot h^{-1} \cdot g^{-1}$ and $O_2/CH_3OH$ molar ratio of 0.29 at 473 K. Espinosa and co-workers [30] have observed that $CH_3OH$ conversion, and $H_2$ and $CO_2$ production increased almost linearly when $O_2$ partial pressure was up to 0.055 atm on Cu//ZnO catalysts. If $O_2$ partial pressure further increased, methanol conversion rapidly decreased to a constant value of 0.03 $mol/g_{cat}.h$ whereas $H_2$ formation was almost suppressed. It was believed that methanol was mainly converted to $CO_2$ and $H_2$ at higher $O_2$ partial pressure range.

An indium tin oxide/alumina ($ITO/Al_2O_3$) nanoparticle catalyst [31] was used for the selective oxidation of methanol to form hydrogen and carbon dioxide. At 68% methanol conversion, the hydrogen selectivity was 73%, and carbon monoxide was only 1-2% of the products.

Methanol partial oxidation to $H_2$ was also explored on noble metal catalysts [43]. On Rh gauze, the reactions were significant at about 603 K and extensive at 903 K. Pt gauze reactions occurred first near 643 K and were extensive at 1223 K. Traxel and Hohn [32] demonstrated that methanol can be converted to $H_2$ at millisecond contact times. Methanol catalytic partial oxidation was catalyzed at $CH_3OH/O_2$ ratios ranging from two to five on Rh and Pt monolith catalysts. Results were similar for both metals. As the ratio increased on Pt, the temperature and conversion decreased from 1373 K and 100% to 823 K and 50% and the $H_2$ selectivity increase from 65% to 75% while the CO selectivity initially rose from 75% to 85% at $CH_3OH/O_2 = 3$, then fell to 70%. The water-gas shift reaction was thought to be a key as high temperature product compositions were within experimental error of water-gas shift equilibrium compositions. The low temperature and high $CH_3OH$ to $O_2$ ratio gave more $H_2$ and $CO_2$ because of more favorable water-gas shift equilibrium although results were far from equilibrium. Supported Pd catalysts also received some attention. A hydrogen selectivity of 96% and conversion of 70% were reported [33] on Pd/ZnO catalysts when a ratio of $O_2/CH_3OH = 0.3$ was in the feed.

### 2.2.2 *Mechanism of methanol partial oxidation to produce $H_2$*

The mechanism of methanol CPO is not completely understood due to its complexity. One of the intriguing aspects of the catalytic partial oxidation of methanol is the variety of reactions that may be occurring simultaneously. The experimental data by Traxel [32] indicated that methanol oxidation reaction was not the only reaction occurring. Additional methanol decomposition may account for the high methanol conversion.

Espisona et al. [30] have proposed a simple Langmuir-Hinshelwood mechanism for the reaction on Cu/ZnO catalysts. They considered methanol O-H bond activation as the first reaction step, forming the surface methoxide species as shown in the first two equations below. The methoxide can be further dehydrogenated to form formaldehyde. The formaldehyde can desorb to the gas phase or dehydrogenate to form a surface formyl species, which results in the formation of CO and H. In the presence of surface oxygen, this formyl species might also be converted to a formate species.

$$CH_3OH \rightarrow CH_3O_s + H_s \qquad \qquad \textbf{Equation 2.9}$$

$$CH_3OH + O_s \rightarrow CH_3O_s + OH_s \qquad \qquad \textbf{Equation 2.10}$$

$$CH_3O_s \rightarrow CH_2O_s + H_s \qquad \qquad \textbf{Equation 2.11}$$

$$CH_2O_s \rightarrow CHO_s + H_s \rightarrow CO_s + H_s \qquad \qquad \textbf{Equation 2.12}$$

$$CHO_s + O_s \rightarrow CO_2H_s \qquad \qquad \textbf{Equation 2.13}$$
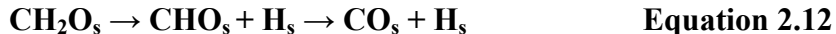
Much has been learned about the methanol partial oxidation by studying methanol decomposition and adsorption on different metals. Kirillov et al. [34] considered that methanol molecules are chemisorbed on the metal surface mainly through oxygen atoms. When methanol is adsorbed on the surface of Group III metals [35] and silver [36], its OH bond weakens, forming M-O bonds. Chemisorbed methoxy group thus formed and then underwent successive dehydrogenation to formaldehyde. CO was formed after complete dehydrogenation of methanol. It has been shown that platinum is the most efficient metal in methanol dehydrogenation due to its well-known ability to form hydrides [34].

One of the main controversies regarding the methanol catalytic partial oxidation mechanism concerns the role of oxygen in hydrogen abstraction. Adsorbed oxygen may either abstract hydrogen from the methanol molecule or simply react with its dissociation products. It was proposed by Valitov and Lakiza [37] that the adsorbed oxygen weakens the C-H and O-H bonds, thus accelerating the reaction.

It was pointed out [38] that the reaction environment is an important factor that affects the methanol decomposition reaction pathways, which may later affect the methanol partial oxidation mechanism. Whether the reaction takes place in the gas-solid system or in an electrochemical environment, the reaction mechanism is different. For example, in gas-solid systems, the formation of surface-bound methoxy groups is considered to be the rate limiting step by some researchers [39]. Dissociation of the OH group in methanol is the first step in the reaction path way. However, in the electrochemical environment, the initial step possibly is the cleavage of a CH bond. The reaction cascade proceeds via intermediates such as $CH_2OH$ and HCOOH [40]. In this research, we'll focus on the reactions in the gas-solid phase.

## 2.3    In situ FTIR studies

Attempts to elucidate the mechanism of catalytic partial oxidation have primarily relied on simulation. Hickman and Schmidt [41] modeled syngas production using a surface kinetic model constructed from kinetics found in the surface science literatures. Deutschmann and Schmidt [42] modeled methane catalytic partial oxidation with surface and gas kinetics and detailed fluid dynamics. Zum Mallen and Schmidt [ 43 ] modeled the methanol partial oxidation over polycrystalline Rh and Pt to study the reaction mechanism. Simulations have been extremely valuable in understanding the catalytic partial oxidation reactions. They have allowed surface

18

and gas phase chemistries to be individually and collectively evaluated to suggest the relative importance of each. Further, mass and heat transfer limitations can be studied. However, they are limited in power since they rely on surface kinetics that are not always well known and can be biased by the choice of which reactions to be included in the mechanism.

Molecular spectroscopy would clearly be valuable in probing the mechanisms occurring during reactions. However, the difficulty lies in developing spectroscopic techniques that are capable of in situ measurements. Many useful characterization techniques, such as Auger, XPS, EELS, LEED, require ultra-high vacuum. However, insights obtained under UHV will not be applicable to autothermal reactions at higher pressures than UHV. For instance, mass transfer limitation may be present at operating pressure but not under high vacuum.

Infrared spectroscopy offers significant potential for in situ study of autothermal reactions. First of all, operation at high pressures is possible. Secondly, the IR signals of several likely surface intermediates, such as CO, formate, hydroxyls, have well defined absorption bands when adsorbed on noble metal catalysts. Finally, infrared spectroscopy is uniquely suited for study of catalytic intermediates and reaction mechanisms because adsorbate-catalyst iterations can be specifically observed.

In situ FTIR studies on catalytic processes have generally been restricted to a few, well studied reactions, such as CO oxidation [44,45] and CO hydrogenation [46,47]. Only a few studies have looked at catalytic partial oxidation using in situ FTIR.

Baerns and coworkers [48, 18] studied Rh-catalyzed partial oxidation of methane using DRIFTS and a temporal-analysis-of-product (TAP) reactor. They found that the interaction of $CO_2$ and carbon deposits from methane led to a fast reverse Boudouard reaction to form CO. A rapid increase in the CO band intensity over time was noted after a catalyst was exposed to $CH_4$ and $CO_2$. Interaction of $CH_4$ with $Rh/Al_2O_3$ led initially to only $CO_2$, followed by a CO band that increased until 20 minutes. After that time the CO band decreased to zero. At the same time the CO band was decreasing, a negative band appeared at the expected location for OH. This negative band resulted from subtraction of the catalyst spectra from the in situ spectra and suggested that surface OH groups reacted with $CO_2$ to form CO. Surface formate was also detected in their DRIFTS experiments, but was deemed a spectator species.

Weng and coworkers [49] investigated the partial oxidation of methane to syngas on Rh and Ru catalysts using time-resolved in situ FTIR spectroscopy. Supported Rh and Ru catalysts were pressed into self-supporting disks for study in transmission mode. Reactants were introduced into a high temperature IR cell, and the spectra of both gas phase and surface species were monitored over time. Rh catalysts in a reduced state catalyzed the direct partial oxidation to CO. Oxidized Rh, however, produced $CO_2$ as the primary product. Ru catalysts always produced $CO_2$ as the primary product. From these results, they suggested that the direct partial oxidation of methane occurs on reduced Rh, while on Ru the indirect mechanism is responsible for CO formation.

Elmasides and coworkers used DRIFTS and XPS to study methane partial oxidation on $Ru/TiO_2$ catalysts [50,51]. They found that the oxidation state of Rh had a significant effect on the selectivity toward syngas, with metallic Ru giving much higher syngas selectivity that oxides of

Ru. In their in situ DRIFTS experiments, they detected adsorbed CO at all conditions up to maximum temperature of 1073K. On the basis of this work, they proposed that syngas was formed by a direct route on metallic Ru.

Basini et. al. utilized in situ DRIFTS to study the chemistry of rhodium clusters during catalytic partial oxidation of methane [52]. IR signals associated with $Rh^I(CO)_2$ species, linear carbonyls, bridged carbonyls, and hydridocarbonyl species were detected under different reactive conditions. During methane catalytic partial oxidation, surface carbonyl complexes at all temperatures between 573 K and 1073 K were detected. Total oxidation products were detected only when $CH_4$ and $O_2$ were flowed simultaneously and occurred with a simultaneous decrease in the IR adsorption bands of surface carbonyl complexes. Based on these results, they proposed that $CO_2$ and $H_2O$ were formed by reaction between primary partial oxidation products.

Stevens and Chuang reported in situ DRIFTS results for $CO_2$ reforming of methane and its coupling with partial oxidation at temperatures between 673 K and 873 K [53]. Pulsing oxygen during $CO_2$ reforming of methane produced CO IR bands and increased CO and $H_2$ production, suggesting that $CH_4$ activation was the rate-limiting step for $CO_2$ reforming and oxygen promoted this reaction. They also pulsed water into $CO_2$ methane reforming and interpreted the lack of a hydroxyl peak to mean that steam reforming played a minor role.

In situ DRIFTS results have been reported by Peppley and coworkers [54] on the production of hydrogen from methanol steam reforming. Following adsorption of methanol and steam on a $Cu/ZnO/Al_2O_3$ catalyst, infrared bands for methoxy, hydroxyl and formate groups were noted.

The authors noted that bands due to adsorbed CO, methyl biformate, and methyl formate were absent, and used these results to omit these species from their reaction mechanism.

Davis and coworkers studied methanol steam reforming, water-assisted formic acid decomposition and water-gas shift reactions on Pt promoted ceria [55]. A normal kinetic isotope experiments associated with the formate coverage monitored by in situ DRIFTS under steady state conditions using $CO + H_2O$ and $CO + D_2O$ were conducted. Experiments of isotope formic acid decomposition and decomposition of adsorbed methanol species under steam were also performed. Bridged OH groups, which are associated with reduced defect centers on the surface of the oxide, were formed at low temperatures for the Pt-promoted thoria catalyst. It was suggested that the active sites for water-gas shift reaction, water-assisted formic acid decomposition and methanol steam reforming are associated with these oxygen-deficient centers.

Evin et al [56] used in situ DRIFTS to study the effect of alkali dopants on scission of C-H bonds in formate and methoxy decomposition. It was found that there is a systematic decrease in the band position corresponding to $v(CH)$ of both formate and adsorbed methanol molecule with increasing atomic number of the alkali metal. This shift indicated that formate and methoxy species pre-adsorbed on the catalyst surface were more reactive for dehydrogenation steps in the catalytic cycle for the Li and Na-doped $Pt/CeO_2$ catalysts compared to undoped $Pt/CeO_2$.

Methanol steam reforming over ex-hydrotalcite Cu–Zn–Al catalysts was studied using IR [57]. Mechanism information was obtained from the results of adsorption and coadsorption of methanol, water, CO, $CO_2$ and $H_2$ on the catalyst. It was proposed that methanol steam reforming

22

occurs over the Cu–Zn–Al catalysts via the adsorbed methoxy groups/ adsorbed formate ions/ adsorbed CO/ $CO_2$ sequence.

## 2.4    Ignition studies

A study of the ignition process is helpful for understanding the reaction mechanism. In addition, a detailed knowledge of ignition is of prime importance due to both economic and safety concerns [58].

Early ignition studies [59] focused on fuel-lean gas-air mixtures on heated metal bars, and were inspired by the consideration of natural gas storage safety.  The dimensions of metal bars were varied and heated under natural gas and air mixtures. It was found that the surface temperature required for natural gas/air gas phase ignition was higher for surfaces that were active for catalytic oxidation of natural gas than for noncatalytic surfaces. The catalytic ignition temperatures of mixtures on several metals increased with increase in natural gas content.

Hiam and coworkers [60] measured the catalytic ignition temperatures as a function of reactant concentration for various hydrocarbon/$O_2$ mixtures. The catalysts used were platinum filaments heated electrically. The hydrocarbons ranged from $C_1$ to $C_4$ paraffins. The ignition temperatures of butane and propane decreased with increasing fuel concentration in the reactant mixtures. The decrease of ignition temperature with increasing fuel concentration in lean butane air mixture was also observed by Cardoso and Luss [61]. These studies focused on very low fuel concentration, <1%. From this series of experiments, rapid determination of the rates of catalytic oxidation was realized. The results suggested that dissociative chemisorption of the hydrocarbon

molecule with rupture of the carbon-hydrogen bond is the rate determination step in catalytic oxidation of alkanes.

Cho and Law [62] accurately determined the catalytic ignition temperatures of a variety of fuel/oxygen/nitrogen mixtures over extended ranges of fuel concentrations on platinum wires. Fuel type, oxygen concentration and flow velocity were also considered. Ignition temperature of propane/air mixtures was not sensitive to variation in the flow velocity. The catalytic ignition temperature of propane and butane decreased with fuel concentration for both the lean and moderately rich mixtures and was only weakly dependent on the oxygen concentration. These results implied that oxygen on the catalyst surface is in abundance and adsorption of saturated hydrocarbons is difficult.

Griffin et al [63] studied both gas and catalytic ignition of fuel lean mixtures of methane and ethane in air over platinum. They concluded that surface reactions are ignited at higher surface temperatures for metals with higher catalytic properties. This result was explained by the change of local concentration of reactants adjacent to the heated surface. Their experiments also suggested that the sharp maximum in surface temperature required for gas phase ignition results from transient heating of the surface as ignition occurs. In their studies [64,65], OH and O species were defined as ignition-enhancing species which lead to a lower required surface temperature for gas phase ignition on platinum. Surface ignition temperatures were obtained for ethane and methane to gain understanding of the surface oxidation kinetics.

Ignition and extinction behavior of various hydrocarbons was examined over platinum foils by Veser and Schmidt [66]. The surface ignition temperature was found to decrease with increasing chain length of the hydrocarbons, which is explained by the decreasing C-H bond strength of the alkanes. The surface ignition temperature decreased with increasing fuel to air ratio was mainly due to the competition between oxygen and hydrocarbon adsorption on the catalyst surface.

Detailed simulation of catalytic ignition of methane/oxygen mixture over platinum was conducted by Bui et al [67]. The surface ignition of methane/oxygen/nitrogen mixtures over a platinum foil was modeled at atmospheric pressure by including 20 surface reactions and seven surface species. The simulation results showed that the adsorption of methane and oxygen is competitive and controls the ignition temperature. Ignition of catalytic methane oxidation over platinum in a monolith reactor was modeled [68]. It is usually difficult to get an exact ignition temperature in a monolith reactor. Therefore, by comparing the experimental results on Pt foils, the model showed that the catalyst surface is essentially oxygen-poisoned before ignition, both for fuel lean and fuel rich mixtures.

The fast light off characteristics of catalytic partial oxidation of methane and higher alkanes was noticed by Leclerc and Schmidt et al. [69,70]. It was found that the monolith reactor can be ignited and produce high selectivities to $H_2$ and CO in less than five seconds. This was accomplished by internal heating of the catalyst, using combustion to produce $CO_2$ and $H_2O$ and then rapidly switching from the combustion ratio to the syngas ratio. These studies further proved that the catalytic partial oxidation reactions have the ability to respond quickly to a transient load.

Ignition and extinction of ethane-air was investigated [71] over Pd, Rh, Ir, and Ni foils. Heterogeneous ignition temperatures were generally in the order Pt < Pd < Rh < Ir < Ni. These results correlated well with the metal-oxygen bond strength: Pt and Pd with the lowest M-O bond strength had the lowest ignition temperatures and ignited in the leanest fuel mixtures, while Rh, Ir, and Ni with high M-O bond strengths had high ignition temperatures and deactivated in excess air.

Recently, ignition of catalytic partial oxidation of methane oxygen mixture with a large amount of $H_2O$ and $CO_2$ in the feed has been experimentally and numerically studied [72]. The dilutions of $H_2O$ and $CO_2$ were 46.3% and 23.1%, respectively. The key reaction controlling catalytic ignition was believed to be the surface oxidation of CO to $CO_2$, which was the main exothermic step in the induction zone. The key parameter controlling the extinction was the CO coverage, which led to catalyst poisoning.

Limited information on the ignition of methanol partial oxidation is available. Hohn and Traxel [32] reported an estimated ignition temperature of 423 K for methanol partial oxidation on Rh and Pt monoliths. A comparable study on the ignition of methanol combustion [73] was studied over supported Pt and Cu catalysts. The onset of the reactions started at room temperatures when the catalysts were pre-reduced while both catalysts became active at 473 K if in the oxidized state.

## 2.5    References

1 A.M. Adris, B.B. Pruden, C.J. Lim, J.R. Grace. Can. J. Chem. Engg. 74 (1996) 177

2 H. Liander, Trans. Faraday Soc. 25 (1929) 462

3 P.D.F. Vernon, D. Phil. Thesis, University of Oxford, 1990

4 D.A. Hickman, E. A. Haupfear, L. D. Schmidt, Catal. Lett. 17 (1993) 223

5 M. Huff, P.M. Torniainen, L. D. Schmidt, Catal. Today, 21 (1994) 113

6 M. Prettre, Ch. Eichner, M. Perrin, Trans. Faraday Soc. 42 (1946) 335

7 D. Dissanayake, M.P. Rosynek, C.C.C. Kharas, J.H. Lunsford, J. Catal. 132 (1991) 117

8 V.R. Choudhary, A.M. Rajput, B. Prabhakar, J. Catal. 139 (1993) 326

9 D.A. Hickman, L. D. Schmidt, Science 259 (1993) 343

10 M.G. Poirier, J. Trudel, D. Guay, Catal. Lett. 21 (1993) 99

11 A.T. Ashcroft, A.K. Cheetham, J.S. Foord, M.L.H. Green, C.P. Grey, A.J. Murrell, P.D.F. Vernon, Nature 344 (1990) 181

12 Y.F. Chang, H. Heinemann, Catal. Lett. 21 (1993) 215

13 O.V. Buyevskaya, D. Wolf, M. Baerns, Catal. Lett. 29 (1994) 249

14 W.J.M. Vermeiren, E. Blomsma, P.A. Jacobs, Catal. Today, 13 (1992) 427

15 A.P.E. York, T. Xiao, M.L.H. Green, Topics in Catal. 22 (3-4) (2003) 345

16 A.P.E. York, D.Phil. Thesis, University of Oxford, 1993

17 F. van Looij, E.R. Stobbe, J.W. Geus, Catal. Lett. 50 (1998) 59

18 K. Walter, O.V. Buyevskaya, D. Wolf, M. Baerns, Catal. Lett. 29 (1994) 261

19 D.A. Hickman, L. D. Schmidt, J. Catal. 138 (1992) 267

20 D.A. Hickman, E.A. Haupfear, L. D. Schmidt, Catal. Lett. 17 (1993) 223

21 P.M. Torniainen, X. Chu, L. D. Schmidt, J. Catal. 146 (1994) 1

22 V.R. Choudhary, A.M. Rajput, B. Prabhakar, Catal. Lett. 15 (1992) 363

23 V.R. Choudhary, A.M. Rajput, V.H. Rane, Catal.Lett. 16 (1992) 269

24 Y.H. Hu, E. Ruckenstein, J. Catal. 158 (1996) 260

25 C.T. Au, H.Y. Wang, J. Catal. 167 (1997) 337

26 W.Z. Weng, Q.G. Yan, C.R. Luo, Y.Y. Liao, H.L. Wan, Catal. Lett. 74 (2001) 37

27 T. Liu, C. Snyder, G. Veser, Ind. Eng. Chem. Res. 46 (2007) 9045

28 C.T. Au, H.Y. Wang, H.L. Wan, J. Catal. 158 (1996) 343

29 S. Velu, K. Suzuki, T. Osaki, Catal. Lett. 62 (1969) 159

30 L.A. Espinosa, R.M. Lago, M.A. Pena, J.L.G. Fierro, Topics in Catal. 22 (2003) 245

31 A. Kulprathipanja, J.L. Falconer, Appl. Catal. A: general 261 (2004) 77

32 B.E. Traxel, K.L. Hohn, Appl. Catal. A: general 244 (2003) 129

33 M.L. Cubiero, J.L.G. Fierro, J.Catal. 179 (1998) 150

34 S.A. Kirillov, P.E. Tsiakaras, I.V. Romanova, J. Mol. Struct. 651-653 (2003) 365

35 J. Kao, W.A. Goddard, J. Am. Chem. Soc. 121 (1999) 10928

36 A. Yee, S.J. Morrison, H. Idriss, J. Catal. 186 (1999) 279

37 N.K. Valitov, S.M. Lakiza, Russ. J. Phys. Chem. 49 (1975) 1853

38 C. Hartnig, E. Spohr, Chem. Phys. 319 (2005) 185

39 B. Barros, A. Garcia, L. Ilharco. J. Phys. Chem. B 105 (2001) 11186

40 C. Lu, C. Rice, R.I. Masel, P.K. Babu, P. Waszczuk, H.S. Kim, E. Oldfield, A. Wieckowski, J. Phys. Chem. B 106 (2002) 9581

41 D.A. Hickman, L. D. Schmidt, AICHE J. 39 (1993) 1164

42 O. Deutschmann, L. D. Schmidt, AICHE, J. 44 (1998) 15

43 M.P. Zum Mallen, L. D. Schmidt, J. Catal. 161 (1996) 230

44 X. Xu, D.W. Goodman, J. Phys. Chem. 97 (1993) 7711

45 G.M. Hoffman, M.D. Weisel, C.H.F. Peden, Surface Science 253 ( 1991) 59

46 M.W. Balakos, S.S.C. Chuang, G. Srinivas, M.W. Brundage, J. Catal. 157 (1995) 51

47 C.S. Kellner, A.T. Bell, J. Catal. 71 (1981) 296

48 O.V. Buyevskaya, K. Walter, D. Wolf, M. Baerns, Catal. Lett. 38 (1996) 81

49 W.Z. Weng, M.S. Chen, Q.G. Yan, T.H. Wu, Z.S. Chao, Y.Y. Liao, H.L. Wan, Catal. Today, 63 (2000) 317

50 C. Elmasides, D.I. Kondarides, W. Grunert, X.E. Verykios, J. Phys. Chem. B 103 (1999) 5227

51 C. Elmasides, D.I. Kondarides, S.G. Neophytides, X.E. Verykios, J. Catal. 198 (2001) 195

52 L. Basini, A. Guarinoni, A. Aragno, J. Catal. 190 (2000) 284

53 R.W. Stevens, S.S.C. Chuang, 17th North American Catalysis Society Meeting, Toronto, 2001

54 B.A. Peppley, J.C. Amphlett, L.M. Kearns, R.F. Mann, Appl. Catal. A: general 179 (1999) 31

55 G. Jacobs, P. M. Patterson, U.M. Graham, A.C. Crawford, A. Dozier, B.H. Davis, J. of Catal. 235 (2005) 79

56 H.N. Evin, G. Jacobs, J. Ruiz-Martinez, U.M. Graham, A. Dozier, G. Thomas, B.H. Davis, Catal. Lett. 122 (2008) 9

57 M.A. Larrubia Vargas, G. Busca, U. Costantino, F. Marmottini, T. Montanari , P. Patrono, F. Pinzari, G. Ramis, J. of Molecular Catal. A: Chemical 266 (2007) 188

58 G. Veser, J. Frauhammer, L. D. Schmidt, G. Eigenberger, Studies in Surf. Sci. and Catal. 109 (1997) 273

59 H.F. Coward, P.G. Guest, J. Am. Chem. Sot. 49 (1927) 2479

60 L. Hiam, H. Wise, S. Chaikin, J. Catal. 9-10 (1968) 272

61 M. Cardoso, D. Luss, Chem. Eng. Sci. 24 (1969) 1699

62 P.Cho, C.K. Law, Combustion and Flame, 66 (1986) 159

63 T.A. Griffin, L.D. Pfefferle, AICHE J. 36 (1990) 861

64 L.D. Pfefferle, T.A. Griffin, M. Winter, D.R. Crosley, M.J. Dyder, Comb. Flame, 76 (1989) 325

65 T.A. Griffin, L.D. Pfefferle, M.J. Dyder, D.R. Crosley, Comb. Sci. Techol. 65 (1989) 19

66 G. Veser, L.D. Schmidt, AICHE J. 42 (1996) 1077

67 P.A. Bui, D.G. Vlachos, P.R. Westmoreland, Surf. Sci. 385 (1997) L1029

68 G. Veser, J. Frauhammer, Chem. Engg. Sci. 55 (2000) 2271

69 C.A. Leclerc, J.M. Redenius, L.D. Schmidt, Catal. Lett. 79 (2002) 39

70 L.D. Schmidt, E.J. Klein, C.A. Leclerc, J.J. Krummenacher, K.N. West, Chem. Engg. Sci. 58 (2003) 1037

71 M. Ziauddin, G. Veser, L.D. Schmidt, AICHE J. 46 (1997) 159

72 A. Schneider, J. Mantzaras, S. Eriksson, Combustion Sci. Technol, 180 (2008) 89

73 C. Jiang, D.L. Trimm, M.S. Wainwright, Chem. Engg. Tech. 18 (1995) 1

# Chapter 3 Experimental and characterization method

## 3.1    Experimental apparatus

An experimental apparatus was constructed in order to study catalytic partial oxidation in situ under both steady-state and transient conditions. The primary components of this apparatus are a flow control and reactant introduction system, a mass spectrometer, and, most importantly, a Fourier Transform infrared spectrometer. A simplified schematic of the reaction system is shown in **Figure 3.1**.
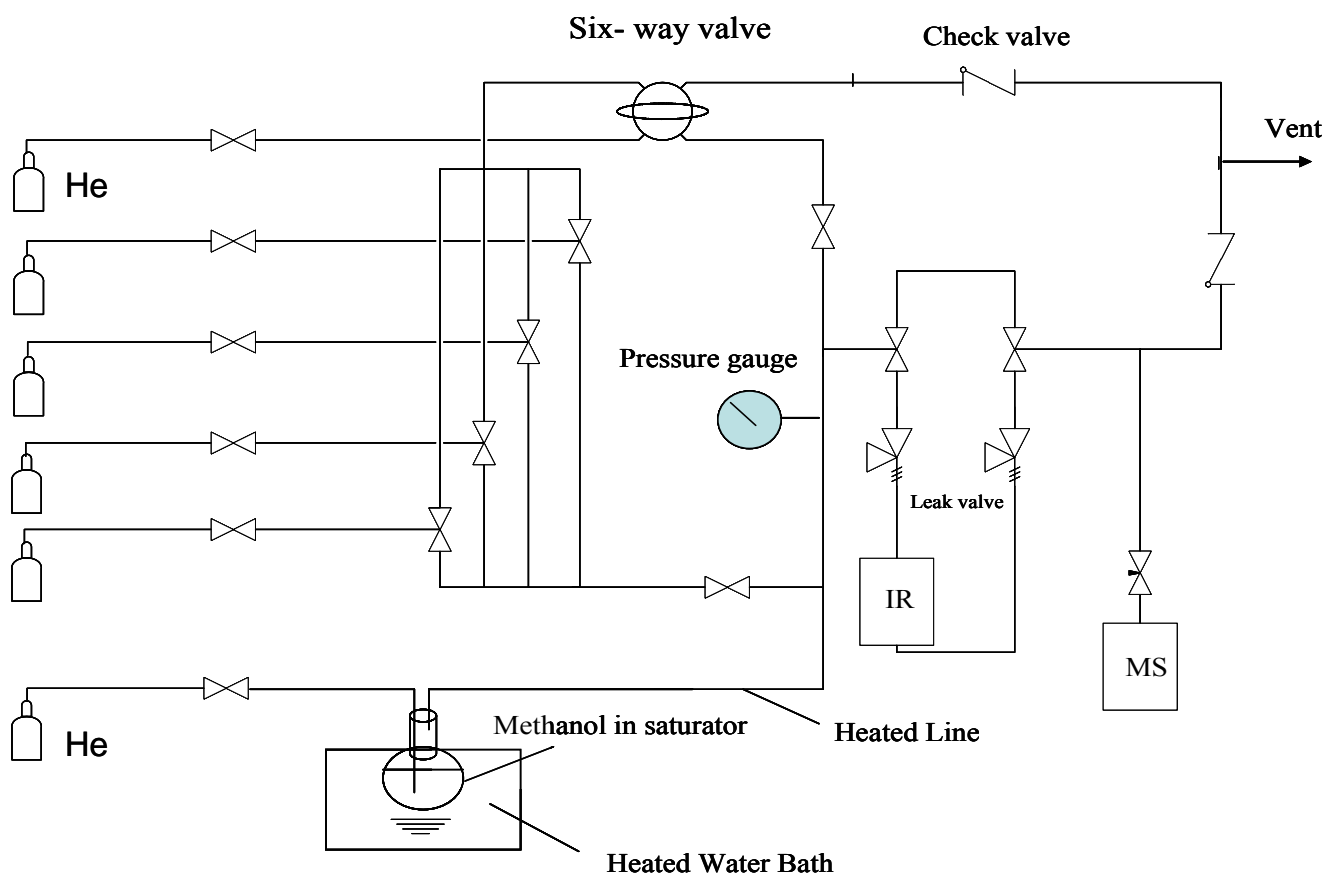


**Figure 3.1 Reaction system**

The components of the flow control and reactant introduction system were selected to allow precise control and measurement of pressure and inlet feed concentrations. Furthermore, the system is designed to allow several gases to be fed simultaneously so that maximum flexibility in the operation can be realized. For example, it is desired to feed gaseous $O_2$ with a diluents inert gas such as He or, alternatively, to feed liquid fuels to be vaporized and mixed with other gases.

These components mainly include valves, a pressure gauge, digital mass flow controllers, heating tapes, and a saturator. The leak valves installed before and after the reactor can maintain the pressure under 1 atm in the reactor. Three sets of mass flow controllers, large range (0-2 SLM), mid range (0-100 SCCM) and small range (0-50 mL/min), regulate flow rates for fuels such as $CH_4$ and other light hydrocarbons, $O_2$, He, $H_2$, CO, and $CO_2$. The saturator is used to feed methanol or other liquids into a carrier gas. The saturator is immersed in a water bath. The concentration of the liquid fuels is controlled by changing the vapor pressure of liquid by heating the water bath to different temperatures. A six-way valve will allow any of the reactants to be pulsed into the reactor. With this design, it is possible to study the reactions under steady-state or transient conditions.

A quadrupole mass spectrometer (Pfeiffer OMNISTAR) is connected on-line for continuous monitoring of reaction products. The mass spectrometer has a stainless steel capillary for gas sampling, which can be heated to prevent the products from condensing. A needle valve was also used to control the sampling.

The FTIR spectrometer (ThermoNicolet 870) allows surface adsorbates to be monitored at most reaction conditions. It is connected to the flow control system, which is used to prepare inlet gas mixtures. During the research, a commercial high temperature/high pressure DRIFTS cell (Spectra-Tech, Model No. 0031-901) has been used as the main reactor. The original configuration of this cell was not suitable for studying CPO in an autothermal mode. Two major obstacles existed. First, the catalytic partial oxidation autothermal condition couldn't be reached. Although the reaction could be ignited, it died immediately after the external heating stopped. Second, water produced from reaction condensed on the IR window, which prevented IR analysis.

The causes behind these problems were the cell configuration and flow pattern in the cell. The original configuration of the reactor (**Figure 3.2a**) was comprised of a 2mm deep and 5mm wide ceramic sample cup in the DRIFTS cell, in which around 30 mg of catalyst can be loaded. The ceramic sample cup had a porous bottom, which allowed gas to exit the reactor. The ceramic sample cup was also equipped with a heater assembly, which was capable of heating the catalysts up to 1173 K. A type-K thermocouple made up of a positive Chromel wire and a negative Alumel wire was inserted just in the catalyst to accurately measure the temperature. A dome with a zinc selenide window for IR beam transmission was placed over the heater assembly to contain the gasses and was cooled by inner circulating distilled water.

There was only one gas inlet (1$^{st}$ inlet) and two outlets, a gas outlet and a vacuum outlet, before modification. Test experiments were done using the first inlet and the gas outlet. Gas flow enters from inlet 1 on the lower part of the reactor and makes its way around the sample cup, and then

34

flows back down through the sample cup, coming out from the bottom of the sample cup (gas outlet). For autothermal operation, the reactant flow rate needs to be high enough to generate the same amount of heat that is lost to the environment. With high reactant flow rate, it was found that the gas flow out of the reactor was much less than the gas feed. Pressure accumulated in the reactor until the inlet leak valve opened, releasing some of the gases. This indicated that the bottom of the sample cup was not porous enough to allow the reaction products to exit.

Another issue with the original configuration of the cell was the flow pattern in the cell. Because of the location of the first inlet, reactants flowed from the bottom up to the window and then down to contact the catalyst in the sample cup. This circulating flow pattern, together with the small porosity of the second outlet, led to the mixing of products and reactants. Water, one of the products, could condense on the IR window. The reactant concentration was also lowered, resulting in the extinction of the reaction immediately after ignition.

The cell was modified by adding a second inlet on the upper part of the reactor as shown in **Figure 3.2b**. Using the second inlet instead of the first inlet allows gases to enter from the top of the reactor. A hole was drilled at the bottom of the sample cup. A quartz disc with a high porosity was used to cover the hole to support catalysts. The flow pattern of this design is close to a packed bed configuration typically used to study catalytic partial oxidation.

With this new set up, reactant gas flows into the reaction chamber from the second inlet and down through the sample. Water condensation on the window was prevented at high temperature with this modification. Autothermal operation was successfully achieved.
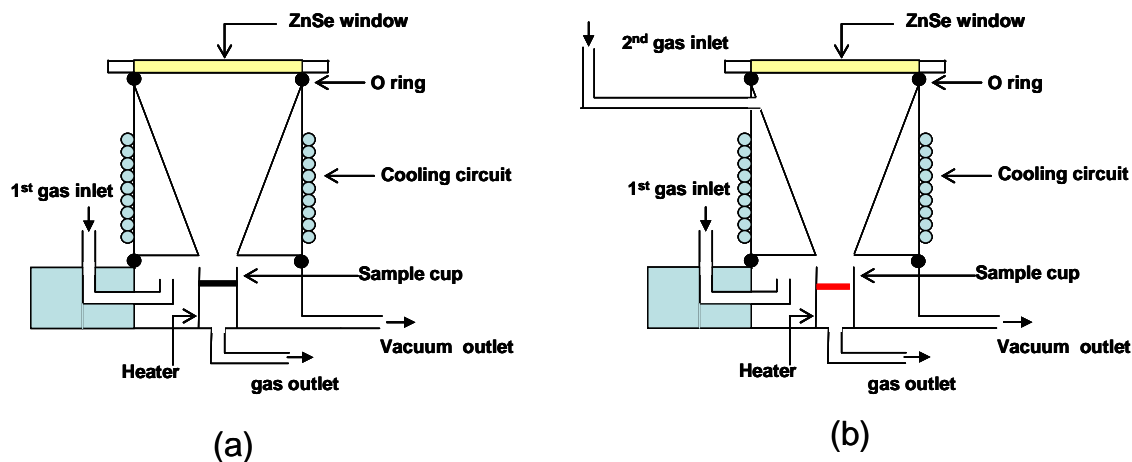
**Figure 3.2 DRIFTS cell configuration: (a) original configuration and (b) modified configuration.**

## 3.2 Catalyst preparation

The incipient wetness impregnation method was used to prepare all catalysts. In this procedure, the support is contacted with a certain amount of solution of the metal precursor. The sample is dried and calcined. Because the amount of solution containing the precursor does not exceed the pore volume of the support, this method is also known as dry impregnation.

Pt/$Al_2O_3$ catalysts, both chloride containing ($Pt_{Cl}$) and chloride free (Pt), were prepared by impregnating the support ($\gamma$-$Al_2O_3$, powder $S_{BET}$ = 121 m$^2$/g)) with aqueous solutions of $H_2PtCl_6.6H_2O$ and $Pt(NH_3)_4(NO_3)_2$, respectively. Rh/$Al_2O_3$ powder catalysts are prepared by impregnating the $\gamma$-$Al_2O_3$ with aqueous solutions of $Rh(NH_3)_4(NO_3)_2.2H_2O$. Impregnated catalysts were dried for 12 hr at room temperature and then for 24 hr at 383 K. The solids were

calcined for 10 hr in flowing $O_2/Ar$ at 773 K. $10\%Pt_{Cl}/Al_2O_3$, $2\%Pt_{Cl}/Al_2O_3$, $2\%$ $Pt/Al_2O_3$, and $2\%Rh/Al_2O_3$ were used in the research.

## 3.3    Characterization methods

### 3.3.1  *Infrared spectroscopy*

Infrared spectroscopy can identify adsorbed species and provide information when these species are chemisorbed on the surface of the catalysts. The infrared regions are classified as in **Table 3.1**. The vibration wavelengths of the molecules in this study are mostly in the mid infrared region.

**Table 3.1 Classification of infrared radiation**

| Region | Frequency ($cm^{-1}$) | Wavelength (um) | Energy (meV) |
|--------|----------------------|-----------------|--------------|
| Near Infrared | 12500 - 4000 | 0.8 - 2.5 | 496 - 1240 |
| Mid Infrared | 4000 - 200 | 2.5 - 50 | 25 - 496 |
| Far Infrared | 200 - 12.5 | 50 - 800 | 1.2 - 25 |

Several forms of infrared spectroscopy are commonly in use, as illustrated in **Figure 3.3**. The most common form is transmission infrared spectroscopy. Transmission IR can be applied if the bulk of the catalysts adsorbs weakly. This usually works for catalysts with typical oxide supports for frequencies above 1000 $cm^{-1}$. 10-100 mg of catalyst can be pressed into a self-supporting disk. In order to guarantee deeper penetration of the incident ray and less specular reflection of the sample surface due to sample's strong absorption, the sample typically is typically diluted in KBr before being pressed into a disk of a few tenths of a millimeter in thickness.
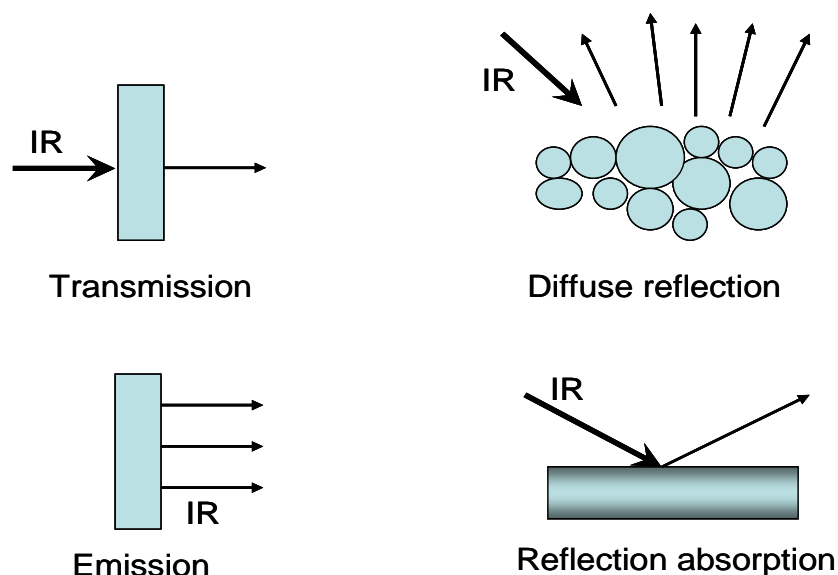
**Figure 3.3 Different infrared spectroscopy techniques**

In the diffuse reflectance mode, samples can be measured as loose powders, which can avoid the diffusion limitation associated with tightly pressed samples. Pressing samples into disks can prevent interacting of reactants with the catalysts. Diffuse reflectance infrared Fourier transform spectroscopy (DRIFTS or DRIFT) is a common technique that collects and analyzes scattered IR energy. It is used for measurement of fine particles and powders, as well as rough surface (e.g., the interaction of a surfactant with the inner particle, the adsorption of molecules on the particle surface).

Measurements of supported catalysts in diffuse reflection and transmission mode are limited to frequencies above what the support absorbs (about 1250 cm$^{-1}$). Infrared emission spectroscopy (IRES) offers an alternative in this case. When a material is heated to about 373 K or higher, it emits a spectrum of infrared radiation in which all the characteristic vibrations appear as clearly recognizable peaks. Thus, low frequencies such as metal-oxygen bond are easily accessible.

Reflection absorption infrared spectroscopy (RAIRS), referred as infrared reflection absorption spectroscopy (IRAS), is used to detect gases adsorbed on the surfaces of metal single crystal or polycrystalline foils. Absorption bands in IRAS are much weaker in intensity than transmission bands in supported catalysts measurements.

Among these infrared spectroscopy techniques, DRIFTS has many advantages. For example, sampling is fast and easy because little or no sample preparation is required. For strongly scattering or absorbing particles, DRIFTS has fewer limitations than transmission mode. Thus dilution is not required. This is a huge advantage when trying to analyze samples under reaction conditions, where undiluted samples are preferred. Furthermore, spectra can be recorded and changes can be analyzed at elevated temperature and/or under pressure provided that commercial DRIFTS apparatus is available. To study catalytic partial oxidation on supported catalysts in situ, DRIFTS is a good choice.

**Figure 3.4** shows the mechanism for generating the DRIFTS spectrum of a powder. When the IR beam enters the sample, it can either be reflected off the surface of a particle or be transmitted through a particle. The IR energy reflecting off the surface is typically lost. The IR beam that passes through a particle can either reflect off the next particle or be transmitted through the next particle. This transmission-reflectance event can occur many times in the sample, which increases the path length. Finally, such scattered IR energy is collected by a spherical mirror that is focused onto the detector. The detected IR light is partially absorbed by particles of the

sample, bringing the sample information. The infrared adsorption spectrum is described by the Kubelka-Munk function:

$$\frac{K}{S} = \frac{(1-R_\infty)^2}{2R_\infty}$$

**Equation 3.1**

in which

$K$ is the absorption coefficient, a function of the frequency $\nu$

$S$ is the scattering coefficient

$R_\infty$ is the reflectivity of a sample of infinite thickness, measured as a function of $\nu$

It is well known that particle size is a key variable in a diffuse reflectance measurement because large particle will result in the scattering of the energy, leading to the shift of the spectrum baseline and the broadening of IR bands. Thus, it is important to grind the sample particles to 5 microns or less.
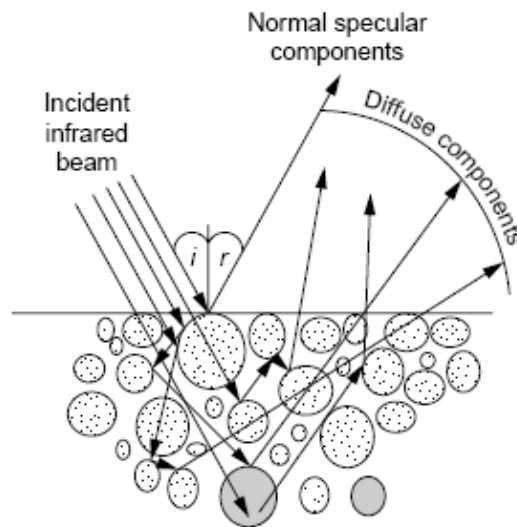


**Figure 3.4 IR beam pathways of DRIFTS [1].**

### 3.3.2 *H₂ chemisorption*

The measurement of metal dispersion in supported metallic catalysts requires adsorption exclusively or predominately on the metal surface. The chemisorption of $H_2$, CO, $O_2$ and NO has been the most frequently used methods [2].

The use of chemisorption requires the measurement of the gas uptake. From the amount of gas uptake, the number of metal surface atoms, thus the metal surface area and metal dispersion, can be estimated. In this process, the monolayer uptake model is used to define the corresponding chemisorption stoichiometry as follows. The chemisorption stoichiometry for a monolayer, $X_m$, is defined as the average number of surface metal atoms associated with the adsorption of each adsorbate molecule. If $n_s$ is the number of metal atoms per unit area of surface, $n_m^s$ is the monolayer adsorbate uptake, and $n_T$ is the total number of the metal atoms, the total surface area, A, is given by:

$$A = n_m^s \, X_m \, n_s^{-1} \qquad\qquad \textbf{Equation 3.2}$$

and metal dispersion is

$$\textbf{Dispersion (\%)} = n_s n_T = n_m^s \, X_m n_T \qquad\qquad \textbf{Equation 3.3}$$

The calculation described above is based on an idealized monolayer model. Correction from measured equilibrium uptake may be needed to get proper adsorption estimation. The error factor includes the incorporation of gas into the bulk of the metal, the adsorption of gas on the support, and the phenomena of gas solubility and reaction to form a separate or quasi-separate phase. Although these factors exist unavoidably to some extent, efforts can be made to reduce the effect. For example, $H_2$ gas instead of CO was chosen to conduct the chemisorption studies,

considering $H_2$ solubility is a negligible contribution (less than$10^{-3}$ atom % at 273K and 1atm) [3] compared to adsorption. CO can form carbonyls on both platinum and rhodium, which are not easy to desorb even at high temperatures. The adsorption of $H_2$ on the alumina support (spillover) is less compared to $O_2$ and CO, which is another reason that the $H_2$ chemisorption method was used in the research.

### 3.3.3 *TEM (Transmission Electron Microscopy)*

Transmission electron microscopy (TEM) uses transmitted and diffracted electrons. Specimen images may be obtained with either bright field or dark field illumination. In bright field illumination, a primary electron beam of high energy and high intensity passes through a condenser to produce parallel rays, which impinge on the sample. Because the attenuation of the beam depends on the density and the thickness, the transmitted electrons form a two-dimensional projection of the sample mass, which is subsequently magnified by the electron optics to produce a bright field image.

The dark field image is obtained from diffracted electron beams, which are slightly off angle from the transmitted beam by suitably tilting the specimen with respect to the microscope axis. The identity of the diffracted beam which is used for dark field image formation is identifiable from the diffraction pattern from which it is selected. Thus dark field illumination is, when used in conjunction with bright field illumination, a powerful technique to assist in phase identification and crystal orientation in polycrystalline specimen.

TEM is the commonly applied form of electron microscopy for studying supported catalysts. It can be used to determine the size and shape of supported particles. Detection of supported

particles requires that there is sufficient contrast between particles and support. Resolution of TEM is far superior to that of optical microscopes due to the fact that electrons are used for the source of illumination rather than visible or ultra-violet light. Optical microscopes are limited to a resolution in the order of 100 nm whereas modern TEM demonstrate resolutions approaching 0.2nm [4].

### 3.3.4 *Mass spectrometry*

Mass spectrometry is used to measure the molecular mass of a sample using a mass spectrometer. Mass spectrometers can be divided into three fundamental parts: the ionization source, the analyzer, and the detector. The sample has to be introduced into the ionization source of the instrument. Once inside the ionization source, the sample molecules are ionized. These ions are extracted into the analyzer region of the mass spectrometer where they are separated according to their mass (m) -to-charge (z) ratios (m/z). The separated ions are detected and this signal is sent to a data system where the m/z ratios are stored together with their relative abundance for presentation in the format of a m/z spectrum. The analyzer and detector of the mass spectrometer, and often the ionization source too, are maintained under high vacuum to give the ions a reasonable chance of traveling from one end of the instrument to the other without any hindrance from air molecules. The entire operation of the mass spectrometer, and often the sample introduction process, is under complete data system control on modern mass spectrometers.

The main function of the mass analyzer is to separate the ions formed in the ionization source of the mass spectrometer according to their mass-to-charge (m/z) ratios. There are a number of mass analyzers currently available, the better known of which include quadrupole, time-of-flight

(TOF) analyzers, magnetic sectors **,** and both Fourier transform and quadrupole ion traps. The mass spectrometer used in this research has a quadrupole analyzer, and is therefore called a quadrupole mass spectrometer.

Quadrupole mass spectrometers consist of an ion source, ion optics to accelerate and focus the ions through an aperture into the quadrupole filter, the quadrupole filter itself with control voltage supplies, an exit aperture, an ion detector, detection electronics, and a high-vacuum system. The quadrupole filter consists of four rods or electrodes arranged across from each other as shown in **Figure 3.5**. As the ions travel through the quadrupole they are filtered according to their *m/z* value so that only a single *m/z* value ion can strike the detector and and all other ions are thrown out of their original path. The quadrupole mass spectrometer is the most common used mass analyzer because of its compact size, fast scan rate and low price.
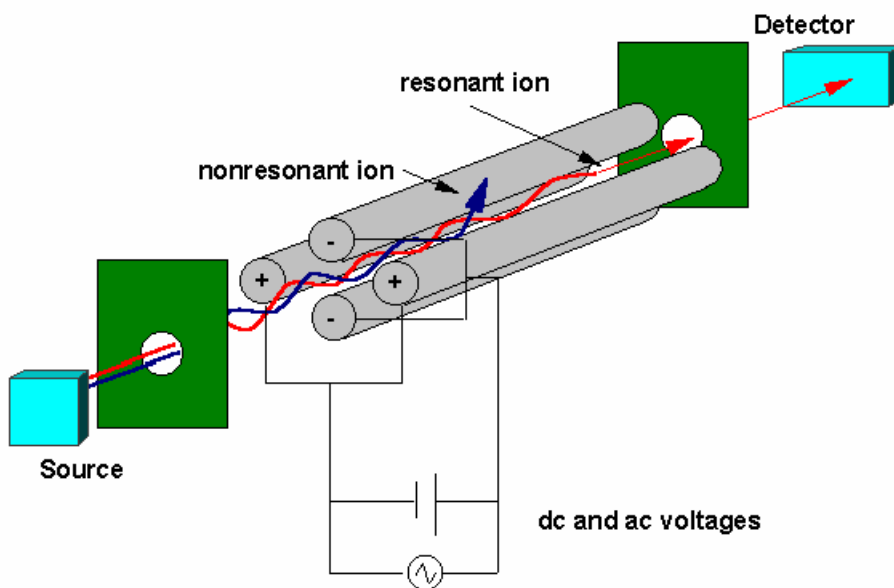


**Figure 3.5 Quadrupole mass spectrometer [5]**

## 3.4    References

1 T. Armaroli, T. Bécue, S. Gautier, Oil & Gas Sci. and Tech. – Rev. IFP, 59 (2004) 215

2 J.R. Anderson, *Structure of Metallic catalysts* , Academic press, London (1975)

3 C.J. Smithell, *Gases in Metals*, Chapman and Hall, London (1937)

4 H. Curtis, *Biology, 5th Edition*. New York: Worth, (1989) 96

5 B.M. Tissue, http://www.chem.vt.edu/chem-ed/ms/quadrupo.html. Copyright © 2000

# Chapter 4 In situ infrared study of the catalytic ignition of methane on Pt/Al$_2$O$_3$

## 4.1    Introduction

Catalytic ignition of methane has been studied in both the combustion and partial oxidation regimes over various metals catalysts [1,2,3]. Most studies have focused on accurately measuring the temperature at which either surface or surface-initiated gas phase ignition occurs. Mass spectrometry or gas chromatography was usually used for monitoring gas phase species concentrations. Several studies have also been devoted to modeling methane ignition considering the surface chemistry as well as the gas phase chemistry and transport processes. However, there is a lack of experimental information about how the surface species change as the temperature is raised towards the ignition temperature. The effect of the surface state of platinum on catalytic ignition is also not well known. This work uses in situ diffuse reflectance infrared Fourier transform (DRIFT) spectroscopy to investigate the light-off of the catalytic partial oxidation of methane over Pt/Al$_2$O$_3$.

## 4.2    Experimental

### 4.2.1  *Catalyst preparation*

Pt/Al$_2$O$_3$ catalysts, chloride containing (Pt$_{Cl}$) and chloride free (Pt), have been prepared by impregnating the support ($\gamma$-Al$_2$O$_3$ powder, S$_{BET}$ = 121 m$^2$/g) with aqueous solutions of H$_2$PtCl$_6$•6H$_2$O and Pt(NH$_3$)$_4$(NO$_3$)$_2$, respectively. After drying for 12 h at room temperature and then for 24 h at 383 K, the solids were treated for 10 hr in flowing O$_2$/Ar at 773 K. Prior to each

experiment, $Pt_{Cl}$ and Pt catalysts sample were pretreated in the DRIFT cell according to the following procedure as shown below : oxygen (T = 773 K, t = 1 h) → helium (T = 773 K, t = 10 min) → $H_2$ (T = 773 K, t = 1 h) → helium (T = 773 K, t = 10 min) → helium (room temperature).
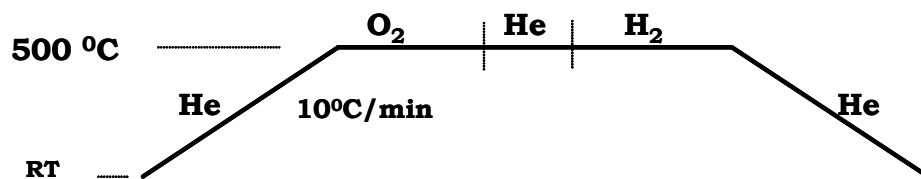


**Figure 4.1 Pretreatment procedure for the reduced catalysts.**

**Table 4.1 Average Pt particle size, dispersion and surface ignition temperatures, Ti, for $Pt_{Cl}$ and Pt catalysts.**

| Catalysts | Catalyst state | Dispersion (%) | Particle size (nm) | Ti (K) |
|---|---|---|---|---|
| 10% $Pt_{Cl}$ | Freshly reduced | 0.58-0.65[a] | 1.7-1.9 [b] | 548 |
| | Oxidized | 0.50-0.58 [a] | 1.9-2.2 [b] | 588 |
| | Aged | 0.22-0.27 [a] | 4-5 [b] | 532 |
| 2% $Pt_{Cl}$ | Freshly reduced | 0.90[c] | 1.2 [a] | 590 |
| 2% Pt | Freshly reduced | 0.89 [c] | 1.2 [a] | 558 |
| 10% Pt | Freshly reduced diluted with $Al_2O_3$ (2:1) | 0.25 [c] | 4.4 [a] | 519 |

[a] Assuming D = 1.1/d(nm) [4].

[b] TEM measurement.

[c] $H_2$ chemisorption.

This resulted in freshly reduced $Pt_{Cl}$ and Pt catalysts. Some $Pt_{Cl}$ samples were only treated in oxygen at 773 K for 1 h, resulting in an oxidized $Pt_{Cl}$ catalyst. An exposure of the reduced $Pt_{Cl}$ sample to 35 successive oxidation–reduction-reaction cycles resulted in the so-called aged $Pt_{Cl}$ catalyst. The average particle sizes of the prepared $Pt_{Cl}$ and Pt catalysts were determined by means of a transmission electron microscope (TEM) and by means of $H_2$ pulse chemisorption. The results are shown in **Table 4.1**.

### 4.2.2 *$CH_4$ adsorption and light-off experiments*

For each experiment 0.03 g of catalyst powder was placed into the ceramic cup of a commercial high-temperature high pressure diffuse reflectance cell (Spectra-Tech) with a ZnSe window. The ceramic cup, porous on the bottom, can be heated up to 1173 K and permits the flow of the gases through the sample. A chromel–alumel thermocouple was inserted into the powdered sample to measure the bed temperature. A controller was used to control the heating power and, therefore, the bed temperature. The cell, residing in a ThermoNicolet NEXUS 870 infrared spectrophotometer bench with a liquid nitrogen cooled MCT detector, was connected to a control panel, which allowed us to prepare gas mixtures at atmospheric pressure. A quadrupole mass spectrometer (Pfeiffer OMNISTAR) was connected online for continuous monitoring of the reactor effluent.

He (99.99%), $CH_4$ (99.99%), and $O_2$ (99.996%) flows to the DRIFT cell were controlled via mass flow controllers (Unit instrument) at a total flow rate in the range of 300~650 sccm (standard cubic centimeter per minute). For some experiment a $CH_4$ cylinder with a purity of

48

only 99% (CP grade) was used in order to flow a mixture of $CH_4$ and ppm of CO (contained as impurity, but not quantifiable with our analytical instruments).

The experiments were performed according to the following procedure. After the pretreatment of the solid, mixtures of $CH_4$/He or $CH_4$/$O_2$/He were introduced into the DRIFT cell at 323 K, and then the temperature was slowly increased (10 K/min) while IR spectra were periodically collected at a resolution of 4 cm$^{-1}$ with 20 co-added scans. For the light-off experiments using $CH_4$/$O_2$/He mixtures, the catalyst ignition temperature was measured when the thermocouple temperature increased rapidly beyond the controller set point. All data points were reproducible to within ±3 K.

Some experiments were also performed in a microreactor flow system. A higher catalyst load, 0.3 g, was used with this system in order to increase the signals of the gas phase products monitored by the mass spectrometer. The catalyst, supported by a glass wool plug, was placed in the quartz microreactor. A thermocouple was inserted in the center of the catalyst bed in order to monitor the temperature of the bed. The reactor was mounted centrally in a vertical furnace, the temperature of which was monitored using a chromel–alumel thermocouple situated on the wall at the mid point of the furnace. Flows were controlled using the same gas control panel as with the DRIFT cell. The same catalyst pretreatment procedures were also used as with the DRIFT cell.

### 4.2.3 *Calorimetric measurements*

The determination of the heat of adsorption of oxygen was performed using a Calvet-type microcalorimeter. The microcalorimetry unit, which consisted of an assembly of an aluminum

block with two integral thermoelectric enclosures, was constructed by International Thermal Instrument Company (Model # CR-100-1). A high temperature silicone oil (Acros Organics) was used to make a good thermal contact between the cell wall and the inner wall of the cavity of the microcalorimeter. The microcalorimeter unit was located in a well insulated forced-air oven to isolate the system from the environment. Roughly one gram of catalyst was placed in the sample cell to form a catalyst bed a few millimeters thick. Each catalyst was pretreated under vacuum by heating at a rate of 2 K/min to 773 K. The sample was then oxidized under a stagnant atmosphere of $O_2$ (UHP, Praxair) for 2 h, with periodic purge and refill cycles to replenish the environment with fresh $O_2$. The sample was subsequently evacuated for 0.5~1.0 h and then reduced under a stagnant atmosphere of $H_2$ (99.95%) for 4.5 h, with periodic purge and refill cycles to replenish the environment with fresh $H_2$. Following this procedure, the sample chamber was evacuated under dynamic vacuum at a temperature of 773 K for an additional 10 h, after which the sample was allowed to cool to room temperature and the gas-dosing manifold was charged with $O_2$ to a pressure ranging between 6.0 and 10.0 Torr. Manifold pressures were measured using a 615 Å high accuracy Baratron absolute pressure sensor (MKS Instruments). A LabView programmed Virtual Instrument (VI) was used to control the sequential dosing of $O_2$ to the sample and record the evolved heat and manifold pressures required for determining the total heat of adsorption and the amount adsorbed. The dry catalyst mass was used to determine the differential heats of adsorption as a function of $O_2$ uptake per gram of catalyst. Further details about the microcalorimetry technique can be found in a recent review by Cardona-Martinez and Dumesic [5].

## 4.3    Results and discussion

### 4.3.1  *Methane adsorption on platinum*

#### 4.3.1.1 *Aged 10% Pt$_{Cl}$ catalyst*

The interaction of methane with the reduced aged 10% Pt$_{Cl}$ catalyst in the absence of gas phase oxygen has been investigated in the 323~773 K range using a 50% CH$_4$/He mixture at a flow rate of 300 sccm. Two surface states of platinum have been considered: an oxygen-free surface and an oxygen-covered surface obtained by chemisorption of oxygen at room temperature.

The IR results obtained after admission of CH$_4$/He on the oxygen-free surface of the aged 10% Pt$_{Cl}$ catalyst are shown in **Figure 4.2**. A weak IR band at 2047 cm$^{-1}$ appears at 373 K. As the temperature is increased, this IR band, ascribed to the linear CO species adsorbed on the reduced surface of Pt [6], shifts to 2075 cm$^{-1}$ and increases to a maximum at 620 K while a broad weak IR band centered at 1800 cm$^{-1}$, assigned to multibound CO species [7], is progressively formed. The shift in the wavenumber of the linearly adsorbed CO can be attributed to a dipole–dipole interaction between the linear CO species on the surface as the amount of this species increases [8]. As no formation of carbon-containing reaction products has been observed by Mallens et al. [9] on reduced Pt sponge when interacting with CH$_4$, the involvement of oxygen from the support must be assumed to explain the initial formation of adsorbed CO. The carbonaceous adspecies originated by dissociative adsorption of methane may react with the hydroxyl groups of the support [10] for which the surface concentration may reach 19 OH nm$^{-2}$ [11] for a fully hydrated alumina. Increasing the temperature beyond 620 K causes the multibound CO species to disappear first at 670 K because of its low heat of adsorption [7], while the IR band of the

51

linear CO species decreases along with a shift to 1992 cm$^{-1}$ at 673 K before disappearing at 770 K. The formation of $H_2$ was also observed in the gas phase with the mass spectrometer from 733 K as shown in **Figure 4.3**. These results reveal that the dissociative adsorption of $CH_4$ on the oxygen-free surface of the aged 10% $Pt_{Cl}$ occurs from 373 K leading to carbon monoxide and hydrogen and is enhanced with the increase of temperature. Martins et al. [12] also observed the dissociative chemisorption of methane occurring above 373 K. As methane has a stable molecular structure, its activation requires a high reaction temperature even on noble metals. For instance, the overall energy of activation for the methane dissociation has been estimated at around 50 kJ/mol on Pt sponge [9].
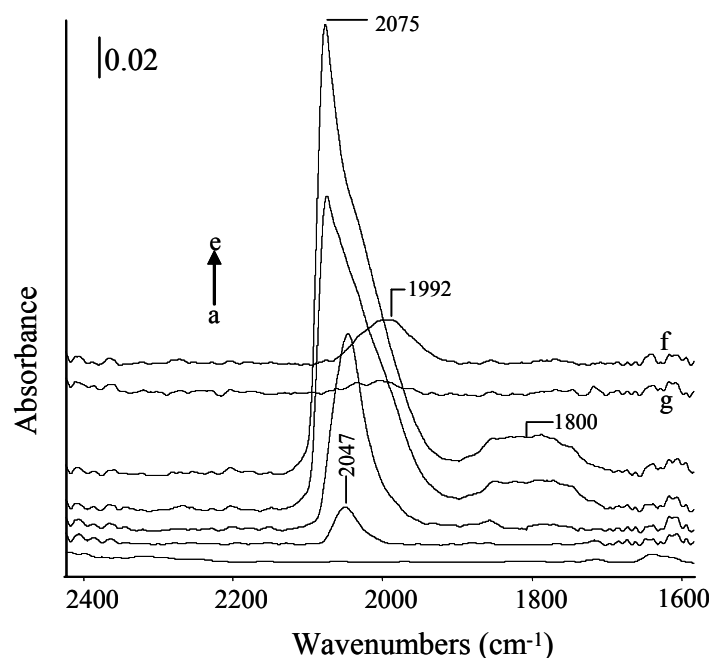


**Figure 4.2 Evolution with temperature of IR spectra of adsorbed species formed when interacting 50% $CH_4$/He with aged 10% $Pt_{Cl}$ catalyst with an oxygen-free surface: (a) 343K, (b) 373K, (c) 433K, (d) 533K, (e) 613K, (f) 673K, and (g) 773K.**

52
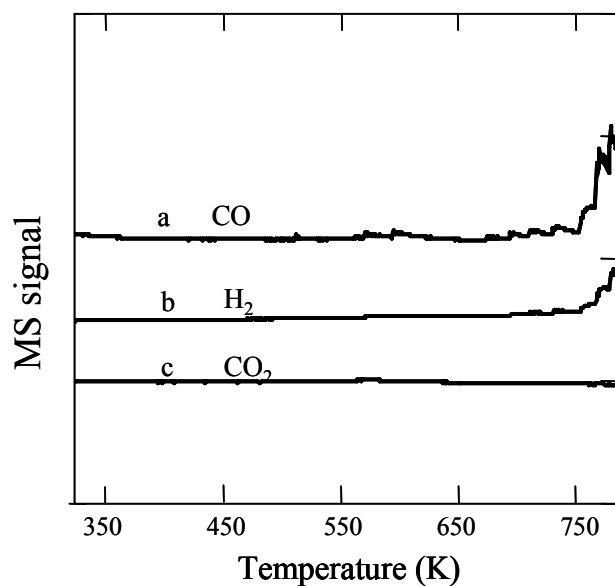
**Figure 4.3 MS spectra of outlet stream during CH₄/He interacting with aged 10% Pt_Cl catalyst with an oxygen-free surface: (a) CO, (b) H₂, and (c) CO₂.**

**Figure 4.4** shows the IR spectra of the adsorbed species when interacting CH$_4$/He with the oxygen-covered surface of the aged 10% Pt$_{Cl}$ in the 323 ~ 773 K range. A weak IR band appears at 2065 cm$^{-1}$ from 403 K. This IR band is assigned to the linearly adsorbed CO. The position of this IR band is higher than the one formed on the oxygen-free surface at the same temperature (2065 cm$^{-1}$ versus 2047 cm$^{-1}$ for the oxygen-free surface).
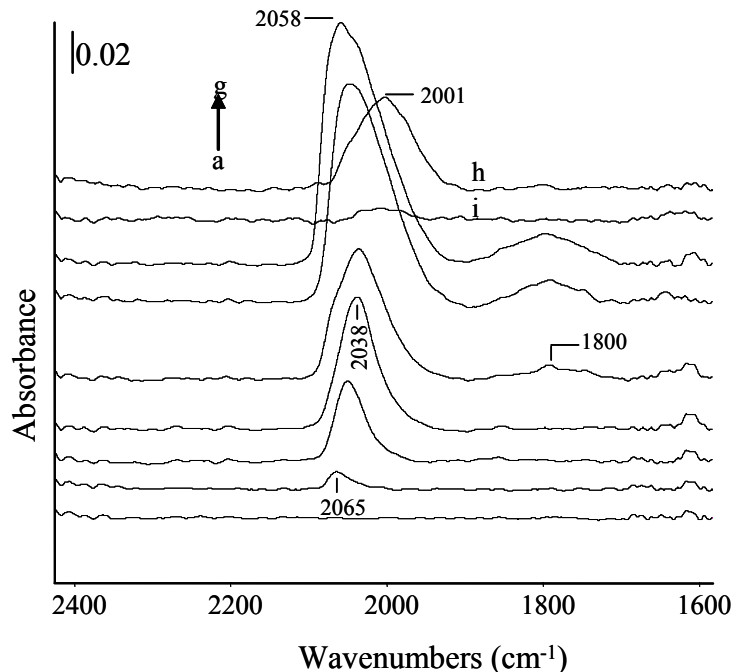
**Figure 4.4 Evolution with temperature of IR spectra of adsorbed species formed when interacting 50% CH₄/He with aged 10% Pt_Cl catalyst with an oxygen-covered surface: (a) 383K, (b)403K, (c) 443K, (d) 463K, (e) 503K, (f) 663K, and (g) 673K, (h) 733K, and (i) 773K.**

The position of the IR band of the linear CO species can characterize the surface state of the catalyst [13,14]. It can also characterize particle size [15]; however, in these experiments the same 10% $Pt_{Cl}$ catalyst was used so particle size effects on wavenumber are expected to be negligible. Levy et al. [14] observed a slight increase of the wavenumber of the linear CO species from 2075 cm$^{-1}$ for a freshly reduced $Pt/Al_2O_3$ sample at 298 K to 2085 cm$^{-1}$ for a sample with oxygen on the surface. The shift in wavenumber observed in our experiments, then, clearly indicates that the surface is initially covered by adsorbed oxygen. As the temperature is increased from 403 to 503 K, this IR band increases and shifts to lower wavenumbers: 2037 cm$^{-1}$ at 503 K, indicating that some of the adsorbed oxygen species are progressively removed from the surface

by reaction with the product of the decomposition of $CH_4$. From 503 to 673 K this IR band continues to increase and reaches a maximum along with a shift to high wavenumbers ($2058cm^{-1}$ at 673 K), while a broad weak IR band at 1800 $cm^{-1}$ assigned to multibound CO species is progressively formed. The shift in linearly adsorbed CO wavenumber is attributed to a dipole–dipole interaction between the linear CO species on the surface of Pt as the amount of this species increases [8]. Increasing the temperature beyond 673 K shows that the multibound CO species disappears at 723 K while the IR band of the linear CO species decreases along with a shift to 2001 $cm^{-1}$ at 733 K before disappearing at 773 K. The formation of hydrogen was observed in the gas phase from 723 K with the mass spectrometer while a small amount of $CO_2$ was detected from 523 to 643 K.

### 4.3.1.2 *Freshly reduced 10% Pt$_{Cl}$ catalyst*

The same experiments have been performed on the freshly reduced 10% Pt$_{Cl}$ catalyst considering the two surface states: the oxygen-free and the oxygen-covered surface obtained by chemisorption of oxygen at room temperature. Contacting the $CH_4$/He mixture with the oxygen-free surface led to the formation of the linear CO species at a similar temperature (373 K) to that on the oxygen-free surface of the aged catalyst with, however, a lower position of the IR band: 2040 $cm^{-1}$ compared to 2050 $cm^{-1}$. This red shift of the IR band is likely caused by the decrease of the particle size from ~5 nm for the aged catalyst to ~2 nm for the freshly reduced catalyst. Fanson et al. [15] observed, for instance, a red shift of the IR band of the linear CO species adsorbed on a Pt/SiO$_2$ from 2076 to 2058 $cm^{-1}$ as the dispersion was increased from 0.6 to 0.99. Similar trends to that with the oxygen-free surface of the reduced aged catalyst have been observed concerning the evolution of the adsorbed CO species with the increase of the temperature.

The interaction of the $CH_4$/He mixture with the oxygen covered surface of the freshly reduced 10% $Pt_{Cl}$ led also to the formation of the linear CO species but at a higher temperature (423 K) than that obtained with the same surface state of the aged catalyst. The same trend as on the aged catalyst has been observed for the adsorbed CO species, especially the increase of the IR band of the linear CO species along with a shift to lower wavenumbers: from 2050 $cm^{-1}$ at 423 K to 2042 $cm^{-1}$ at 463 K, indicating that the surface is initially covered by oxygen which is progressively removed by reaction with the product of the dissociation of methane. Apparently the presence of adsorbed oxygen on the Pt surface is delaying the dissociative adsorption of methane, evidenced by the formation of the linearly adsorbed CO species, to a higher temperature. The delay is larger for the freshly reduced catalyst than for the aged catalyst. Under these reaction conditions, i.e. with no gas phase oxygen in the mixture, carbon monoxide is the main carbonaceous product initially obtained.

### 4.3.2 *Interaction of $CH_4$ / $O_2$ / He with platinum*

**Figure 4.5** shows the IR spectra during the interaction of $CH_4$ with the aged 10% $Pt_{Cl}$ catalyst in the presence of gas phase oxygen using a 40% $CH_4$ / 20% $O_2$ / He mixture in the 323~520 K range. These temperatures are below the surface ignition temperature, as will be seen later. The aged 10% $Pt_{Cl}$ catalyst has been used in order to perform several experiments with the same catalyst without having to worry about catalyst stability. At 483 K an IR band appears at 1594 $cm^{-1}$ ascribed to adsorbed carbonate species on the alumina support [16]. It is thought that adspecies originated by dissociative adsorption of methane react with adsorbed oxygen species to form $CO_2$ which then interacts with the support to form carbonates. The intensity of the IR band of the carbonate species increased with the rise of the temperature. While carbon dioxide was

56

detected in the gas phase from 503 K and increased with the temperature, neither carbon monoxide nor hydrogen was observed with the mass spectrometer for the range of temperatures considered. A blank experiment performed using the $\gamma$-$Al_2O_3$ support alone did not reveal the formation of carbonaceous species, indicating that the support is not active under these conditions. Thus, in the presence of gas phase oxygen, the dissociative adsorption of methane on the platinum surface is delayed to higher temperature and leads to the formation of carbon dioxide below the ignition temperature.
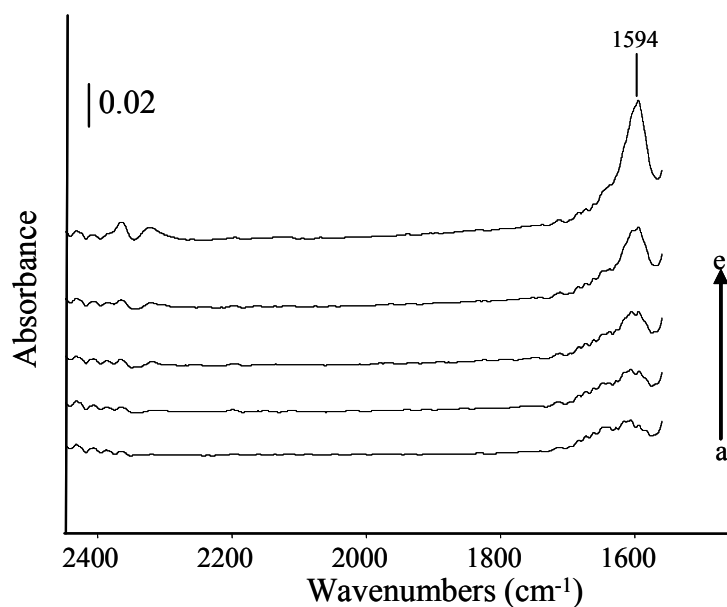


**Figure 4.5 Evolution of IR spectra with temperature during reaction on aged 10% Pt$_{Cl}$ catalyst using 40% CH$_4$/ 20% O$_2$ / He mixture: (a) 453K, (b) 473K, (c) 493K, (d) 513K, (e) 533K.**

Similar experiments have been performed in the 323~520 K range on the same aged 10% Pt$_{Cl}$ catalyst using different mixture compositions where the partial pressure of oxygen was varied. The trend of the evolution of the carbonaceous species was the same as observed above;

57

however, the temperature at which adsorbed carbonate species appeared on the support was found to depend on the partial pressure of oxygen. The lower the partial pressure of oxygen, the lower the temperature at which carbonate appeared. Carbonate appeared at 453 and 413 K for 40% $CH_4$ / 11.4% $O_2$ / He and 40% $CH_4$ / 5% $O_2$ / He, respectively.

A 40%$CH_4$ / 20%$O_2$ / He mixture containing a few ppm of carbon monoxide (which results from the use of $CH_4$ cylinder with a purity of 99%) was used to perform similar experiment from 323 K to below the ignition temperature (see below). The IR spectra obtained in the 1700~2300 $cm^{-1}$ range when contacting this mixture with the freshly reduced 10% $Pt_{Cl}$ catalyst are depicted in **Figure 4.6**. It can be seen at 323 K an IR band of the linear CO species at 2078 $cm^{-1}$ compared to the one obtained at 2065 $cm^{-1}$ with the mixture containing no oxygen (**Figure 4.6f**), indicating the presence of adsorbed oxygen on the surface [13,14,17]. Increasing the temperature led to a progressive decrease of the IR band at 2078 $cm^{-1}$ before its disappearance at 500 K and the appearance  of an IR band at 2108 $cm^{-1}$ from 343 K due to the linear CO species adsorbed on $Pt^{2+}$ sites [18].
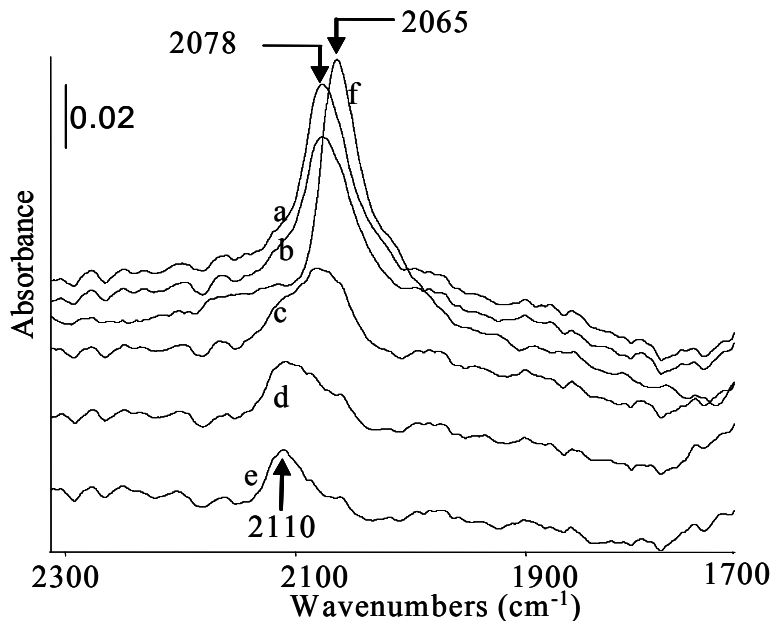
**Figure 4.6 Evolution of IR spectra with temperature when interacting (a)-(e) CH₄/O₂/ppmCO/He and (f) ) CH₄/ppmCO/He with the freshly reduced 10% Pt$_{Cl}$ catalyst: (a) 323K, (b)343K, (c) 378K, (d) 418K, (e) 498K, and (f) 323K.**

These results, combined with the ones of the preceding section, suggest that in the presence of gas phase oxygen, the surface of the catalyst is mainly covered by oxygen until the ignition temperature, which delays the adsorption of $CH_4$. A competitive adsorption between these species is then assumed, in agreement with the suggestion of Veser and Schmidt [19]. As the mixture becomes more oxygen rich, the partial pressure of $O_2$ above the surface increases and so does its rate of adsorption. Therefore, it is more difficult for $CH_4$ to find adsorption sites on the platinum surface, resulting in an increase in the temperature at which carbonate appears. This behavior can be simply illustrated considering the evolution of the coverage of methane $\theta_{CH4}$ and oxygen $\theta_O$ on the platinum surface assuming competitive adsorption of oxygen and methane. Assuming that oxygen adsorbs dissociatively while methane adsorbs nondissociatively, the following formulas result:

59

$$\theta_{CH_4} = \frac{K_{CH_4} P_{CH_4}}{1 + K_{CH_4} P_{CH_4} + (K_{O_2} P_{O_2})^{1/2}}$$
<div align="right">**Equation 4.1**</div>

$$\theta_{O} = \frac{(K_{O_2} P_{O_2})^{1/2}}{1 + K_{CH_4} P_{CH_4} + (K_{O_2} P_{O_2})^{1/2}}$$
<div align="right">**Equation 4.2**</div>

where $K_{CH4}$ and $K_{O2}$ are the adsorption constants of methane and oxygen, respectively. The dissociative adsorption of oxygen is in agreement with experimental investigations while the assumption of the nondissociative adsorption of methane is a gross simplification. Surface reactions between the adsorbed species are neglected; the coverage of both methane and oxygen are simply determined by the adsorption–desorption equilibrium.

**Figure 4.7** shows the evolution of $\theta_{CH4}$ and $\theta_O$ with the adsorption temperature for different $CH_4$ and $O_2$ partial pressures considering constant heats of adsorption of 18 kJ/mol [20] and 155 kJ/mol (for a high coverage) [21] for methane and oxygen, respectively. The heat of adsorption for $O_2$ was obtained from the literature, rather than from our data, so that a more precise value at complete oxygen coverage could be used. It can be observed that the coverage of oxygen is very high, even for low partial pressures of oxygen, while the coverage of methane is very low. Methane coverage rises exponentially as the temperature increases, but this rise is delayed to higher temperature for higher oxygen partial pressure. There likely is a threshold surface concentration of carbonaceous species that allows the production of enough carbonate species to be detected by our IR experiments. Use of higher partial pressures of oxygen delays the formation of this threshold concentration to higher temperatures, leading to the observation that carbonate species were not detected until higher temperatures for higher $O_2$ partial pressure.
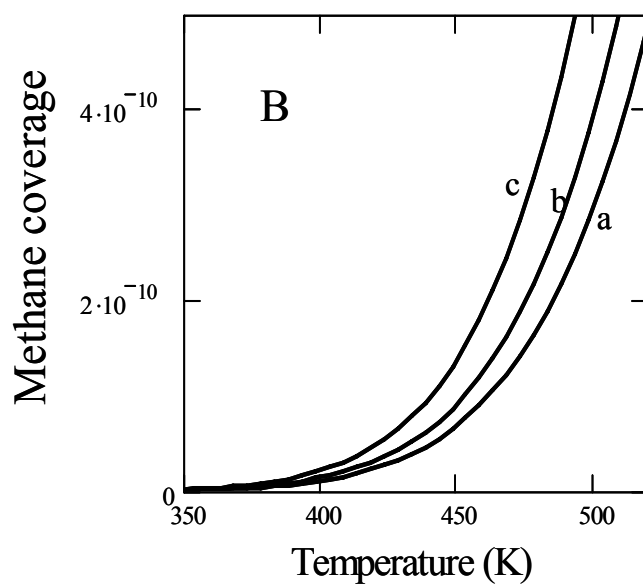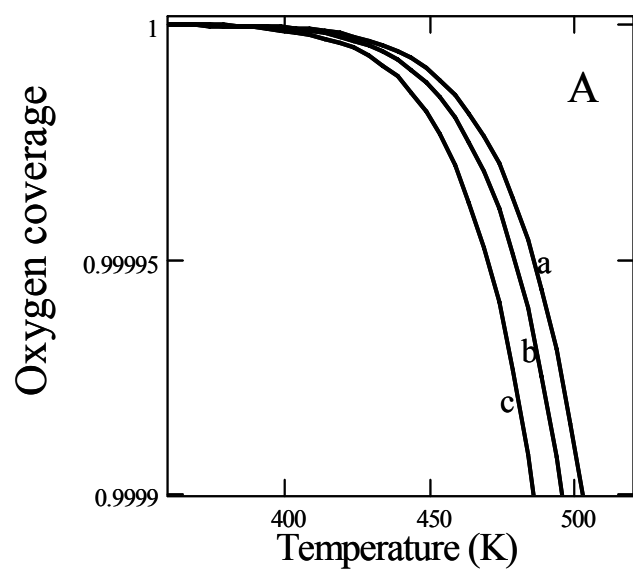
**Figure 4.7 Theoretical coverage of CH$_4$ (A) and oxygen (B) on a Pt surface at several temperatures considering competitive adsorption in the absence of surface reaction with (a)P$_{CH4}$ = 40 × 10$^3$ Pa and P$_{O2}$ = 20 × 10$^3$ Pa, (b) 11.4 × 10$^3$ Pa, and (c) 5 × 10$^3$ Pa.**

### 4.3.3 *Surface ignition temperature*

The temperature of the surface ignition was measured for the aged 10% $Pt_{Cl}$ catalyst with different gas compositions. A 40% $CH_4$/x% $O_2$/He mixture, for which x was varied in order to obtain the $CH_4/O_2$ ratios of 2–8, was continuously fed at room temperature and atmospheric pressure into the DRIFT cell at a flow rate of 650 sccm. The catalyst was heated by increasing the temperature (10 K/min) of the ceramic cup. The surface ignition temperature was then determined by a sudden rapid increase in the temperature. The results are reported in **Figure 4.8**. It can be seen that the ignition temperature decreases with increasing the $CH_4/O_2$ ratio, as observed in the literature. For instance, Behrendt et al. [22] reported a decrease about 120 K of the surface ignition temperature of Pt foils at atmospheric pressure as the $CH_4/O_2$ ratio was increased from 2 to 9. The decrease in ignition temperature with decreasing oxygen content of the reaction mixture is in agreement with the observations mentioned above about the temperature at which the carbonate species appeared. That is, a competition between methane and oxygen for surface site is involved in the ignition process. Veser and Schmidt [19] proposed a simple model based on a Langmuir–Hinshelwood mechanism with competitive adsorption of the reactant gases to predict the catalytic ignition temperature of the oxidation of alkanes. The model showed that oxygen desorption was the main factor affecting the surface ignition. In their numerical study of the transient behavior of the partial oxidation of methane, Schwiedernoch et al. [3] also considered that the adsorption–desorption equilibrium for oxygen was slowly shifting towards desorption with the increase of temperature, leading to more and more vacancies on the surface.
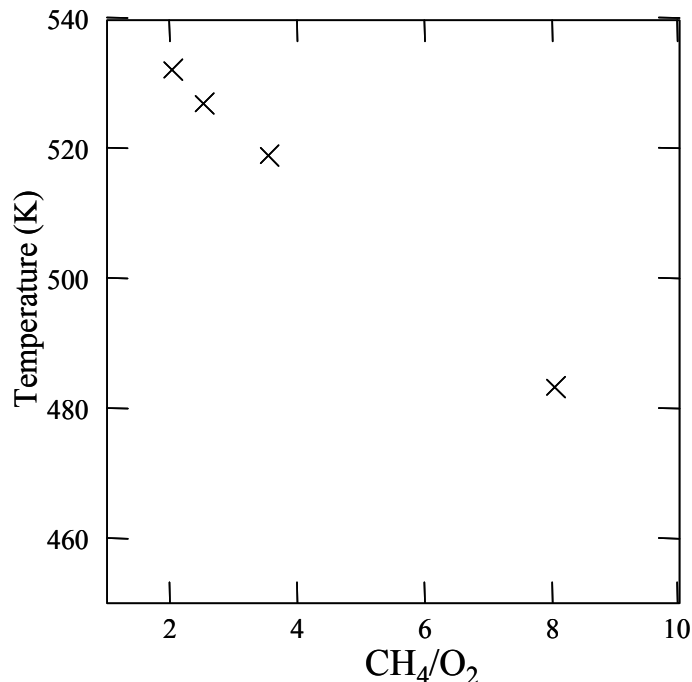
**Figure 4.8 Surface ignition temperatures as a function of the CH$_4$/O$_2$ ratio with the aged 10% Pt$_{Cl}$ catalyst.**

### 4.3.4 *Effect of catalyst state and salt precursor on surface ignition*

**Table 4.1** reports the surface ignition temperatures measured in the light-off experiments performed with a 40%CH$_4$ / 20%O$_2$ / He mixture at a flow rate of 650 sccm over the reduced, oxidized and aged 10% Pt$_{Cl}$ catalysts. The surface ignition temperature is found to change with the catalyst state following the order oxidized (D$_{Pt}$ = 1.9~2.2 nm) > reduced (D$_{Pt}$ = 1.7~1.9 nm) > aged (D$_{Pt}$ = 4~5 nm). Qin et al. [23] observed a similar order with an Rh/MgO catalyst; the ignition temperature of the reduced catalyst was found to be 70 K lower than the unreduced catalyst for which rhodium oxide covers the surface. The presence of chlorinated species on catalysts surface has been invoked in several studies to account for changes in activities of catalysts prepared using chloride salts compared to chloride-free catalysts. For instance, Volter et al. [24] observed that added chloride mainly deactivates Pt samples in the catalytic combustion

of n-heptane. Paulis et al. [25] showed the inhibitory effect of chlorine, assigned to the formation of oxychlorided platinum species, on the catalytic activity of $Pt/Al_2O_3$ catalyst for complete oxidation of toluene. The aged 10% $Pt_{Cl}$ catalyst has been obtained after exposure to a number of successive oxidation–reduction-reaction cycles. It is possible that the slow removal of chlorinated species after such treatments is responsible for the lower ignition temperature obtained with the aged catalyst compared to that with the freshly reduced and oxidized 10% $Pt_{Cl}$ catalysts. For this reason, the chloride effect was investigated by performing light-off experiments using catalyst samples prepared from a nitrate precursor. The ignition temperature observed with 2% $Pt_{Cl}$ and 2% Pt samples, which have almost the same dispersion, are shown in **Table 4.1**. As seen in this table, there is indeed a chloride effect since the ignition temperature is ~30 K lower with the chloride-free sample. However, comparing the results observed with 2% Pt and 10% Pt (diluted in alumina in order to have nearly the same number of accessible Pt surface sites as 2% Pt), with particle sizes of ~1.5 and ~4.5 nm, respectively, shows that the ignition temperature is ~40 K lower with the bigger particle size. Therefore, the influence of chloride alone does not explain why the aged $Pt_{Cl}$ catalyst has a lower ignition temperature than the freshly reduced $Pt_{Cl}$ catalyst; particle size also plays a role.

### 4.3.5 *Oxygen-metal bond strength*

The surface ignition results obtained with our platinum catalysts can be explained by considering the Pt–oxygen bond strength, that is, the heat of adsorption of $O_2$. Differential heats of adsorption as a function of oxygen coverage of freshly reduced and aged 10% $Pt_{Cl}$ catalysts are shown in **Figure 4.9**. The oxygen coverage was based on the saturation coverage of oxygen over the catalyst, as measured by the maximum oxygen uptake observed during the microcalorimetry experiment. It can be observed that the heats of adsorption are lower for the aged 10% $Pt_{Cl}$,

64

indicating that oxygen is less strongly adsorbed on the catalyst with bigger particle size. Briot et al. [26] have also found by calorimetric measurement that the heat of adsorption of oxygen on their aged $Pt/Al_2O_3$ catalyst with a particle size of 12 nm was lower than that on the fresh catalyst with an average particle diameter of 2 nm. Wang and Yeh [27] observed a decrease of the heat of adsorption of oxygen about 100 kJ/mol as the particle size of the $Pt/Al_2O_3$ catalyst was increased from 1 to 2.2 nm. Drozdov et al. [28] have found that oxygen is bound more weakly on platinum metal than on the bulk oxide. The order of the surface ignition temperature obtained with our different 10% $Pt_{Cl}$ catalyst states follows the oxygen heat of adsorption trend. This can also explain why a higher temperature was observed for the appearance of the linearly adsorbed CO species on the freshly reduced catalyst than on the aged catalyst when interacting $CH_4$/He with the oxygen-covered surface. Since the heat of adsorption of $O_2$ is higher on the freshly reduced catalyst than on the aged catalyst, $CH_4$ will find fewer available sites at the same temperature. From these results it can be asserted that the heat of adsorption of oxygen on the platinum surface is a key factor during ignition of the surface reaction.
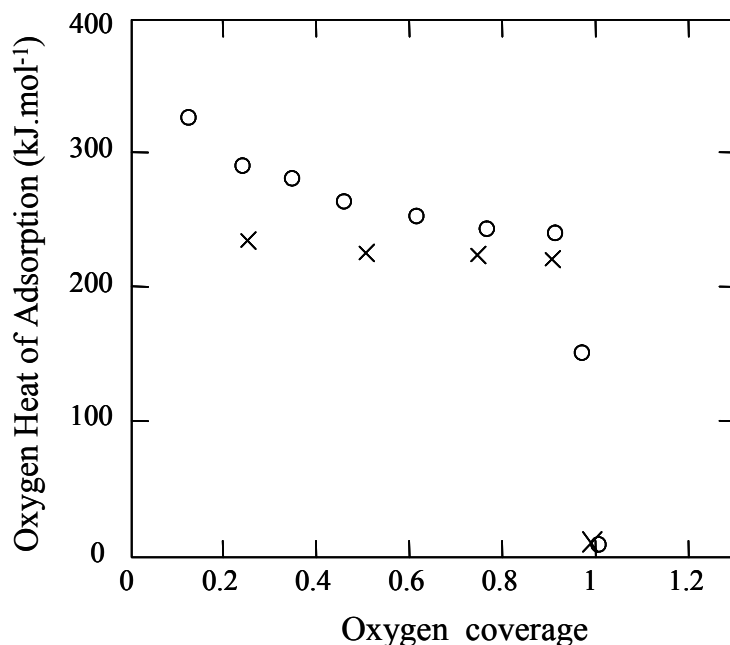
**Figure 4.9: Differential heat of adsorption of oxygen as a function of oxygen coverage at 300K for the (O) freshly reduced and (×) aged 10% Pt$_{Cl}$**

## 4.4    Conclusions

The ignition of the catalytic partial oxidation of methane on 10% Pt/Al$_2$O$_3$ catalysts has been investigated using in situ DRIFT spectroscopy. It has been shown that the ignition temperature decreased with decreasing amounts of oxygen in the CH$_4$/O$_2$/He reactant mixture. Carbonate species adsorbed on the support were observed before the ignition temperature. The temperature at which the carbonate species appeared was lower for lower concentration of oxygen in the mixture. Competition between methane and oxygen is suggested, with adsorbed oxygen mainly covering the surface until the ignition temperature and preventing the dissociative adsorption of methane. This is clearly shown when interacting a CH$_4$/He mixture on an oxygen-free and oxygen-covered surface: the dissociative adsorption of methane, indicated by the appearance of the linearly adsorbed CO species, is delayed to higher temperatures on the latter surface.

Moreover, the interaction of the $CH_4/O_2/ppm$ CO/He mixture led to the formation of the linearly adsorbed CO species at 2078 $cm^{-1}$ compared to 2065 $cm^{-1}$ with the $CH_4$/ppm CO/He mixture containing no oxygen, suggesting that the surface was covered with oxygen prior to catalytic ignition. The heat of adsorption of oxygen was found to be a key factor during the ignition of the surface reaction. This has been confirmed by correlating the order obtained for the ignition temperature on the different catalyst states: oxidized ($D_{Pt}$ = 1.9~2.2 nm) > freshly reduced ($D_{Pt}$ = 1.7~1.9 nm) > aged ($D_{Pt}$ = 4~5 nm) with the measured differential heats of oxygen adsorption and the literature data where it is reported that the oxygen-metal bond strength is lower for bigger particles of Pt and higher for bulk Pt oxide.

## 4.5    References

1 C.A. Leclerc, J.M. Redenius, L.D. Schmidt, Catal. Lett. 79 (2002) 39.

2 A.K. Avci, D.L. Trimm, A.E. Aksoylu, Z.I. Onsan, Catal. Lett. 88 (2003)17.

3 R. Schwiedernoch, S. Tischer, C. Correa, O. Deutschmann, Chem. Eng. Sci. 58 (2003) 633.

4 M. Boudart, G. Djega-Mariadassou, The Kinetics of Heterogeneous Catalytic Reactions, Princeton University Press, Princeton, NJ, 1984.

5 N. Cardona-Martinez, J.A. Dumesic, Adv. Catal. 38 (1992) 149.

6 O. Dulaurent, D. Bianchi, Appl. Catal. A: Gen. 196 (2000) 271.

7 A. Bourane, O. Dulaurent, D. Bianchi, J. Catal. 196 (2000) 115.

8 F. Stoop, F.J.C.M. Toolenaar, V. Ponec, J. Catal. 73 (1982) 50.

9 E.P.J. Mallens, J.H.B.J. Hoebink, G.B. Marin, J. Catal. 167 (1997) 43.

10 P. Ferreira-Aparicio, I. Rodriguez-Ramos, A. Guerrero-Ruiz, Appl. Catal. A: Gen. 148 (1997) 343.

11 J. Haber, A. Kozlowska, R. Kozlowski, J. Catal. 102 (1986) 52.

12 R.L. Martins, M.A. Baldanza, M.M.V.M. Souza, M. Schmal, in: X. Bao, Y. Xu (Eds.), Studies in Surf. Sci.and Catal. 147 (2004) 643.

13 J. Sarkany, M. Bartok, R.D. Gonzalez, J. Catal. 81 (1983) 347.

14 P.J. Levy, V. Pitchon, V. Perrichon, M. Primet, M. Chevrier, C. Gauthier, J. Catal. 178 (1998) 363.

15 P.T. Fanson, W.N. Delgass, J. Lauterbach, J. Catal. 204 (2001) 35.

16 L.H. Little, *Infrared Spectra of Adsorbed Species*, Academic Press, London, New York, 1966.

17 A. Bourane, D. Bianchi, J. Catal. 202 (2001) 34.

18 Y. Barshad, X. Zhou, E. Gulari, J. Catal. 94 (1985) 128.

19 G. Veser, L.D. Schmidt, AICHE J. 42 (1996) 1077.

20 G. Veser, J. Frauhammer, Chem. Eng. Sci. 55 (2000) 2271.

21 T. Matsushima, Surf. Sci. 157 (1985) 297.

22 F. Behrendt, O. Deutschmann, R. Schmidt, J. Warnatz, in: Proceedings of the 211th National Meeting, Symposium on Heterogeneous Hydrocarbon Oxidation, Division of Petroleum Chemistry Inc., ACA New Orleans, LA, March 24–29, 1996.

23 D. Qin, J. Lapszewicz, X. Jiang, J. Catal. 159 (1996) 140.

24 J. Volter, G. Lietz, H. Spindler, H. Lieske, J. Catal. 104 (1987) 375.

25 M. Paulis, H. Peyrard, M. Montes, J. Catal. 199 (2001) 30.

26 P. Briot, A. Auroux, D. Jones, M. Primet, Appl. Catal. 59 (1990)141.

27 C. B. Wang, C.T. Yeh, J. Catal. 178 (1998) 450.

28 V.A. Drozdov, P.G. Tsyrulnikov, V.V. Popovskii, N.N. Bulgakov, E.M. Moroz, T.G. Galeev, React. Kinet. Catal. Lett. 27 (1985) 425.

# Chapter 5  In situ IR investigation of activation and catalytic ignition of methane over Rh/Al$_2$O$_3$ catalysts

## 5.1    Introduction

Methane conversion into higher hydrocarbons has become extremely attractive in recent years because of abundant natural gas resources and steadily depleting oil reserves. Methane steam reforming is a traditional way to utilize natural gas resources through syngas. However, this method has several drawbacks. It is energy intensive and produces an unsuitable hydrogen to CO ratio for many subsequent products. Thus, catalytic partial oxidation (CPO) of CH$_4$ has attracted interest as a potential replacement for steam reforming. The interest in this reaction is that the products with a more preferable H$_2$ to CO molar ratio of 2:1 can be used directly as a feedstock for methanol or higher hydrocarbons production. In addition, because of its exothermicity, CPO can run autothermally once ignited.

While the potential of CPO for syngas generation is considerable, the reaction mechanism is not yet well understood. For example, some experimental work shows that CPO proceeds directly from the reaction of CH$_4$ and O$_2$ to yield CO and H$_2$ [1]. However, it has been shown by other authors [2, 3, 4, 5] that, over a variety of catalysts, an indirect route is followed. First, all the oxygen is consumed for the complete combustion of part of the methane; the residual methane subsequently is reformed by steam and CO$_2$. A study of the ignition process is helpful for understanding the reaction mechanism. Moreover, a detailed knowledge of ignition is of prime importance due to both economic and safety concerns [6].

70

Catalytic ignition has been studied previously in different regimes over various catalysts. Schmidt et al. [7] studied different hydrocarbon-air mixtures over several noble metal foils and found that the total gas flow rate did not influence the results within experimental error. Pt was the most studied metal due to the fact that it constitutes the most investigated and best understood oxidation catalyst. It also exhibits the simplest behavior. Schmidt et al. [7] proposed that the Pt surface was covered mainly by oxygen up to ignition; then oxygen desorption was the decisive step for catalytic ignition by creating free sites for methane adsorption. As described in chapter 4, the ignition temperatures on different states of $Pt/Al_2O_3$ were measured. The whole process was conducted in a DRIFTS cell reactor and monitored by both an IR and a mass spectrometer. The ignition temperature was higher with increasing $O_2$ in the reactant mixture. By measuring the heat adsorption of $O_2$ on different state of $Pt/Al_2O_3$, it was demonstrated that the competition between $CH_4$ and $O_2$ for surface sites controlled the ignition process. The desorption of $O_2$ from the Pt metal created the sites for methane adsorption and activation [8].

The ignition mechanism may differ from one catalyst to another and even vary from foil to supported catalyst. For example, Rh and Ir foils only show surface ignition in a fuel-rich atmosphere and deactivate rapidly under fuel-lean conditions. Pt and Pd show surface ignition over a very wide range of equivalence ratios from very fuel-lean to extremely fuel-rich mixtures [7]. Thus, it is necessary to have a thorough study on individual catalysts. Supported Rh on alumina is the main focus of this work since Rh catalysts have been found to be the most selective and stable for methane partial oxidation [9]. The present study focuses on the surface intermediates, the surface states, and the ignition process of methane partial oxidation on

supported rhodium as the temperature is raised to the ignition temperature. Interaction of several catalysts and catalyst states with $CH_4/He$ and $CH_4/O_2/He$ were also examined with in situ DRIFTS coupled with mass spectrometry.

## 5.2    Experimental

### 5.2.1  *Catalyst preparation*

$Rh/Al_2O_3$ powder catalysts were prepared by impregnating the $\gamma$-$Al_2O_3$ powder ($S_{BET}$ = 121 $m^2/g$, Alfa Aesa) with aqueous solutions of $Rh(NH_3)_4(NO_3)_2 \cdot 2H_2O$ (Alfa Aesa). After drying for 12 h at room temperature and then for 24 h at 383 K, the solids were calcined for 10 h in flowing $O_2/Ar$ at 773 K. For this research, a metal loading of 2% by weight was used.

Four different catalysts were studied: fresh, aged, sintered, and oxidized. The fresh catalyst is defined as the calcined catalyst that had never been used. The aged catalyst was obtained by letting the fresh catalyst undergo 35 cycles of temperature increase and decrease under $CH_4/O_2/He$ and $CH_4/He$ mixtures. The sintered catalyst was obtained after exposure of the fresh catalyst to He at 1073 K for 10 h.  Some fresh catalyst was treated only in flowing $O_2$ at 773 K for 1hr followed by a brief He evacuation, resulting in an oxidized catalyst. Before each experiment, fresh, aged and sintered catalysts experienced in situ pretreatment under various gases to generate two states: reduced and $O_2$-covered reduced.  To obtain a reduced state, the temperature of the catalyst was increased to 773 K at a speed of 10 K/min under flowing He. Then the catalyst was oxidized with flowing $O_2$ for 60 min, followed by He purge for 5 min. After that, the catalyst was reduced with $H_2$ at 773 K for 60 min followed by He evacuation. Low temperature $O_2$ coverage was realized by flowing $O_2$ at 323 K for 30 min over the corresponding

reduced catalyst, resulting in the state designated $O_2$-covered reduced. Four catalysts and their different states are listed in **Table 5.1**.

### 5.2.2 *Catalyst characterization*

Catalyst metal dispersions were determined by pulse $H_2$ chemisorption, assuming an adsorption stoichiometry of one hydrogen atom per surface metal atom [10]. The $H_2$ chemisorption experiment was performed on an AMI 200 equipped with a TCD detector. About 150 g of catalyst, supported by a glass wool plug, was placed in the quartz U tube reactor. $H_2$ pulse adsorptions were carried out at room temperature on the oxidized catalyst and the reduced states of the fresh, aged, and sintered catalysts. The degree of Rh dispersion was calculated from the amount of $H_2$ adsorbed.

Metal particle sizes of these catalysts were measured using TEM (JEOJEM 2010F). Samples were ultrasonically dispersed in acetone and spread over perforated copper micro grids. The photo images of catalysts were taken and the catalyst particle sizes were estimated from the average of approximately 600 particles.

### 5.2.3 *In situ infrared spectroscopic studies*

Infrared diffuse reflectance (DRIFTS) spectra were recorded on a Nicolet NEXUS 870 infrared spectrometer using an in-situ DRIFTS cell attached to a gas supply system, which prepared gas mixtures at atmospheric pressure for transient response and catalytic studies. For each experiment, 0.03 g of catalyst powder were placed into the ceramic cup of a modified commercial high-temperature high-pressure DRIFTS cell (Spectra-Tech: Model No. 0031-901) with a ZnSe window. The cell was modified by drilling a hole at the bottom of the ceramic cup.

A more porous thin ceramic frit was used to cover the hole and support the catalysts, which lowered the pressure drop. The catalysts can be heated to 1173 K. A chromel-alumel thermocouple (type K) was inserted into the powdered sample to measure the bed temperature. The FTIR spectrometer with a liquid nitrogen cooled MCT detector allows surface adsorbates to be monitored at any reaction condition. Gases flowing to the DRIFTS cell were controlled via mass flow controllers. The time required for reaching a new steady-state in the DRIFTS cell after changing the feed was about 10s.

A quadrupole mass spectrometer (Pfeiffer OMNISTAR) was connected on-line for continuous monitoring of the reactor effluent. Gases used in the study were He (99.99%), $CH_4$ (99.99%), $O_2$ (99.996%) and CO (99.3%). He was passed through a molecular sieve column to remove trace quantities of water.

The methane adsorption experiments were performed in the DRIFTS cell. A mixture of 50 vol % $CH_4$ in helium at a total flow rate of 520 cc/min was introduced to the DRIFTS cell at 323 K after pretreatment of the catalyst. The catalyst temperature was slowly increased while IR spectra were collected every 10 K at a resolution of 4 $cm^{-1}$ with 20 co-added scans.

Reaction ignition experiments were performed in the same DRIFTS cell at a total gas flow rate between of 300 and 650 cc/min. $CH_4/O_2/He$ were introduced into the DRIFTS cell at 323 K, and then the catalyst temperature was slowly increased (10 K/min) while IR spectra were collected at selected time intervals. The catalytic ignition temperature was defined as the temperature beyond

which the thermocouple temperature increased rapidly beyond the controller set point. All data points were reproducible to within ± 3 K.

The oxidation states of rhodium during reaction were characterized by IR peak position using CO as a probe molecule. The temperature of the catalyst was increased slowly under the reaction mixture to a desired temperature, which was lower than the ignition temperature. The reaction mixture flowed in the system for 3min, and then the cell was purged with He for 3 min. After evacuation, the catalyst was cooled to 373 K quickly. At this temperature, 30 ppm CO in helium was pulsed into reactor through a six-way valve, and the spectra were recorded immediately with five co-added scans. The cooling time was short (close to 2 min), and the change of the catalyst state during this process is assumed to be negligible.

### 5.2.4 *TPSR (temperature programmed surface reaction)*

For each experiment, 0.4 g of catalysts was placed on a quartz wool plug in the U-tube reactor. A thermocouple was inserted in the center of the catalyst bed in order to monitor the temperature of the bed. The reactor was mounted centrally in a vertical furnace, the temperature of which was monitored using a chromel-alumel thermocouple situated on the wall at the midpoint of the furnace. Use of this reactor increased the signal of the mass spectrometer because of the larger amount of catalyst employed. Before each experiment, the catalysts were treated to give the desired states. After the catalyst was cooled to 323 K under He, the reactor was fed a mixture of 50 vol % $CH_4$ in helium with a total flow rate of 520 cc/min. Temperature programmed surface reactions were carried out at temperatures from 323 K to 773 K at a heating rate of 7 K/min. Gas phase products were analyzed by the mass spectrometer.

## 5.3  Results

### 5.3.1  *Characterization*

The characterization results from $H_2$ chemisorption and TEM measurements are listed in **Table 5.1**. The four catalysts showed different dispersions; i.e., different number of accessible sites. The order of metal dispersion is: oxidized catalyst (27%) < sintered catalyst (28%) < fresh catalyst (37%) < aged catalyst (74%). These results are quite surprising, especially with the aged catalyst having the highest dispersion. One might expect the dispersion to decrease due to sintering (as in the case of platinum). Rh particle sizes of aged, fresh, and sintered catalyst are 1.8 nm, 2.9 nm, and 4.2 nm, respectively, increasing with decreasing dispersion. The metal particle size of the oxidized catalyst was only 0.8 nm, from which a higher dispersion is expected. The low dispersion of the oxidized catalyst is likely due to the incorporation of some metal atoms into the support structure to form a phase that is not easy to reduce at room temperature [11]. The characterization results implied that treatment was very important for $Rh/Al_2O_3$.

### 5.3.2  *Ignition process and temperatures*

Ignition temperatures were measured at a $CH_4$ to $O_2$ ratio of two (40%$CH_4$/20%$O_2$/He) under a total gas flow rate of 650 cc/min on the reduced fresh catalyst in the DRIFTS cell. IR spectra during the interaction of reactant mixture with the catalyst are shown in **Figure 5.1**. From spectra a through e, carbonate progressively formed on the alumina support from 463 K, evidenced by the increasing peak intensity at 1596 cm$^{-1}$ [12]. Spectrum f was collected after ignition and shows a big peak of $CO_2$ gas at 2346 cm$^{-1}$ and adsorbed CO at 2000 cm$^{-1}$. In addition to carbonate formation, a very small amount of $CO_2$ desorbed for temperatures above 463 K,

suggesting that $CH_4$ dissociated before reaction ignition. Adspecies from this process reacted with oxygen to form carbonate and $CO_2$. Mass spectroscopy results also reveal that $H_2$, CO, $CO_2$ and $H_2O$ were the main products after reaction ignition at the stabilized temperature of 773 K under autothermal conditions. Selectivity for CO and $H_2$ is higher than that of $CO_2$ and $H_2O$.
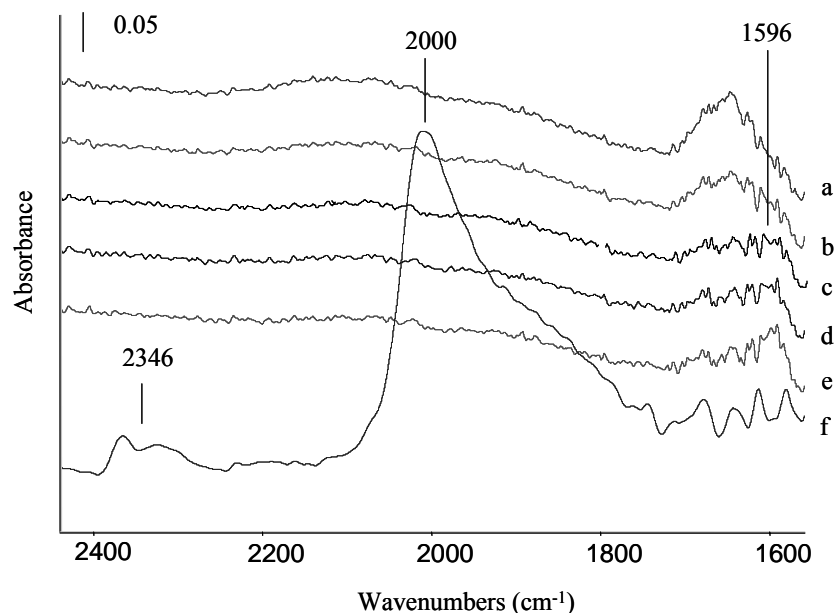


**Figure 5.1: Evolution of the IR spectra with temperature during reaction on the reduced fresh 2%Rh/Al$_2$O$_3$ using a 40%CH$_4$/20%O$_2$/He mixture: (a) 373K, (b) 423K, (c) 463K, (d) 483K, (e) 503K, (f) 1053K.**

The same experiments were performed on the oxidized, reduced aged and reduced sintered catalysts in the DRIFTS cell. The ignition temperatures are listed in **Table 5.1.** The reduced fresh catalyst has the lowest ignition temperature, 513 K. Ignition temperatures for the reduced aged and sintered catalyst are 598 K and 623 K, respectively. Since the reduced fresh, aged and sintered catalysts were all treated the same before reaction, the differences in the ignition temperature must be caused by catalyst characteristics, such as particle size, which perhaps led to

different interactions between reactants and catalysts. The ignition temperature on the oxidized

catalyst is 596 K. It is difficult to directly compare this value to the others because of the

different pretreatment procedure.

Ignition temperatures on the reduced fresh catalyst with different $CH_4/O_2$ ratios from 1.16 to 8

and a total flow rate of 650 cc/min were also measured. As shown in **Figure 5.2**, the ignition

temperature was lower when there was a higher $O_2$ concentration in the reactant mixture. These

results are the opposite from the results obtained on alumina supported platinum catalysts [8].

Results shown in this section imply that the ignition process on $Rh/Al_2O_3$ could not simply be

related to the heat of adsorption of oxygen, as was suggested for $Pt/Al_2O_3$.
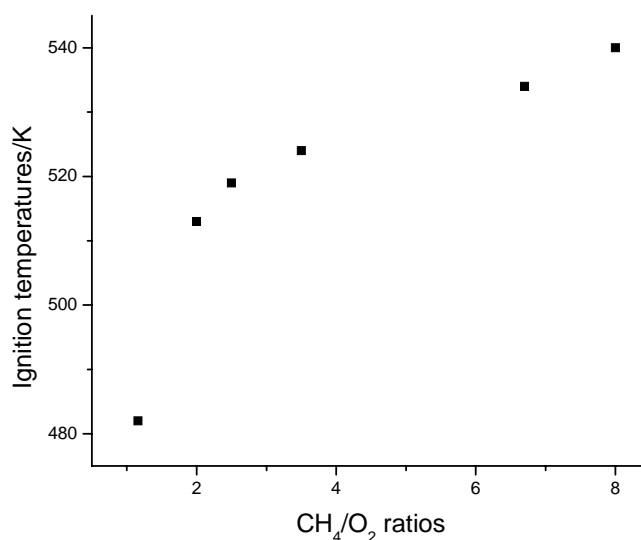


**Figure 5.2: Evolution of the ignition temperature with $CH_4/O_2$ ratio**

### 5.3.3 *Methane adsorption*

**5.3.3.1** *Methane adsorption on reduced state catalysts*

Methane adsorption experiments have been performed using a $CH_4/He$ mixture with $O_2$ omitted. The IR spectra obtained after admission of methane and helium on the reduced fresh catalyst are shown in **Figure 5.3.** At 423 K, a weak IR bank appears at 2010 cm$^{-1}$. This IR band has been ascribed to the linear CO species adsorbed on reduced Rh [13,14]. As temperature is increased, the band intensity increases while a broad weak IR band centered at 1850 cm$^{-1}$, assigned to bridged CO species adsorbed on reduced Rh [15], is progressively formed. The formation of CO was also observed in the gas phase mass spectroscopic data, as shown by the solid line in **Figure 5.4.**
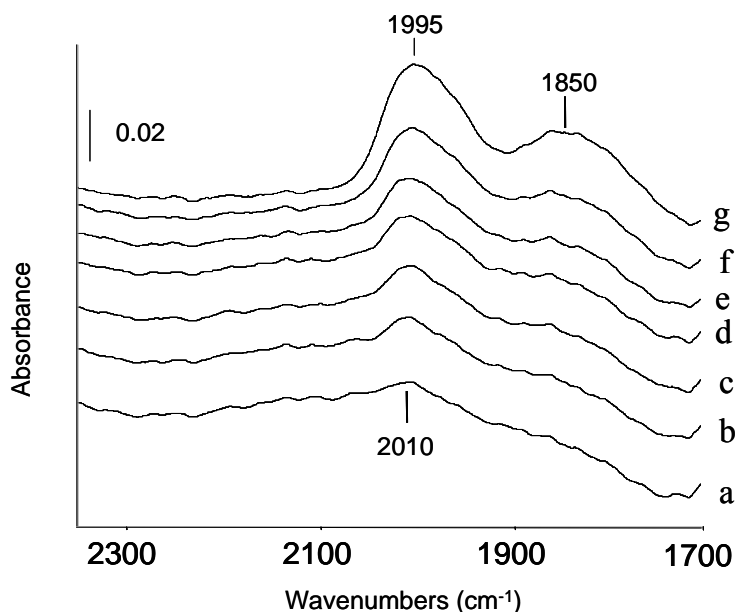


**Figure 5.3: IR spectra after interaction of 50%CH$_4$/He with the reduced fresh catalyst at different temperatures: (a) 423, (b) 433, (c) 443, (d) 453, (e) 463, (f) 483, (g) 513 K.**
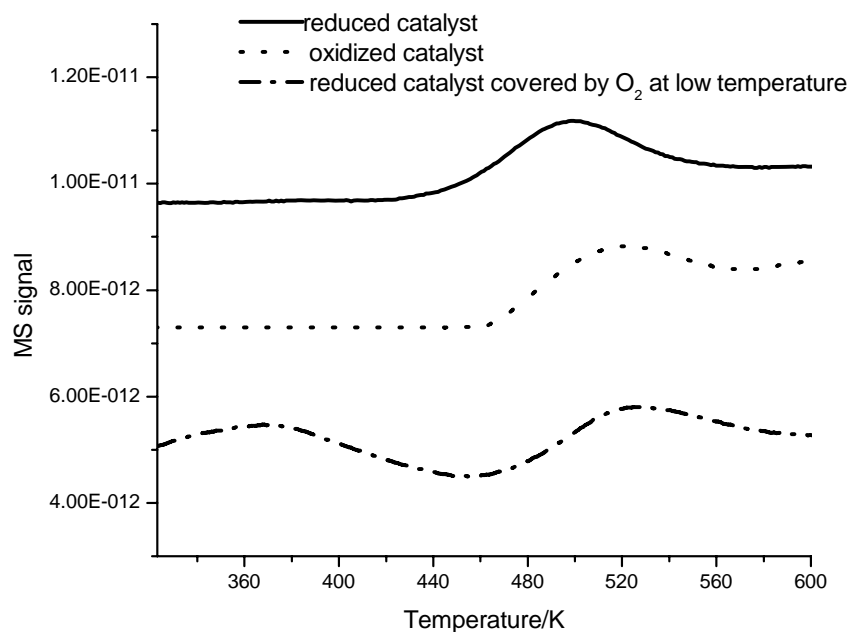
**Figure 5.4: Mass spectra of m/z = 28 during methane adsorption on different states of 2%Rh/Al$_2$O$_3$ using 50%CH$_4$/He mixture.**

### 5.3.3.2 *Methane adsorption on O$_2$-covered reduced states*

**Figure 5.5** shows the IR spectra when methane was adsorbed on the reduced fresh catalyst covered by chemisorbed O$_2$ (O$_2$-covered reduced fresh catalyst). At 463 K, a weak peak assigned to linearly adsorbed CO on metallic Rh appears at 2023 cm$^{-1}$ [14]. At the same temperature, a small broad shoulder formed at the wavenumbers centered at 2100 cm$^{-1}$ [15]. It is assumed that CO adsorbed on several different oxidation states of Rh coexist in this region. Therefore, these species are referred to CO adsorbed on Rh$^{n+}$ (1 $\leq$ n $\leq$ 3) for simplicity, representing higher oxidation states of Rh [15]. The peak intensity increased, became narrower, and shifted to lower wavenumbers centered at 2086 cm$^{-1}$ with increasing temperature, thus indicating that some of the Rh$^{n+}$ was reduced during methane adsorption. As temperature increases, the bridged CO species

80

also appears at 1864 cm$^{-1}$. Both linear and bridged CO species shift to lower wavenumbers with increasing temperature.
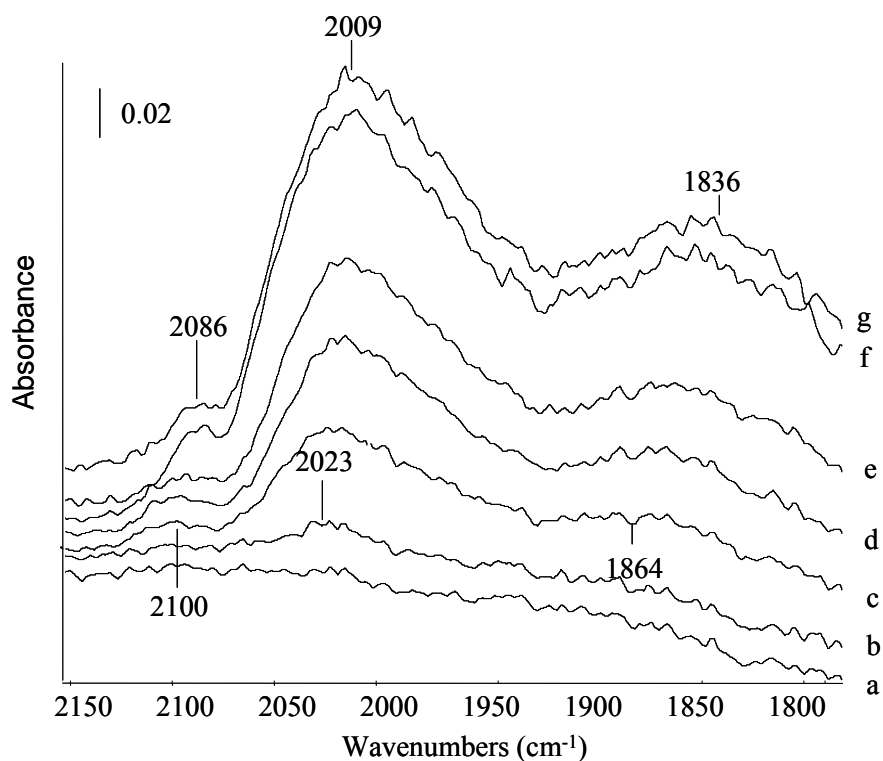


**Figure 5.5: IR spectra after interaction of 50%CH$_4$/He with the fresh reduced catalyst covered by chemisorbed O$_2$ at different temperatures: (a) 453, (b) 463, (c) 533, (d) 573, (e) 633, (f) 733K, and (g) 773K.**

**Figure 5.6** shows the evolution of the IR spectra when methane was adsorbed on an O$_2$-covered reduced aged catalyst. Linear CO bands appear at 2034 cm$^{-1}$ at 523 K; they increase and shift to lower wavenumbers as temperature increases. A very weak band, assigned to CO adsorbed on Rh$^{n+}$, appears at 2100 cm$^{-1}$ and increases with increasing temperature. The intensity of the peak and its increase is not significant; nevertheless the peak still exists at a temperature of 603 K but is overshadowed by the large tail of linearly adsorbed CO. **Figure 5.7** shows the IR spectra

evolution when methane was adsorbed on $O_2$-covered reduced sintered catalyst. As the temperature is increased, a weak peak at the wavenumber of 2039 cm$^{-1}$ appears. This peak is assigned to linear CO adsorbed on reduced Rh and progressively shifts to lower wavenumbers as temperature is increased.
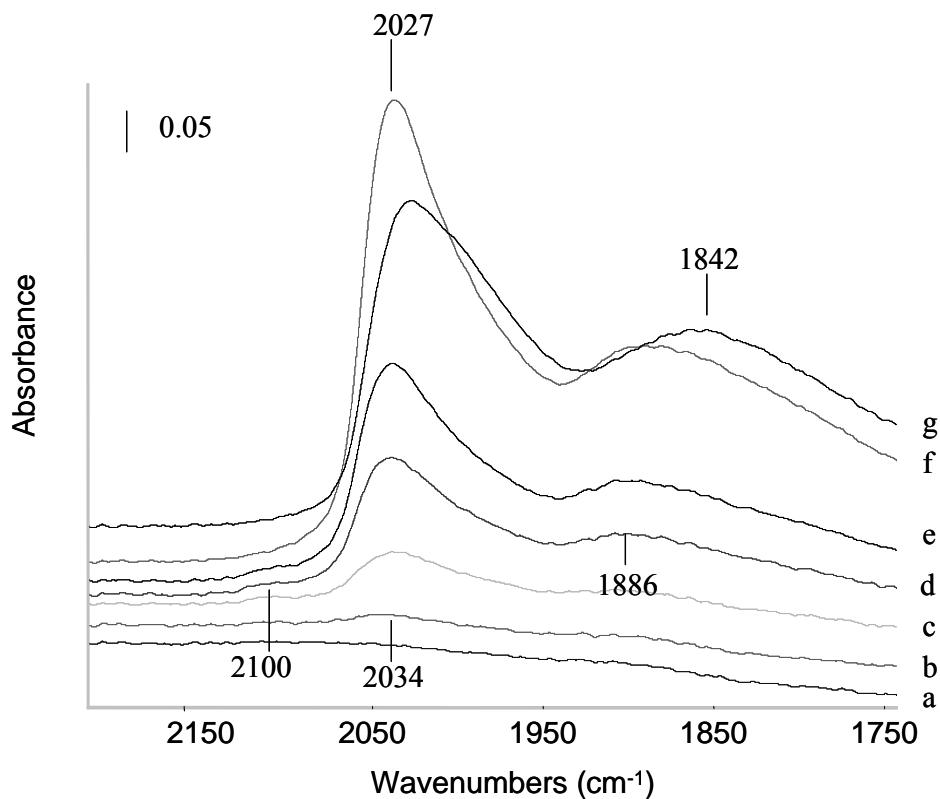


**Figure 5.6: IR spectra after interaction of 50%CH$_4$/He with the reduced aged catalyst covered by O$_2$ at different temperatures: a) 513K, b) 523K, c) 563K, d) 583K, e) 603K, f) 683K, and g) 773K.**
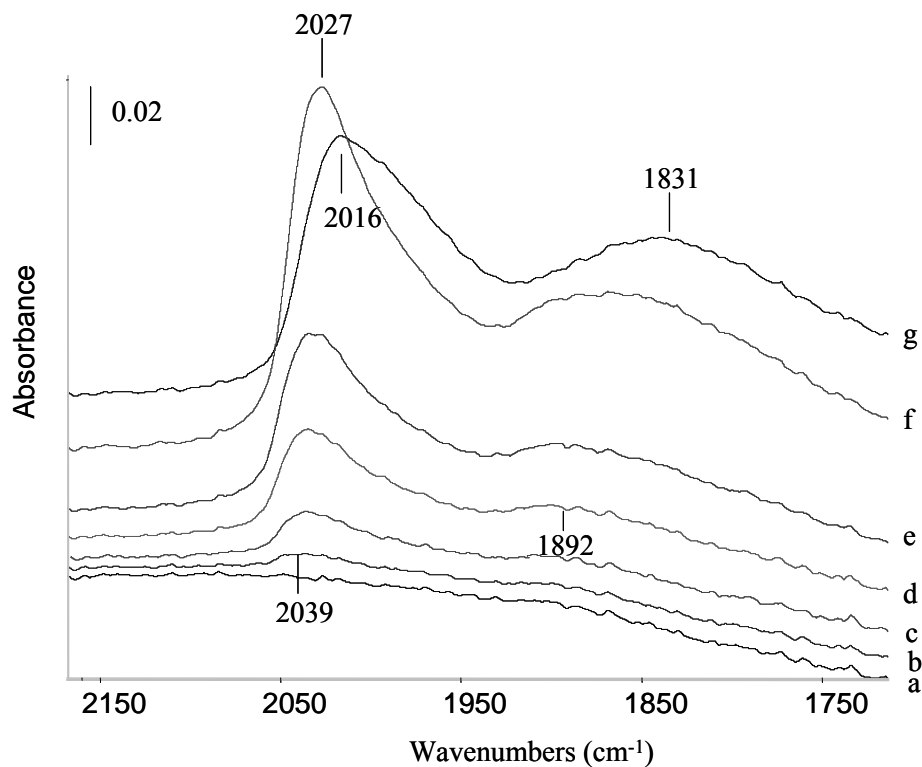
**Figure 5.7: IR spectra after interaction of 50%CH₄/He with the reduced sintered catalyst covered by chemisorbed O₂ at different temperatures: a) 513K, b) 523K, c) 553K, d) 573K, e) 593K, f) 653K, and g) 773K.**

### 5.3.3.3 *Methane adsorption on oxidized catalyst*

**Figure 5.8** shows the evolution of the IR spectra with temperature during methane adsorption on the oxidized catalyst. At 483 K, linear CO adsorbed on reduced Rh forms at a wavenumber of 2036 cm⁻¹ [14], and displays a shift to lower wavenumbers with increasing temperature. At the same temperature, CO adsorbed on $Rh^{n+}$ appears at the wavenumber centered at 2110 cm⁻¹. This peak becomes narrower and shifts to approximately 2087 cm⁻¹, indicating that the catalyst is progressively reduced during methane adsorption. At a temperature of 683 K, the peak almost completely disappears.

83
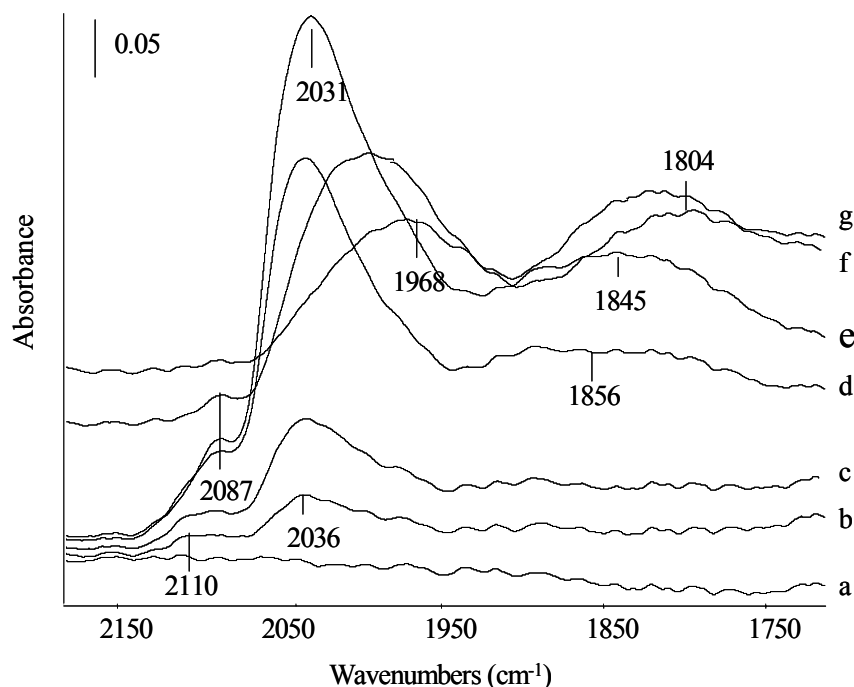
**Figure 5.8: IR spectra after interaction of 50%CH₄/He with the oxidized catalyst at different temperatures: a) 473K, b) 483K, c) 493K, d) 533K, e) 553K, f) 653K, and g) 723K.**

### 5.3.4 *Catalysts oxidation state characterization during the reaction ignition process*

FTIR spectroscopic studies of CO adsorption are widely used to characterize highly dispersed $Rh/Al_2O_3$ catalysts. The first investigation was reported by Yang and Garland [16]. It is now generally believed that eight types of adspecies with different Rh oxidation states are formed when CO is chemisorbed on dispersed Rh surface. IR bands of the different adsorbed CO species on different oxidation states of rhodium are listed in **Table 5.2** [15]**.**

The single band at 2042~2076 cm$^{-1}$ is assigned to CO molecules linearly adsorbed on the rhodium atoms on the surface of rhodium metal crystallites. The corresponding oxidation state of rhodium is Rh$^0$. The single band appearing at 1900 -1920cm$^{-1}$ is assigned to a CO molecule bridged between two neighboring Rh atoms with oxidation state of zero. Yao and Rothschild

[17] have suggested that the broad band peaking between 1850 and 1930 cm$^{-1}$ should be assigned to a mixture of bridged species with different structures on Rh$^0$. Infrared band at 2095 and 2027 cm$^{-1}$ were assigned to the symmetric and antisymmetric stretching modes for adsorbed species known as gem-dicarbonyl. These two bands are on Rh$^+$ and do not shift with increasing CO coverage. Monocarbonyl also exists on Rh$^+$ at the wavenumber in the range of 2080~2100 cm$^{-1}$. Further higher IR bands of CO on oxidation states Rh$^{2+}$ and Rh$^{3+}$ appear above 2100 cm$^{-1}$. The positions of different carbonyls and the corresponding metal oxidation states are very useful for this study.

The catalysts were characterized by CO adsorption after the catalysts were heated to four different temperatures with reactant mixtures having different CH$_4$ to O$_2$ ratios (1.16, 2, 3.5, and 8). Reduced fresh catalysts were used for this series of experiments.

**Figure 5.9** shows the IR spectra of the adsorbed CO at 373 K obtained after temperatures reached 438, 463, 488 and 513 K under a reaction mixture with a CH$_4$ to O$_2$ ratio of 2. The spectrum of the adsorbed CO after reaching 438K **(Figure 5.9a)** reveals strong bands at 2025 cm$^{-1}$, 2065 cm$^{-1}$, 2095 cm$^{-1}$, and a broad band centered at 1900 cm$^{-1}$ associated with bridged CO species [15]. The band at 2065 cm$^{-1}$ can be assigned to the linearly adsorbed CO on reduced rhodium while the 2025 cm$^{-1}$ band can be assigned to CO symmetric stretching mode adsorbed on Rh$^+$ referred to geminal dicarbonyl species, Rh$^+$(CO)$_2$ [15]. According to Rice [15] and Solymosi [18], geminal carbonyl gives two peaks representing the symmetric and asymmetric modes, respectively. The two bands should have the same intensity (same integrated peak area) and should not shift with changing CO coverage. It is apparent that the band at 2095 cm$^{-1}$ is

markedly more intense than the one at 2025 cm$^{-1}$. This peak could be due to several different species.
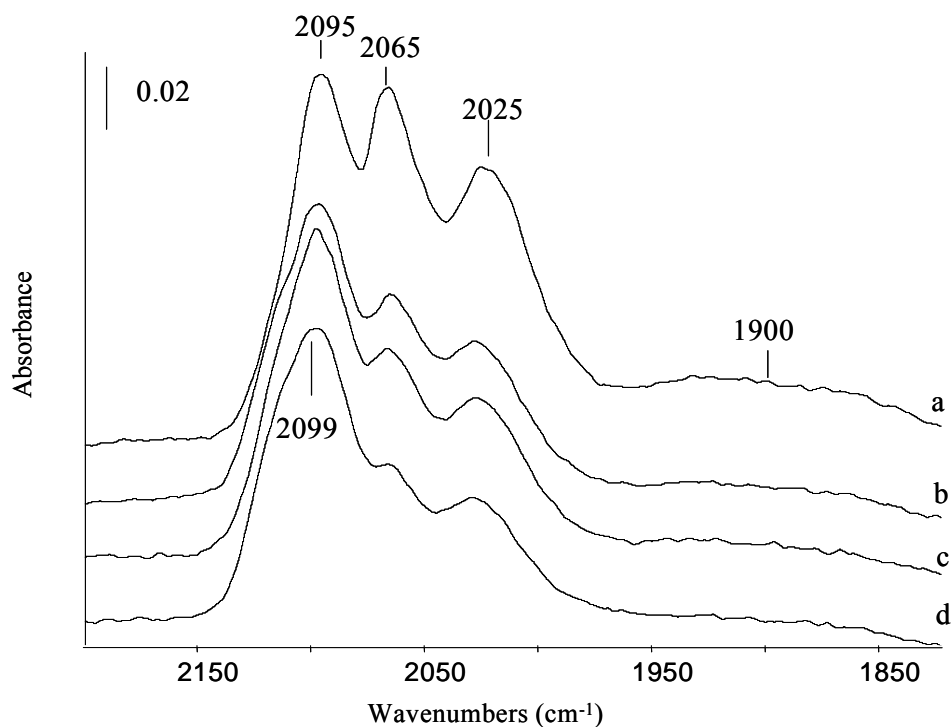


**Figure 5.9: IR spectra of adsorbed CO on the surface of fresh 2%Rh/Al$_2$O$_3$ at 373 K after increasing temperature from room temperature to (a) 438 (b) 463 (c) 488 and (d) 513 K under 40%CH$_4$/20%O$_2$/He mixture.**

The spectrum of the adsorbed CO after reaching 463 K (**Figure 5.9b**) shows CO species similar to that after reaching 438 K. However, the intensity of symmetric mode of the geminal dicarbonyl species at 2025 cm$^{-1}$, the bridged CO species, and the linear CO species has decreased. The band at 2095 cm$^{-1}$ has nearly the same intensity but has shifted to slightly higher wavenumbers. A shoulder appears as the temperature was raised. In the partial oxidation environment, four components probably coexist at a position around 2095 cm$^{-1}$: asymmetric

stretching mode of adsorbed CO on $Rh^+$, monocarbonyl on $Rh^+$, carbonyl on $Rh^{2+}$ at around 2120 $cm^{-1}$, and the species assigned to carbonyl on $Rh^{3+}$ at around 2136 $cm^{-1}$ [15]. The decrease of asymmetric mode of the geminal carbonyl around 2095 $cm^{-1}$ probably is balanced by an increase of intensities of the other peaks around this wavenumber. The decrease in intensity of the gem doublet carbonyl is understandable since this species is thermally unstable [19], and it might be only a transition state between higher oxidation states and rhodium zero.

The same trend is observed for the evolution of the bands of the adsorbed CO species after reaching 488K (**Figure 5.9c**) and 513 K (**Figure 5.9d**) under the reaction mixture. The bridged CO species has almost disappeared. Linear CO species and the geminal doublet decrease with increasing temperature. The intensity change of the peak near 2095 $cm^{-1}$ isn't obvious. Similar trends have been observed using different reactant mixtures with varying partial pressure of oxygen.

## 5.4    Discussion

### 5.4.1 *Methane adsorption*

As shown in **Table 5.1**, the temperature at which the formation of CO occurs varies with catalyst particle size. The temperature for the reduced aged catalyst having a smallest particle size is the lowest at 373 K. It is the highest at 473 K on the reduced sintered catalyst, which has a largest particle size. This suggests that the highly dispersed rhodium activates the dissociation of methane easier than larger particles of rhodium. The positions of the adsorption bands for the earliest linearly adsorbed CO on the reduced catalysts also change from lower wavenumbers to higher wavenumbers with increasing catalyst particle size (2000 $cm^{-1}$, 2010 $cm^{-1}$ and 2033 $cm^{-1}$

for the reduced aged, reduced fresh and reduced sintered, respectively). The difference in the position of the linear CO bands on reduced rhodium sites is a consequence of different particle size. This result agrees with the observation that frequencies of CO species shift to higher wavenumbers for bigger metal particles [20]. It should also be noted that the coverage of CO is expected to be quite low in the methane adsorption experiments. For this reason, the wavenumbers reported for linearly adsorbed CO in **Table 5.1** are quite different than those for linearly adsorbed CO when CO was used as probe molecule (i.e. **Figure 5.9**)

The peak position for the first adsorbed CO peak formed on the reduced fresh state is located at a higher wavenumber than on the $O_2$-covered reduced fresh state. According to Levy et al. [21], the position of the IR band of linearly adsorbed CO species can characterize the surface state of the catalysts. They observed a slight increase of the linear CO species from 2075 $cm^{-1}$ for a freshly reduced $Pt/Al_2O_3$ sample to 2085 $cm^{-1}$ for the sample with oxygen on the surface at 298 K. In our experiments, the difference in wavenumber was observed for the linear CO species at 2010 $cm^{-1}$ (**Figure 5.3a**) on the reduced fresh catalyst and at 2023 $cm^{-1}$ (**Figure 5.5b**) on the $O_2$-covered reduced fresh catalyst. This shift indicates that catalyst surface is initially covered by chemisorbed $O_2$.

As shown in the MS data in **Figure 5.4**, CO gas was formed on the reduced fresh catalyst at 423 K, which was the same temperature as adsorbed CO appeared in IR spectrum. Since there was no oxygen in the gas phase, the CO formed may come from the reaction of the carbonaceous adspecies from methane dissociation with surface OH groups on the support via a redox mechanism [11,22] and/or with low coordinated oxygen of the support [23].

88

Compared to their corresponding reduced catalysts states, CO always forms at higher temperatures on the $O_2$-covered reduced states, indicating that adsorbed oxygen is an important factor in CO formation. There appears to be no correlation between the particle size and the temperature or position at which CO is first observed for $O_2$-covered catalysts. Adsorbed CO forms at 463 K for the $O_2$ covered reduced fresh catalyst and at 523 K for both the $O_2$-covered reduced aged and sintered catalysts. A direct relationship between the ignition temperatures and formation of CO from methane dissociation cannot be easily made from the results of methane dissociation experiments.

### 5.4.2 *$C_2$ species and CO formation during methane adsorption on oxygen-covered catalysts*

Comparing the results on catalysts with and without chemisorbed $O_2$, it is apparent that the existence of chemisorbed oxygen species delayed the formation of CO. From the IR data, methane seems to dissociate at a higher temperature on the $O_2$-covered reduced fresh catalyst than on the reduced fresh catalyst. However, gas phase components produced during methane adsorption on the $O_2$-covered reduced fresh catalyst in **Figure 5.4** suggest that $CH_4$ reacts at a very early stage. In this figure, a small peak appeared immediately after the $CH_4$/He mixture was added to the oxygen-covered catalyst at 323 K. The peak, which can be assigned to $C_2$ species due to ethane or ethylene [24], reaches a maximum at around 373 K and then decreases. Because the most intense signal of CO, ethane and ethylene is m/z = 28, the difference between CO and these $C_2$ species has been made by comparing IR and MS results at the same time. From **Figure 5.5**, it is apparent that formation of CO starts at 463 K on oxygen-covered reduced catalyst, which is consistent with the second increase of the m/z = 28 signal in **Figure 5.4** and indicates

that this second signal results from CO gas. The increase of m/z = 28 signal from 323 K is not

CO because, at this temperature, adsorbed CO hasn't formed yet. An alternative explanation is

that CO was also formed at low temperature and the existence of chemisorbed $O_2$ might prevent

CO from adsorbing on the surface. However, this does not agree with some previous

experimental results. For instance, adsorbed CO was observed immediately in the IR spectrum

when flowing $CH_4$, $O_2$, and ppm of CO simultaneously over $Pt/Al_2O_3$ [8]. In addition, there was

adsorption of CO when ppm of CO was pulsed over the $O_2$-covered reduced Rh catalyst surface.

Because of these results, it is less likely that CO could be appearing when no adsorbed CO was

observed in the IR spectrum. If CO was omitted from consideration for the m/z peak at 28, then

$C_2$ hydrocarbon species are the most likely explanation. Since no signal at m/z = 26 was

observed under the condition of the experiment, acetylene was also eliminated from

consideration.


Accordingly, $CH_4$ appears to dissociate at very low temperature on Rh sites covered by $O_2$. The

result of this dissociation is apparently the formation of the $C_2$ species. The low-temperature $CH_4$

dissociation behavior on $O_2$-covered catalyst was also observed by Ferreira-Aparicia [11,25],

who claimed that a trace of $C_2$ was obtained over rhodium at temperatures as low as 373 K. This

phenomenon didn't happen over the oxidized catalyst (see **Figure 5.4)**, which means only $O_2$ on

top of a reduced catalyst promotes low temperature $CH_4$ dissociation to form $C_2$ species and

oxygen species in the bulk do not have this effect. The decrease of the $C_2$ species indicates that

the adsorbed oxygen on the surface disappeared with increasing temperature. Most likely, some

initial adsorbed oxygen has transformed into strongly bonded O species that are more difficult to

desorb from the rhodium surfaces.

90

Both theoretical and experimental studies indicate that $CH_4$ can adsorb and dissociate at low temperatures. The calculation by Au et al [26] shows that the adsorption energy for $CH_4$ on adsorbed O is very small. Au and Wang [23] found that the activation energy for $CH_4$ dissociation over adsorbed O is zero according to the reaction:

$$CH_{4,\,s} + O_s - CH_{3,\,s} + OH_s \qquad \textbf{Equation 5.1}$$

$CH_3$ radical produced in methane dissociation may react with Os to form $H_3C$-Os, which is less stable than $H_3C$-Rh and, thus, combines with each other to form $C_2$. On the contrary, the binding energy of $CH_3$ on Rh metal is very high ($4.85eV^{cal}$, $4.51eV^{exp}$). This accounts for the fact that $C_2$ products were generated on the $O_2$-covered reduced catalyst but not on the reduced catalysts at low temperatures during the methane adsorption experiments.

CO is formed at relatively high temperatures via CHx (x =0 – 3) species produced by methane dissociation [23]. However, the nature of the first dissociation rhodium sites and the manner by which these sites are formed on the $O_2$-covered catalysts is under question. Higher oxidation states, $Rh^{n+}$, resulting from oxidation of reduced rhodium by adsorbed $O_2$ with increasing temperature is the preferred explanation when the high heat of adsorption of $O_2$ on rhodium is considered. This means desorption of $O_2$ will occur at very high temperatures. Additionally, desorption of $O_2$ occurs at nearly the same temperature for catalysts with different particle sizes [ 27 ]. On the contrary, the results presented herein show that CO appears at different temperatures for the catalysts having different particle sizes: 463 K for $O_2$-covered reduced fresh catalysts and 523 K for both $O_2$-covered reduced aged and sintered catalysts.

In summary, methane can dissociate both on the $O_2$-covered Rh sites at low temperatures and on both higher oxidation state Rh sites and reduced Rh sites at higher temperatures. However, the dissociation products are different. $C_2$ species is formed at the former condition, and the evolution of CO is observed for the latter sites.

### 5.4.3 *CO formation on different catalysts from methane activation*

#### 5.4.3.1 *Effect of pretreatment*

It should be noted that pretreatment, i.e. oxidation and reduction cycling, before each experiment not only removes carbonaceous deposits but also may induce significant structural and morphological alterations of the catalyst system. This could greatly influence the performance of the catalysts. Grunwaldt et al [28] stated that the structure of the Rh particles is strongly dependent on the gaseous atmosphere applied. Treating $Rh/Al_2O_3$ in an oxidizing environment caused not only the oxidation of supported Rh particles but the formation of an oxidized form of Rh at a high temperature, which is difficult to reduce to the metal [29]. However, this partially reducible form, known as the diffuse oxide phase, only forms during calcination under $O_2$ at temperatures higher than 823 K. Some researchers have suggested that $Rh_2O_3$ can be easily reduced to metallic Rh in a reducing environment at 473 K [30,31]. TPR and ESR results [32] showed that 95% of the rhodium is present in the form of metal crystallites after reducing highly dispersed 0.57 wt % $Rh/Al_2O_3$ catalyst. The crystallites consist of 15-20 atoms and probably have a three dimensional structure including two layers of $Rh^0$ atoms and one layer of $Al_2O_3$. The metal support interactions involve $Rh^0$ - $O^{2-}$ bonds. In this case, they exclude the possibility that isolated $Rh^0$ atoms are present after reduction of the catalyst at 597 K. Thus, our treatment cycle at 773 K under $O_2$ followed by $H_2$ reduction has completely reduced the surface of aged,

fresh, and sintered catalysts. In addition, the particle sizes of the catalysts could play an important role in the treatment. Tian et al [14] suggested that the larger the Rh metal particles are, the more difficult it is to disrupt them. This indicates that the oxidation of the reduced sintered catalysts should be most difficult because of its bigger particle size.

### 5.4.3.2 *CO formation on reduced catalysts*

Based on the experimental results discussed herein, CO formation through methane dissociation on reduced catalysts is related to the particle size of different catalysts to a large extent. When $CH_4$ approaches the reduced Rh in a H-end collinear fashion, only a very small activation energy, ca. 7 cal/mol (0.3 eV) [33], is needed for this approach. This means that $CH_4$ can adsorb immediately on the reduced Rh. However, further dissociation of methane on these sites requires additional energy. As reported by Au [23], the total activation energy for formation of adsorbed C atoms on reduced $Rh/SiO_2$ is 285 kJ/mol (3.2 eV). This energy could vary as $CH_4$ dissociates on Rh particles of different sizes. Although there are no values reported with different particle sizes for Rh, comparable data for Pt and Pd having different cluster sizes were provided by Au [34]. For example, the total activation energy for adsorbed C atoms formation on Pd clusters with 12 atoms is 3.68 eV, which is bigger than 3.57 eV on Pd clusters with 7 atoms. From this comparison one could assume that the total activation energy needed for adsorbed C atom formation is less on smaller Rh particles. This could possibly explain why CO formed at the lowest temperature on the reduced aged catalyst with the smallest particle size and at the highest temperature on the reduced sintered catalyst with largest particle size.

### 5.4.3.3 *CO formation on $O_2$-covered catalysts*

The situation for CO formation is different on the catalysts covered by chemisorbed oxygen species. Castner and Matsushima [35,36] have found that diffusion of $O_2$ into the catalyst bulk

and Rh bulk oxidation occurred at temperatures above approximately 400 K. Desorption of $O_2$ occurs at the temperature above 850 K [27] according to Putna et al. With the diffusion of $O_2$ into the bulk as temperature is raised, more and more $Rh^0$ sites are oxidized into higher oxidation states, $Rh^{n+}$. As shown in **Figure 5.5** and **Figure 5.6,** not only linear CO on $Rh^0$ but CO on higher oxidation state Rh (2100 $cm^{-1}$) first appeared at the same temperature, which means that some of the $Rh^0$ sites were oxidized and a mixture of several Rh oxidation states ($Rh^{n+}$) coexisted. The amount of $Rh^{n+}$ formed varies on different catalysts. The peak at around 2100 $cm^{-1}$ increases with increasing temperature in **Figure 5.5,** indicating that the amount of $Rh^{n+}$ on the $O_2$-covered reduced fresh catalyst is significant. One can probably assume that $CH_4$ initially dissociates on these $Rh^{n+}$ sites and some of these sites are progressively reduced into $Rh^0$ under a methane atmosphere, forming CO. The dissociation of methane on partially oxidized Rh sites has also been observed by Buyevskaya et al [37]. $CH_4$ perhaps has no direct access to the bare $Rh^0$ atoms at the beginning because of the chemisorbed O species.

### 5.4.3.4 *CO formation on oxidized catalyst*

Methane adsorption on oxidized catalysts is quite different. Oxidation of the catalyst at 773 K generated a catalyst consisting of large amounts of higher oxidation state Rh. The amount of $Rh^{n+}$ in the oxidized catalyst was high enough to provide $CH_4$ adsorption sites. Since there are no $Rh^0$ sites at the beginning, $Rh^{n+}$ apparently can be the active site for $CH_4$ dissociation. As shown in **Figure 5.8**, the composition of $Rh^{n+}$ changes as the temperature increases under a $CH_4$/He environment. $Rh^+$ and $Rh^0$ appear to be the dominant states at 533 K, which means that catalyst is being reduced with increasing temperature.

### 5.4.4 *Catalysts oxidation state characterization during the reaction ignition process*

When there is gas phase $O_2$ present in the reactant mixture, the catalyst state may change with increasing temperature. This change was characterized using CO as a probe molecule.

As shown in **Figure 5.9**, the intensities of different carbonyl species change as a function of temperature. In order to quantitatively evaluate the change in these adsorbed carbonyl species during the course of the light-off process, deconvolution of the bands in the 1950 - 2160 $cm^{-1}$ range using the software package GRAMS was performed. Four overlapping bands resulting from CO adsorption are assumed as if equal integrated area for each of the two components of the geminal dicarbonyl are equal [15] for all conditions. **Figure 5.10** shows the deconvolution results for the reaction mixture of 40%$CH_4$/20%$O_2$/He at the temperature of 463 K. The peaks from lower to higher energy are: symmetric stretching band of gem doublets on $Rh^+$, linear carbonyl on $Rh^0$, asymmetric stretching band of gem doublets on $Rh^+$, and the combination of linear carbonyl on $Rh^+$, carbonyl on $Rh^{2+}$ and carbonyl on $Rh^{3+}$. This fourth peak is denoted as carbonyl on $Rh^{n+}$ ($1 \leq n \leq 3$), higher oxidation rhodium states. One of the reasons why $Rh^{n+}$ is used is that it is hard to deconvolute the coexisting $Rh^{n+}$ peak into three peaks. Another reason is that they all have higher oxidation states compared to rhodium zero. Even though $Rh^{2+}$ and $Rh^+$ are transition oxidation states, which can be oxidized into $Rh^{3+}$, the total effect of the three should not change. The change of integrated area of different species with temperature and the methane to oxygen ratios used are shown in **Figure 5.11, Figure 5.12,** and **Figure 5.13.** It can be seen that the intensity of the linear CO species decreases with temperature implying $Rh^0$ decreases, while the combined species due to $Rh^{n+}$ increases. In addition, the higher the amount of oxygen in the mixture, the higher the combined integrated area of $Rh^{n+}$ is for any temperature.

**Figure 5.10: Deconvolution result.**
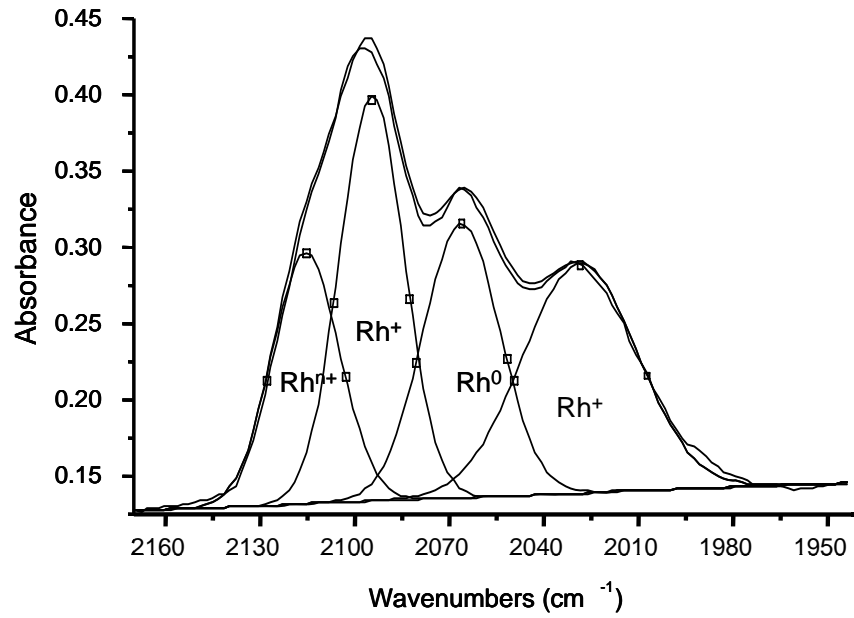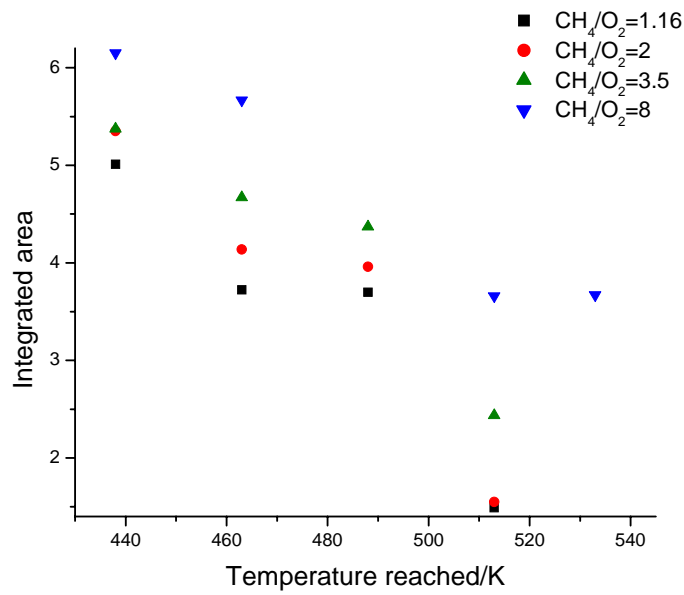


**Figure 5.11: Effect of temperature on the integrated area of carbonyl on $Rh^0$ for different $CH_4/O_2$ ratios.**
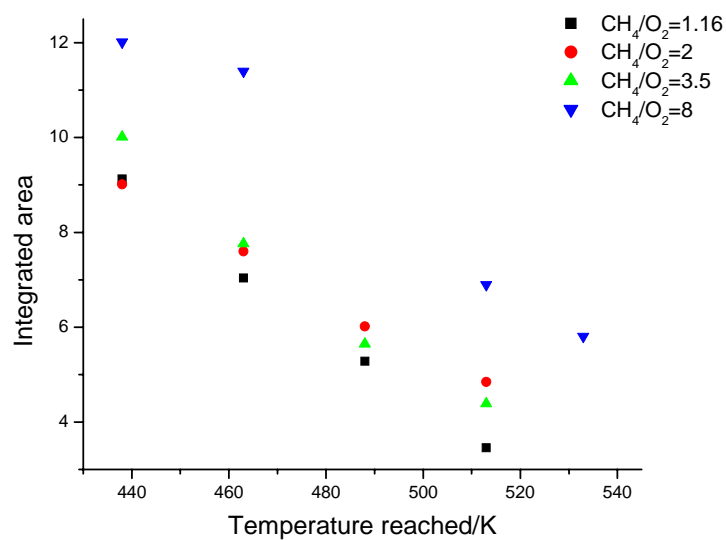
**Figure 5.12: Effect of temperature on the integrated area of carbonyl on $Rh^+$ (geminal carbonyl) for different $CH_4/O_2$ ratios.**
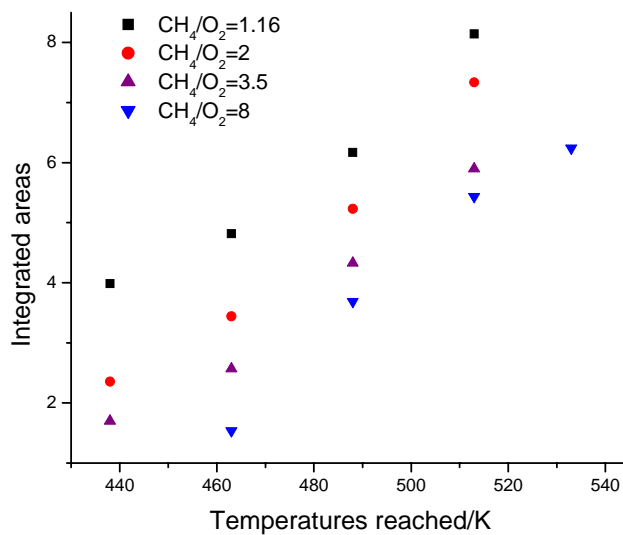


**Figure 5.13: Effect of temperature on the integrated area of carbonyl on $Rh^{n+}$ for different $CH_4/O_2$ ratios.**

The results agree with those obtained through in situ EXAFS study by Grunwaldt et al [28], which showed that the structure of Rh catalyst was gradually changed and Rh was slightly oxidized before ignition under a methane-oxygen (CPO) reaction mixture. The structural change was very similar to the changes in pure $O_2$. This process is reversible. When the reaction mixture is introduced on the reduced fresh catalysts at 323 K, Rh metal is covered with adsorbed O species. As was explained previously on $O_2$-covered catalysts, more and more $Rh^0$ were oxidized into $Rh^{n+}$ with increasing temperature. The extent of oxidation is determined by the $O_2$ partial pressure in the gas mixture. The more $O_2$ in the reactant mixture, the more $Rh^0$ is oxidized. The chemisorbed oxygen species do not desorb from catalyst surface because of supported rhodium catalysts' high affinity for oxygen, instead diffusing into those rhodium sites and producing oxidized Rh sites. This is why the accumulation of higher oxidation states is observed during the ignition process. Reduction of the catalyst occurred once the CPO reaction was initiated.

### 5.4.5 *Summary*

Based on the results from the methane adsorption studies and characterization of catalysts states using CO as a probe molecule, $Rh^{n+}$ sites appear to play an important role in ignition. The more $Rh^{n+}$ sites that exist, the easier reaction ignition occurs. Like $Rh^0$, $Rh^{n+}$ probably also acts as the adsorption and dissociation sites for $CH_4$.

As shown in **Table 5.1**, the trend for reaction ignition temperature (IT) with fixed $CH_4/O_2$ ratio is: IT on fresh reduced catalysts < IT on reduced aged catalysts < IT on reduced sintered catalysts. This is opposite to the trend for amount of $Rh^{n+}$ formed on different $O_2$-covered reduced catalysts during methane adsorption ($O_2$-covered reduced fresh > $O_2$-covered reduced

aged > $O_2$-covered reduced sintered). Methane adsorption on $O_2$-covered reduced catalysts represents an extreme condition for the ignition reaction, which has extremely low $O_2$ partial pressure and, therefore, implies that $Rh^{n+}$ is probably the key factor that affects the reaction ignition on different reduced catalysts. Although rhodium particle size plays an important role in methane dissociation to form CO, it is apparent that $Rh^{n+}$ formation is the slow step in the whole process, which determines the ease of ignition. CO formation is most likely not the rate-determining step, as evidenced by CO formation at almost the same time for $O_2$-covered reduced aged and $O_2$-covered reduced sintered catalysts, though their ignition temperatures are quite different. Ignition on the same reduced catalyst with varying $O_2$ partial pressure in the reaction mixture shows that a higher amount of $Rh^{n+}$ was formed when there is more $O_2$, which, therefore, lowered the ignition temperatures. This is further evidence that the reaction ignition on reduced catalysts is related to $Rh^{n+}$.

## 5.5   Conclusions

It has been found that the dissociative adsorption of methane on rhodium occurs from low temperatures. The types of adsorption sites determine the product composition.  $Rh^0$ sites covered by chemisorbed oxygen are responsible for $C_2$ species (ethane or ethylene) because adsorbed $O_2$ promotes methane dissociation at low temperatures. However, the formation of $C_2$ species is not important in reaction ignition. The formation of CO can occur on bare reduced Rh sites and occurs first on the reduced aged catalyst, which has a smallest particle size. $Rh^{n+}$ sites ($1 \leq n \leq 3$) are probably also active for $CH_4$ dissociation at low temperatures. They are progressively reduced into $Rh^0$ by interaction with $CH_4$, where more CO forms. Pretreatment and the particle size of catalysts play important roles during the process of methane activation on the reduced catalyst states.

The ignition temperatures were found to be lowest on the reduced fresh catalyst, highest on the reduced sintered catalyst, and in between for the reduced aged catalyst. This trend is hypothesized to be due to the amount of $Rh^{n+}$ formed on these three samples. It has also been shown that the ignition temperatures increased with decreased concentration of oxygen in the reactant mixture. The oxidation state of rhodium changes as temperature is raised, as shown by using CO as a probe molecule. Higher oxidation states, $Rh^{n+}$, increase with increasing temperature and with increasing $O_2$ concentration. The results further imply that the ignition of CPO is related to the amount of $Rh^{n+}$ present.

**Table 5.1: Reaction ignition temperatures and methane dissociation on different states of catalysts and related characterization results**

| 2%Rh/Al$_2$O$_3$ | Catalyst states | Characterization results | | Results from methane adsorption experiments | | | Results from reaction experiments |
|---|---|---|---|---|---|---|---|
| | | Dispersion | Particle sizes (nm) | T for the first adsorbed CO appearance (K) | Positions of the first adsorbed CO (cm$^{-1}$) | | Ignition temperatures (K) |
| | | | | | Linearly adsorbed CO on Rh$^0$ | Other adsorbed CO on Rh$^{n+}$ | |
| Aged catalyst | Reduced aged | 74% | 1.8 | 373 | 2000 | | 598 |
| | O$_2$-covered reduced aged | | | 523 | 2034 | 2100 | |
| Fresh catalyst | Reduced fresh | 37% | 2.9 | 423 | 2010 | | 513 |
| | O$_2$-covered reduced fresh | | | 463 | 2023 | 2100 | |
| Sintered catalyst | Reduced sintered | 28% | 4.2 | 473 | 2033 | | 623 |
| | O$_2$-covered reduced sintered | | | 523 | 2039 | No peak or extremely small | |
| Oxidized catalyst | | 27% | 0.8 | 483 | 2036 | 2110 | 596 |

**Table 5.2 Carbonyl species and their frequencies**

| Frequency range ($cm^{-1}$) | Oxidation state | Proposed structure |
|---|---|---|
| 2136 | III | |
| 2116-2120 | II |  |
| 2096-2102<br>2022-2032 | I |  |
| 2080-2100 | I |  |
| 2000-2020 | I |  |
| 2042-2076 | 0 |  |
| 1900-1920 | 0 |  |
| 1845-1875 | 0 |  |

## 5.6　References

1 W. Weng, Q. Yan, C. Luo, Y. Liao, H. Wan, Catal. Lett. 74 (2001) 37.

2 M. Prettre, Ch. Eichner, M. Perrin, Trans. Faraday Soc. 43 (1946) 335.

3 D. Dissanayake, M.P. Rosynek, K.C.C. Kharas, J.H. Lunsford, J.Catal. 132 (1991) 117.

4 A.T. Ashcroft, A.K. Cheetham, J.S. Foord, M. L.H. Green, C.P. Grey, A.J. Murrell, P.D.F. Vernon, Nature 344 (1990) 319.

5 F. van Looij, J.C. van Giezen, E.R. Stobbe, J. W. Geus, Catal. Today 21 (1994) 495.

6 G. Veser, J. Frauhammer, L. D. Schmidt, G. Eigenberger, Studies in Surf. Sci. and Catal. 109 (1997) 273.

7 G. Veser, M. Ziauddin, L. D. Schmidt, Catal. Today 47 (1999) 219.

8 A. Bourane, C. Cao, K. L. Hohn. Appl. Catal. A: Gen. 302 (2006) 224.

9 P.M. Torniainen, X. Chu, L.D. Schmit, J. Catal. 146 (1994) 1.

10 J.P. Candy, A.El Mansour, O.A. Ferretti, G. Mabilon, J.P. Bournonville, J.M. Basset, G. Martino, J. Catal. 112 (1988) 201.

11 P. Ferreira-Aparicio, I. Rodríguez-Ramos, A. Guerrero-Ruiz, Appl. Catal. A: Gen. 148 (1997) 343.

12 L. H. Little, *Infrared Spectra of Adsorbed Species*, Academic Press, London, New York, 1966.

13 W. Weng, M. Chen, Q. Yan, T. Wu, Z. Chao, Y. Liao, H. Wan, Catal. Today, 63 (2000) 317

14 Z. Tian, O. Dewaele, G.B. Martin, Catal. Lett. 57 (1999) 9

15 C.A. Rice, S.D. Worley, C.W. Curtis, J.A. Guin, A.R. Tarrer, J. Chem. Phys. 74 (1981) 6487.

16 A.C. Yang, C.W. Garland, J. Phys. Chem. 61 (1957) 1504.

17 H.C. Yao, W.G. Rothschild, J. Chem. Phys. 68 (1978) 4774.

18 F. Solymosi, M. Pasztor, J. Phys. Chem. 89 (1985) 4789.

19 H. Arai, H. Tominaga, J. Catal. 43 (1976) 131.

20 P.T. Fanson, W. N. Delgass, J. Lautherbach, J. Catal. 204(2001) 35.

21 P. J. Levy, V. Pitchon, V. Perrichon, M. Primet, M. Chevrier, C. Gauthier, J. Catal. 178 (1998) 363.

22 O.V. Buyevskaya, D. Wolf, M. Baerns, Catal. Lett. 29 (1994) 249.

23 C.T. Au and H.Y. Wang, J. Catal. 167 (1997) 337.

24 F. Solymosi, A. Erdohelyi, J. Cserenyi, Catal. Lett. 16 (1992) 399.

25 M. S. Liao, Q. E. Zhang, J. Mol. Catal. A: Chem. 136 (1998) 185.

26 C.T. Au, M.S. Liao, C. F. Ng, Chem. Phys. Lett. 267 (1997) 44.

27 E. S. Putna, J.M. Vohs, R.J. Gorte, Surf. Sci. 391 (1997) L1178.

28 J.D. Grunwaldt, L. Basini, B.S. Clausen, J. Catal. 200 (2001) 321.

29 D.D. Beck, C.J. Carr, J. Catal. 144 (1993) 296.

30 C. Wong, R.W. McCabe, J. Catal. 119 (1989) 47.

31 G. Bayer, H.G. Wiedermann, Thermochem. Acta 15 (1976) 2139.

32 H.F.J. van't Blik, J.B.A.D. van Zon, T. Huizinga, J.C. Vis, D.C. Koningsberger, R. Prins. J. Am. Chem. Soc. 107 (1985) 3139.

33 C. N. Stewart, G. Ehrlich, J. Chem. Phys. 62 (1975) 4672.

34 C.T. Au, M.S. Liao, C.F. Ng, J. Phys. Chem. A. 102 (1998) 3959.

35 D. G. Castner, G. A. Somoriai, Appl. Surf. Sci. 6 (1980) 29.

36 T. Matsushima, J. Catal. 85 (1984) 98.

37 O.V. Buyevskaya, K. Walter, D. Wolf, M. Baerns, Catal. Lett.38 (1996) 81.

# Chapter 6 Study of reaction intermediates of methanol decomposition and catalytic partial oxidation on Pt/Al₂O₃

## 6.1    Introduction

The development of hydrogen fuel-cell-powered vehicles has excited much interest in recent years. However, storage and distribution of $H_2$ remains an unsolved problem for implementation of $H_2$-fueled vehicles. As a result, attention has been focused on the design and operation of compact and efficient devices to generate hydrogen on board a vehicle. Methanol is promising fuel for onboard hydrogen generation because methanol has a high hydrogen to carbon ratio and it can be made from a variety of feedstock, including renewable resources.

The most studied method for methanol conversion is steam reforming. The disadvantage of steam reforming is that external heating is required. Catalytic partial oxidation of methanol offers the potential of producing hydrogen through an exothermic reaction and can be run in an autothermal mode, where the heat necessary for the reaction comes from the reaction itself. The high reaction rates of catalytic partial oxidation lead to smaller reactors. Another advantage of methanol partial oxidation is its rapid response to change during the reaction.

While the advantages of methanol catalytic partial oxidation make it intriguing, the reaction mechanism is not well understood. One of the intriguing aspects of the catalytic partial oxidation of methanol is the variety of reactions that may be occurring simultaneously. Many reaction intermediates may be involved. To study the reaction mechanism, reaction kinetics studies were

carried out on different catalysts [1]. The traditional catalysts employed are similar to those used for methanol steam reforming reactions. For example, Cu based catalysts were studied by many researchers [2]. Noble metal catalysts [3] were also explored for methanol partial oxidation to $H_2$. On Rh gauze, the reactions reach steady-state at about 950 K when methanol to oxygen ratio was 3. On Pt gauze, methanol oxidation reached maximum production at 1200 K. They thought that decomposition behavior is dominant by the breaking of the methanol C-O bond on Pt and formation of carbon on Pt surface at low temperatures. The addition of oxygen serves to reduce surface carbon levels and increase catalytic activity. Traxel and Hohn [4] demonstrated that methanol can be converted to $H_2$ at millisecond contact times on supported Pt and Rh monolith catalysts. Methanol catalytic partial oxidation was catalyzed at $CH_3OH/O_2$ ratios ranging from two to five. Results were similar for both metals. As the ratio increased on Pt, the temperature and conversion decreased from 1373 K and 100% to 823 K and 50%, and the $H_2$ selectivity increase from 65% to 75% while the CO selectivity initially rose from 75% to 85% at $CH_3OH/O_2$ = 3, then fell to 70%. They concluded from the study that the water-gas shift reaction appeared to be a key as high temperature product compositions were within experimental error of water-gas shift equilibrium compositions. Low temperatures and high $CH_3OH$ to $O_2$ ratio gave more $H_2$ and $CO_2$ because of a more favorable water-gas shift equilibrium, although results were far from equilibrium.

These kinetic studies of methanol partial oxidation provided very useful information on which reaction is dominant among many reactions occurring simultaneously. However, there is limited information about the reaction intermediates of the methanol partial oxidation to produce $H_2$ on these catalysts. In addition, different opinions about the reaction intermediates were given in

these limited studies. For example, Gentry et al [5] proposed that $CO_2$ was produced from the decomposition of COOH species formed from addition of O atoms to an HCO intermediate after conducting research on Pt wires. Hodges and Roselaar [6], instead, pointed out that $H_2CO$, an intermediate in the reaction, dissociates to adsorbed CO and H atoms which are subsequently oxidized to $CO_2$ and $H_2O$.

To clarify which reaction intermediates are important, experiments should be conducted at autothermal conditions. In this work, in situ DRIFTS and mass spectrometry were used to detect the intermediate species and elucidate the reaction mechanism of methanol partial oxidation. The results from these studies could provide insight into the mechanism of the reactions at high temperatures.

## 6.2 Experimental

### 6.2.1 *Catalyst preparation*

$Pt/Al_2O_3$ powder catalysts were prepared by impregnating the $\gamma$-$Al_2O_3$ (powder $S_{BET}$ = 121 m$^2$/g) with aqueous solutions of $H_2PtCl_6 \cdot 6H_2O$. After drying for 12 h at room temperature and then for 24 h at 383 K, the solids were calcined for 10h in flowing $O_2$/Ar at 773 K. For this research, a metal loading of 2 wt % was used.

The calcined catalysts were treated to a reduced state or an $O_2$-covered reduced state in the reactor cell before each experiment. To obtain a reduced state of the catalyst, the temperature of the catalyst was increased to 773 K at a speed of 10 K/min under flowing He. Then the catalyst was oxidized with flowing $O_2$ for 60 min, followed by a He purge for 5 min. After that, the

catalyst was reduced with $H_2$ at 773 K for 60min followed by He evacuation. $O_2$ coverage was realized by flowing $O_2$ at 303 K for 30min over the corresponding reduced catalyst, resulting in the state designated $O_2$-covered reduced state. The oxidized catalyst was obtained by treating the catalyst at 773 K under $O_2$ for 1 h followed by brief He evacuation.

### 6.2.2 *In situ infrared spectroscopic studies*

Infrared diffuse reflectance (DRIFTS) spectra were recorded on a ThermoNicolet NEXUS 870 infrared spectrometer using an in situ DRIFTS cell attached to a gas supply system, which prepared gas mixtures at atmospheric pressure for transient response and catalytic studies. For each experiment, 0.03 g of catalyst powder were placed into the ceramic cup of a modified [7] commercial high-temperature high-pressure DRIFTS cell (Spectra-Tech: Model No. 0031-901) with a ZnSe window, which resided within the infrared spectrometer bench. The catalysts can be heated up to 1173 K. A chromel-alumel thermocouple (type K) was inserted into the powder sample to measure the bed temperature. A quadrupole mass spectrometer (Pfeiffer OMNISTAR) was connected on-line for continuous monitoring of the reaction effluent. Reactant gases used were He (99.99%), $O_2$ (99.996%), and $CO_2$ (99.9%). He was passed through a molecular sieve column to remove trace quantities of water. Methanol (Fisher) and other liquids such as formic acid (Sigma, 99%, impurity: 1% $H_2O$) were fed as vapor through a saturator using He as a carrier gas.

The methanol adsorption experiments were performed in the DRIFTS cell reactor. A mixture of 10 vol % $CH_3OH$, formic acid or $CO_2$ in helium at a total flow rate of 300 cc/min was introduced to the DRIFTS cell reactor at 303 K after pretreatment of the catalyst. The catalyst temperature was slowly increased while IR spectra were collected every 10 K at a resolution of 4 cm$^{-1}$ with

20 co-added scans. Formic acid and $CO_2$ desorption experiments were conducted under He after the saturated adsorption of the gases on the catalysts. The temperature of the catalysts was increased gradually while IR spectra were collected to monitor the adsorbed species on the catalyst surface.

Methanol partial oxidation reaction experiments were performed in the same DRIFTS cell at a total gas flow rate between of 300 and 650 cc/min.$CH_4/O_2$/He were introduced into the DRIFTS cell at 303 K. A water bath was used to maintain the temperature of the saturator. The methanol concentration in the feed was controlled by changing the temperature of water bath. The methanol to oxygen ratio was changed by regulating the $O_2$ flow rate. The reaction ignition temperatures were measured by the thermocouple in the catalysts. The catalytic ignition temperature was defined as the temperature beyond which the thermocouple temperature increased rapidly beyond the controller set point. IR spectra were collected at selected time intervals.

## 6.3    Results

### 6.3.1 *Methanol adsorption on $Al_2O_3$*

Adsorption of methanol vapor on $Al_2O_3$ has been done to characterize the IR bands on the support. Spectra a and b in **Figure 6.1** show the spectra of $CH_3OH$ on $Al_2O_3$ before and after evacuation.  They are complicated and indicate simultaneous presence of several adsorbed species on $Al_2O_3$. Bands for different types of hydroxyls appeared at different frequencies. The broad peak around 3267 cm$^{-1}$ [8] is assigned to the stretching mode of the hydrogen-bonded hydroxyls group, compared to the isolated OH group at around 3400 cm$^{-1}$ in spectrum a. The

110

peak at 3267 cm$^{-1}$ disappeared with increasing temperature, indicating that such species is easily

desorbed. The methoxy groups are characterized by the symmetric $\nu(CH_3)$ stretching mode

located at 2990(weak shoulder), 2944 and 2824 cm$^{-1}$. The splitting was due to the Fermi

resonance with a symmetric deformation [9]. The band located at 1647 cm$^{-1}$ is physisorbed

water, which decreased with increasing temperature. A small peak at 1602 cm$^{-1}$ is difficult to

assign to a single chemical species. It could come from carbonate or formate, or a mixture of

them. Actually, carbonate and formate have very similar structures as shown in **Table 6.1**. They

both have OCO vibration bonds.  Due to the existence of the surface OH groups, interaction of

carbonate with   these OH groups could also form C-H bonds. This results in carbonate and

formate adsorption peaks at the nearly same positions. However, it is very important to

distinguish between these two peaks to determine if formate is one of the reaction intermediates.

In order to accomplish this, studies were conducted to monitor the evolution of adsorbed species

on Pt/Al$_2$O$_3$ catalyst with increasing temperature.



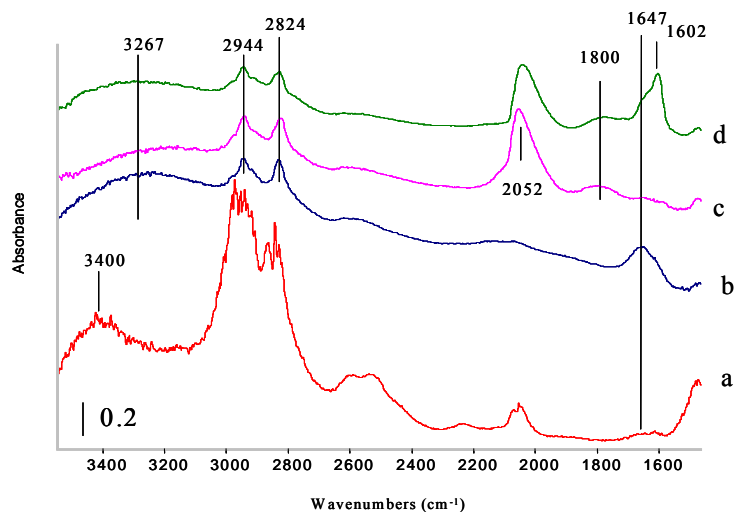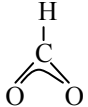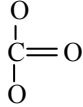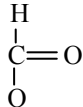**Figure 6.1: IR spectra of methanol adsorption: a) methanol vapor on Al$_2$O$_3$. b) on Al$_2$O$_3$**

**after evacuation at 293K. c) on reduced Pt/Al$_2$O$_3$ after evacuation at 293K. d) on the O$_2$-**

**covered reduced Pt/Al$_2$O$_3$ after evacuation at 293K.**

**Table 6.1 Structures of formate and carbonate**

| Species | Structures |
|---------|------------|
| Bidentate carbonate |  |
| Bidentate formate |  |
| Monodentate carbonate |  |
| Monodentate formate |  |

### 6.3.2 *CO₂ and HCOOH adsorption and desorption of adsorbed species*

Adsorption of $CO_2$ and HCOOH on the reduced Pt/Al$_2$O$_3$ has been done to verify the adsorption bands on the catalyst. **Figure 6.2** is the IR spectra of formate evolution with temperature on the reduced Pt/Al$_2$O$_3$ catalyst. Formate was formed by adsorbing formic acid gas vapor on the catalyst, followed by evacuation under He. Formic acid vapor showed peaks around 1300-1800 cm$^{-1}$ region and 2800-3100 cm$^{-1}$ region as shown in **Figure 6.2**. After evacuation under He, peaks related to formate are apparently complicated. Peak assignment of formate has been studied a lot on $CeO_2$ and supported $CeO_2$ catalysts [10,11]; however, there are not a lot of direct studies on Al$_2$O$_3$ supported Pt catalysts. Thus, the peak assignment on Pt/Al$_2$O$_3$ was made by comparing the shape of spectra collected in this experiment with that of the formate formed on $CeO_2$ and its supported catalysts. Adsorption bands in the region of 1300-1400 cm$^{-1}$ are due to

the symmetric OCO stretching mode and bands between 1500 and 1700 $cm^{-1}$ are because of the asymmetric mode of this group [12]. Peaks at these specific positions can be assigned to monodentate formate or bidentate formate. According to Gopal [13] and Deacon [14], the frequency separation between asymmetric monodentate formate and symmetric monodentate formate should be larger than the same separation for bidentate formate. Furthermore, the frequency separation of the asymmetric and symmetric of free formate ion is around 250 $cm^{-1}$. Thus, peaks at 1668 and 1328 $cm^{-1}$ might be attributed to monodentate formate species with the frequency separation of 340 $cm^{-1}$. The bands at 1598 and 1374 $cm^{-1}$ are assigned to bidentate formate with a frequency separation of 224 $cm^{-1}$, which is smaller than 250 $cm^{-1}$. The peak at around 1627 $cm^{-1}$ is perhaps due to a different type of bidentate formate. Bands related to surface formate also include C-H stretch vibration [11] at 2895 $cm^{-1}$ (bidentate) and a weak band at 2999$cm^{-1}$ (bridged). The peak at 1396 $cm^{-1}$ is attributed to the C-H bending vibration. Apparently, this peak is more dominant than the peak at 1374 $cm^{-1}$.

When the sample was heated up under He, a new peak at 2063 $cm^{-1}$ immediately appeared from a very low temperature (303 K) and increased dramatically with increasing temperature. The appearance of this peak indicates the formation of adsorbed CO on Pt [15], likely because of decomposition of formate species into CO. With increasing temperature, the peaks related to formate species in the region of 1500-1700 $cm^{-1}$ steadily decreased and shifted to lower wavenumbers. The intensities of all other peaks related to formate species also decreased. However, it is clear that bidentate formate is more stable than monodentate formate species, because peaks at 1668 $cm^{-1}$ and 1328 $cm^{-1}$ vanished progressively with increasing temperature while peaks at 1598 and 1374 $cm^{-1}$ still remain at 773 K. Also, a peak at around 3532 $cm^{-1}$ was

formed progressively with temperature. This peak is due to isolated hydroxyl groups, which implied that decomposition of formate species produced OH groups.
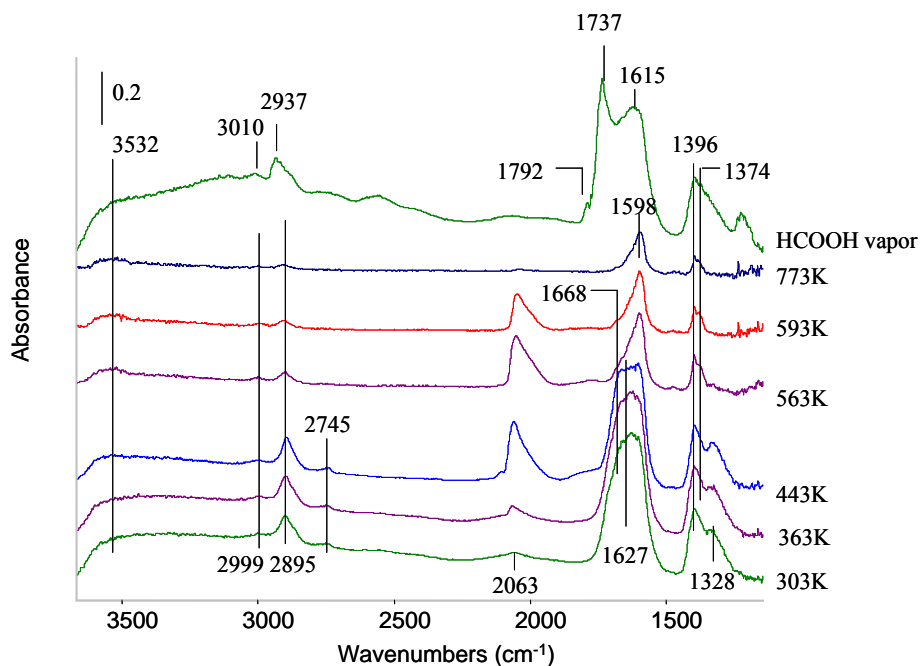


**Figure 6.2 Formate evolution with temperature on reduced Pt/Al$_2$O$_3$**

An attempt was made to create carbonate by adsorbing CO$_2$ gas on the catalyst followed by He evacuation. Several distinct peaks are seen in **Figure 6.3**. The spectra from CO$_2$ treatment (**Figure 6.3)** are extremely similar to those resulting from formic acid treatment (**Figure 6.2**). It is understandable that peaks at 1661, 1635, 1598, 1373, and 1335 cm$^{-1}$ showed up due to the OCO stretching mode. It is surprising that peaks at 1397, 2852 and 2952 cm$^{-1}$ due to C-H bond appeared immediately after the CO$_2$ adsorption, which indicates that the adsorption of CO$_2$ also forms formate on the catalyst surface. This phenomenon agrees with the results and conclusions obtained by Li et al. [16]. The authors observed formation of formate when adsorbing CO$_2$ on CeO$_2$. It was proposed that surface OH groups participated in the reaction to produce formate according to their studies.

When the catalyst was heated in He, a small peak of adsorbed CO appeared at 2055 cm$^{-1}$ and totally disappeared at around 523 K. The appearance of the adsorbed CO indicated the decomposition of the OCO species from $CO_2$ adsorption. However, existence of Pt [17] is necessary for the occurrence of this decomposition reaction.

Slight differences were observed in **Figure 6.2** and **Figure 6.3**. It appears that the OCO group formed from HCOOH adsorption is more readily decomposed into CO than those from $CO_2$ adsorption. The peak at 1373 cm$^{-1}$, attributed to the bidentate OCO mode in the spectra from $CO_2$ adsorption, is more intense than the one from HCOOH adsorption.
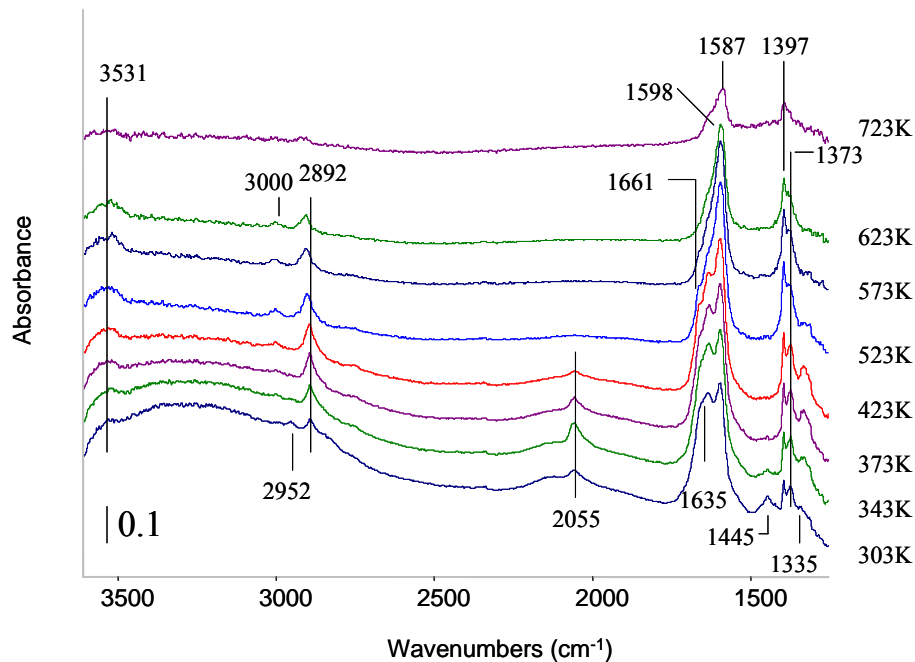


**Figure 6.3 Evolution of adsorbed species on reduced Pt/Al$_2$O$_3$ obtained from CO$_2$ treatment.**

MS spectra of the species evolved as absorbed formic acid and carbon dioxide when progressively heated are shown in **Figure 6.4** and **Figure 6.5**. As seen in these two figures, adsorbed species from both HCOOH and $CO_2$ released CO, $CO_2$ and an extremely small amount of HCOOH with increasing temperature. It is reasonable that HCOOH was one of the products during desorption since we have established that the adsorption of $CO_2$ on the catalyst also formed formate from the spectra in **Figure 6.3**. One difference between the two spectra is that adsorbed species from HCOOH adsorption released $H_2$ while $H_2$ could not be detected from desorption of adsorbed species from $CO_2$ adsorption. Another difference is that CO started to decrease at temperatures beyond 523 K in **Figure 6.5**. However, the CO gas increased even at much higher temperatures from desorption of adsorbed species from HCOOH.
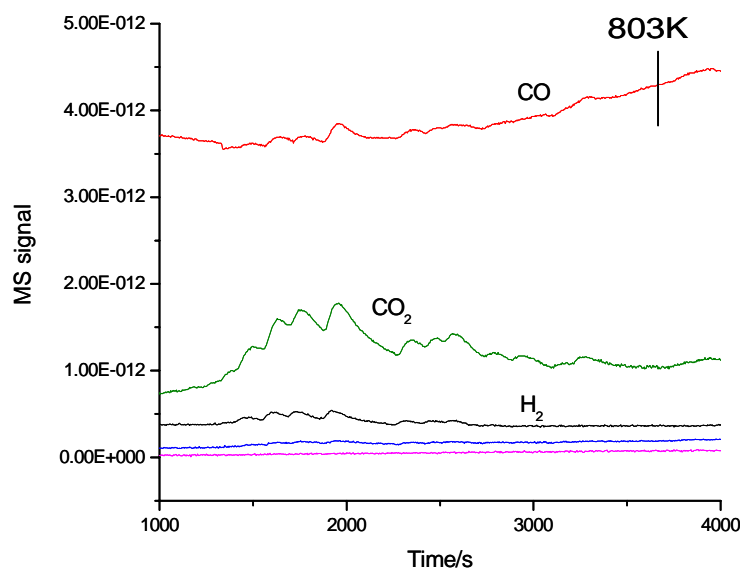


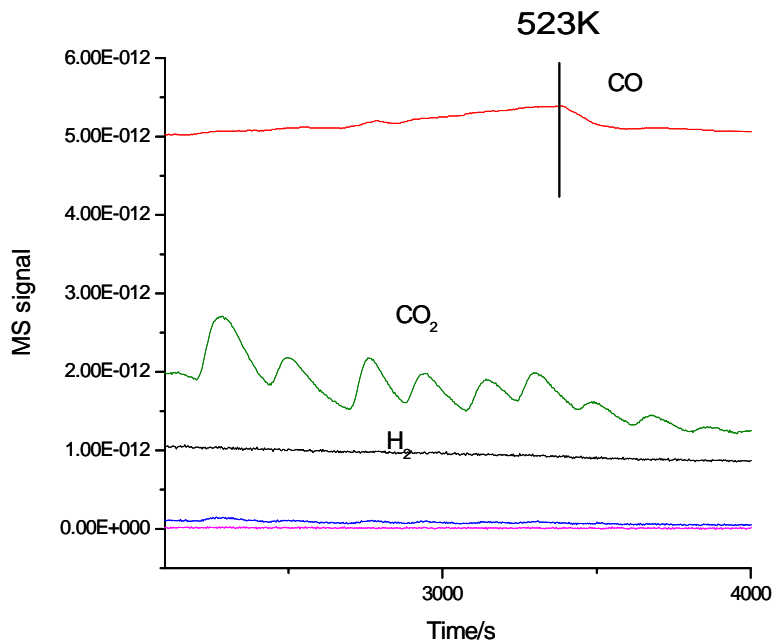**Figure 6.4 MS signal when heating under He after HCOOH vapor adsorption on reduced Pt/Al$_2$O$_3$.**

116

**Figure 6.5 MS signals when heating under He after $CO_2$ adsorption on reduced $Pt/Al_2O_3$**

From the studies of $CO_2$ and HCOOH adsorption and desorption, the IR adsorption bands related to formate species were determined. In addition, the gas phase products of the formate decomposition with temperature were established to be CO, $CO_2$ and $H_2$. These results will give insight to assign the adsorbed peaks found during methanol adsorption on the catalysts.

Mass spectra are shown in **Figure 6.6** during methanol adsorption on $Al_2O_3$ with increasing temperature. Traces of HCOOH was observed in the product at low temperatures immediately after methanol was admitted on the $Al_2O_3$, although the amount is so small that it is hard see any changes due to the scale in **Figure 6.6**. However, this observation is very important because it, combined with the small shoulder of spectrum b at 1602 cm$^{-1}$ in **Figure 6.1**, is evidence for the formation of the formate species on $Al_2O_3$. With increasing temperature, more and more HCOOH was produced from 423 K. Not too long after the HCOOH gas was formed, $CO_2$

appeared in the gas phase, too. CO wasn't formed until 673K. Thus, the formation of $CO_2$ probably results from formate during methanol decomposition on $Al_2O_3$. At 713 K, the amount of formic acid in the product decreased dramatically, while a great amount of $H_2$ and CO was formed. The results from IR and MS tell us that methanol decomposition can occur on $Al_2O_3$, and formation of formic acid starts at low temperatures, although the reaction rate is very low.
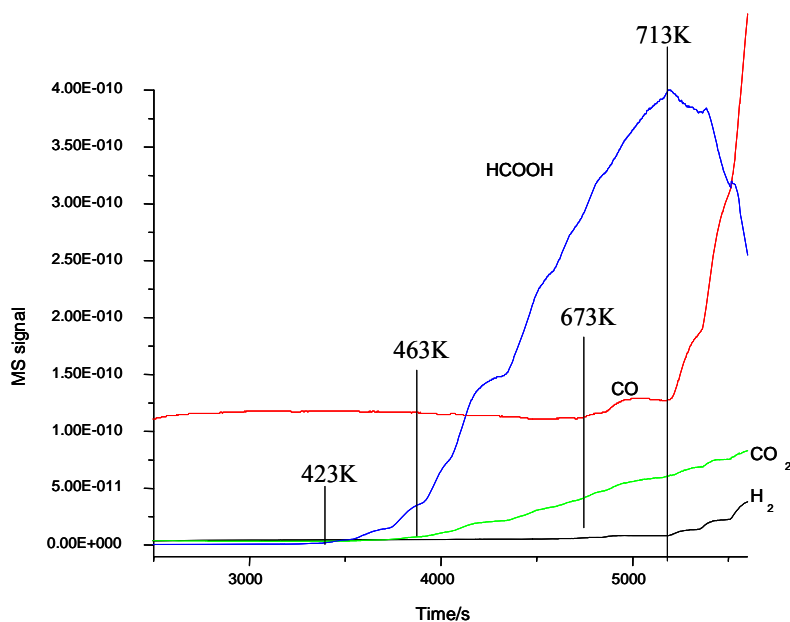


**Figure 6.6: MS spectra during methanol adsorption on $Al_2O_3$.**

### 6.3.3 *Methanol adsorption on Pt/Al$_2$O$_3$*

As shown in **Figure 6.1** (spectrum c), exposure of $CH_3OH/He$ to the reduced $Pt/Al_2O_3$ after evacuation gave a band at 2052 cm$^{-1}$ due to linearly adsorbed CO on Pt [15], together with bands at 2944 and 2825 attributed to methoxy groups. A small peak around 1800 cm$^{-1}$ is due to bridged CO adsorbed on Pt [18]. One of the differences between methanol adsorption on $Al_2O_3$ and $Pt/Al_2O_3$ is that the adsorbed CO peak on Pt appears at the beginning of the adsorption, which

118

indicates that Pt act as a decomposition site to produce CO. The very small bump at 1602 cm$^{-1}$ is assigned to formate, as on Al$_2$O$_3$.

At 293 K, adsorption of CH$_3$OH/He on the O$_2$-covered reduced Pt/Al$_2$O$_3$ results in a large band at 1602 cm$^{-1}$, shown as spectrum d in **Figure 6.1**. This peak is attributed to formate formed on the catalyst. Compared to the methanol adsorption on the same catalyst without adsorbed oxygen, the dramatic increase in intensity of this peak at room temperature implies that oxygen species play an important role on the formation of formate. This point is in agreement with the conclusion that Endo et al. [19] have reached. They claimed that the presence of oxygen molecules, which transform into the dissociated oxygen atoms, is a key to formate formation.

The IR spectra of methanol adsorption on the reduced Pt/Al$_2$O$_3$ as a function of temperature are shown in **Figure 6.7**. A peak appears at 2021 cm$^{-1}$, assigned to linearly adsorbed CO on Pt, once methanol was introduced on the catalyst. The small shoulder on the left is caused by the methanol vapor. This assignment can be made if one compares the spectra with the methanol vapor spectrum on Al$_2$O$_3$. With increasing temperature, the adsorbed CO peak increases and shifts to higher wavenumbers. This shift is apparently due to increased CO coverage. Bridged CO also forms immediately after admission of the adsorption mixture. Two small peaks form at 1617 and 1610 cm$^{-1}$, which are assigned to formate. The two peaks are so small at the beginning that they are not easy to see. However, if stacking all the spectra collected at elevated temperatures together, there is an obvious increasing trend for the peak at 1610 cm$^{-1}$, which shifts to lower wavenumbers with increasing temperature. It was pointed out previously that oxygen species are important to the formation of formate on the catalyst. The formation of this

small peak on the reduced catalyst here is perhaps due to some low coordinated O species on the support [20] or reaction with hydroxyl groups [21]. At 443 K, the intensity of the formate peak increases dramatically. This formate species still remains on the catalyst surface at 773 K.
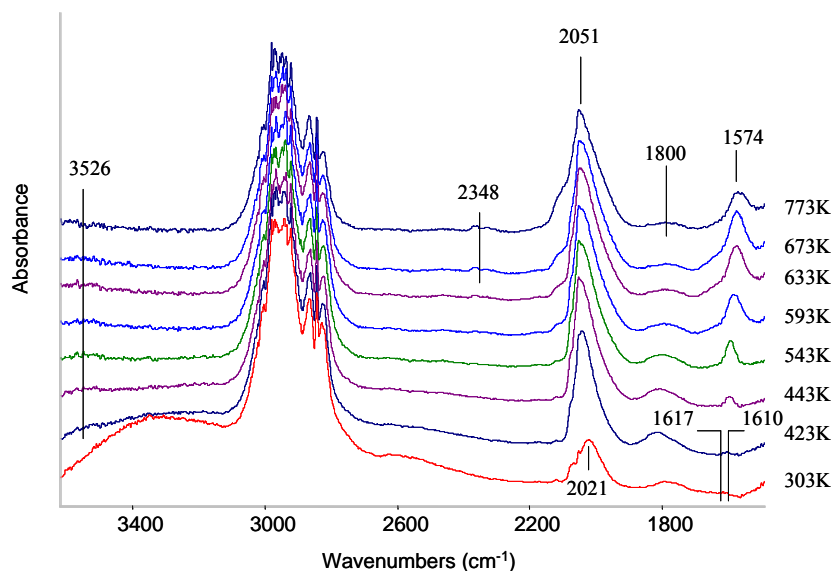


**Figure 6.7: Evolution of IR spectra with temperature during methanol adsorption on reduced Pt/Al$_2$O$_3$.**

**Figure 6.8** is the IR spectra evolution with temperature when adsorbing methanol on the O$_2$-covered reduced Pt/Al$_2$O$_3$. Linearly adsorbed CO peak on Pt appeared at 2028 cm$^{-1}$ at 303 K. This peak shifts first to higher wavenumbers and then slightly to a little lower wavenumbers with increasing temperature. A great amount of formate was formed immediately after the methanol was introduced on the catalyst at 303 K, shown as the peak at 1610 cm$^{-1}$. This peak shifts to lower wavenumbers with increasing temperature and still remains at 873 K. The band at 1396 cm$^{-1}$ further confirms the formation of formate at low temperatures. The amount of CO$_2$ produced in the decomposition is not large.
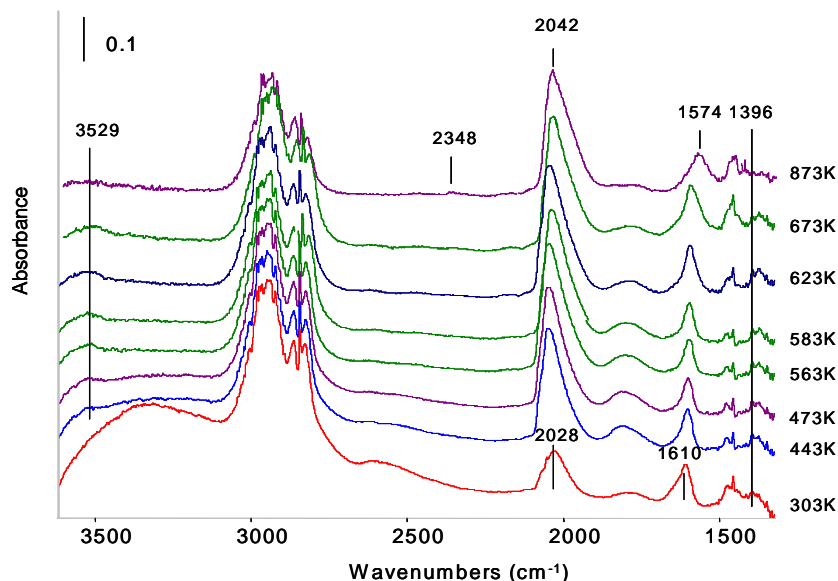
**Figure 6.8 Evolution of IR spectra with temperature during methanol adsorption on O₂-covered reduced Pt/Al₂O₃.**

The MS spectra of methanol adsorption on the $O_2$-covered reduced Pt/Al₂O₃ are shown in **Figure 6.9**. Much less HCOOH and $CO_2$ are produced compared to $H_2$ and CO. For this reason, the curves for HCOOH and $CO_2$ are multiplied by a constant. The product profile during methanol decomposition on the $O_2$-covered reduced Pt/Al₂O₃ suggests that there are several stages of reactions. As shown in the figure, traces of formic acid appear in the gas phase immediately after methanol was admitted into the reactor, which confirms the IR observation of the formate peak at 303 K. Before 423 K, only HCOOH appears as a product. From 423 K, more HCOOH is produced and small amounts of $H_2$ and $CO_2$ also are observed. From 463 K, CO starts to appear due to desorption of adsorbed CO species. Also, much more $CO_2$ is produced in the gas phase at this stage. Compared to the MS profile on Al₂O₃ during methanol decomposition, the temperature for $H_2$ production is much lower than that for methanol decomposition on Al₂O₃. It

121

is apparent that the main products were formic acid and $CO_2$ at the temperatures before 673 K on $Al_2O_3$. The earlier formation of CO and $H_2$ on the $O_2$-covered reduced $Pt/Al_2O_3$ than on $Al_2O_3$ indicates that Pt is the site promoting $H_2$ and CO production. From 563 K, both HCOOH and $CO_2$ decreased. The sharp decrease of formic acid and $CO_2$ at the same time indicates that formate mainly decomposed into CO in this temperature range. Formic acid kept decreasing with increasing temperature while $CO_2$ started to increase again at 653 K. At 873 K, $CO_2$ had another sharp decrease.



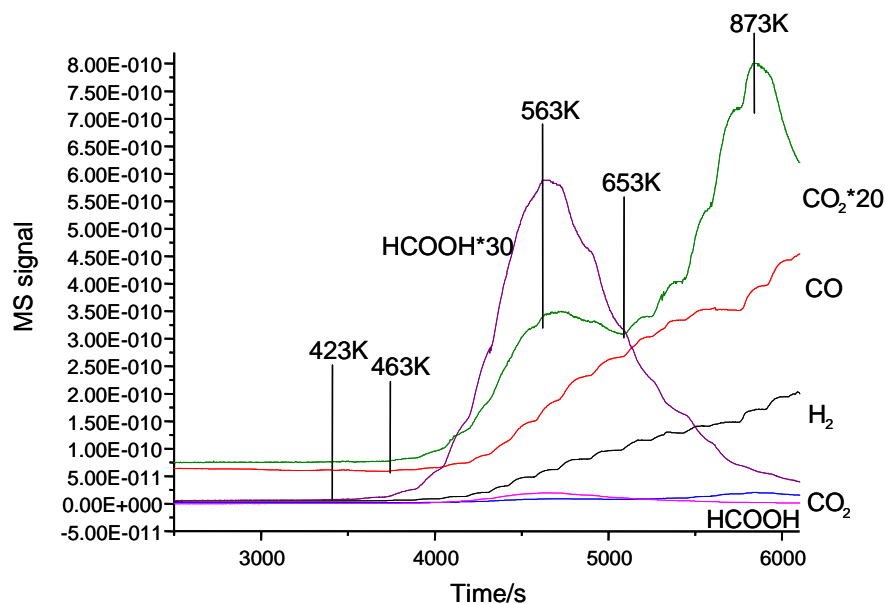**Figure 6.9: MS spectra of major products during $CH_3OH$/He adsorption on the $O_2$-covered reduced $Pt/Al_2O_3$**

Methanol decomposition on $Al_2O_3$ and on $Pt/Al_2O_3$ forms an important intermediate, formate. This brings up the question of how formate is formed. **Figure 6.10** shows the IR spectra under He after exposure of methanol and He mixture on the $O_2$-covered reduced $Pt/Al_2O_3$ at room

temperature. The methoxy group decreases with time and the formate group increases, which implies that the formate group likely results from methoxy dehydrogenation.
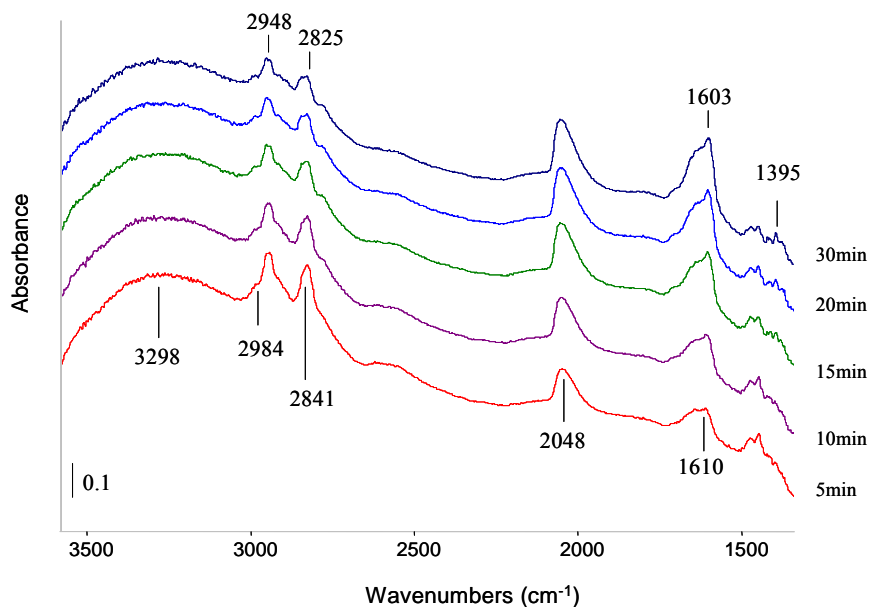


**Figure 6.10 Evolution of adsorbed species on the O$_2$-covered reduced Pt/Al$_2$O$_3$ at room temperature with time.**

### 6.3.4 *Transient and steady state methanol partial oxidation reactions*

Reaction ignition experiments were run in the same DRIFTS cell reactor. The catalyst ignition temperature was measured when the thermocouple temperature increased rapidly beyond the controller set point. CH$_3$OH/O$_2$/He was introduced into the DRIFTS cell at 303 K. The ignition occurred immediately after the reactant mixture flew over both the reduced and the oxidized Pt/Al$_2$O$_3$ catalysts with any methanol to oxygen ratio.

Transient reactions were run with different oxygen to methanol ratios at different temperatures. The ratios used were 2, 3.3, and 4. The composition of the product gases was examined by QMS

(quadrupole mass spectrometer). Data for steady-state and transient reactions using different methanol to oxygen ratios on the supported Pt are presented in **Figure 6.11**. Water was detected by the MS; however, it was hard to record reliably because of the background level.

Only a small amount of HCOOH was produced in the partial oxidation reactions. In order to make the change more obvious, the actual MS signals are multiplied by a factor of 20 in **Figure 6.11**. Compared to the large amount of the HCOOH in the methanol decomposition on the reduced catalyst, this small amount of HCOOH gas produced when there is $O_2$ in the feed implies that $O_2$ plays a role in the transformation of formate into other species. It appears that trends for $CO_2$ and HCOOH are always reversed when the methanol to oxygen ratios change: the more $O_2$ in the feed, the less HCOOH and the more $CO_2$ were detected in the product. This phenomenon indicates that formate formed on the $O_2$-covered sites is more likely to decompose into $CO_2$ than desorb as HCOOH. $O_2$ concentration also affects the selectivity of $H_2$. $H_2$ increases when methanol to oxygen ratio increases.

Temperature also caused changes in product composition. When the temperature increases, the concentrations of CO and $H_2$ increase while the concentrations of $CO_2$ and HCOOH decrease.
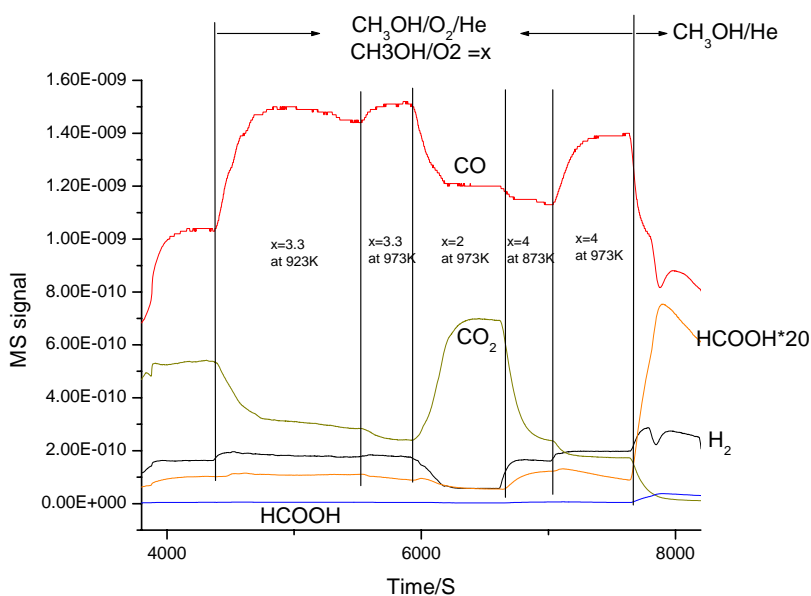
**Figure 6.11: MS spectra for transient reactions of methanol partial oxidation on the reduced Pt/Al$_2$O$_3$.**

## 6.4    Discussion

According to results from both methanol decomposition and partial oxidation, we propose the following pathways for CO$_2$, CO and H$_2$ formation. First, methanol dissociates on the catalyst to form methoxy groups. The initial formation of this group as the intermediate has been established by other researchers [22,23]. The study by McCabe et al [24] provided the evidence of methoxy dehydrogenation to adsorbed CO and H. The abstraction of H atoms from methoxy group is shown in the following equation [25]. These H adatoms tend to form OH$^-$ at low temperatures.

$$CH_3O_s \rightarrow CH_2O_s + H_s \rightarrow CHO_s + 2H_s \rightarrow CO_s + 3H_s \qquad \textbf{Equation 6.1}$$

The intermediate between formyl species ($CHO_s$) and adsorbed CO, however, was not identified by these researchers. Our study shows that formate is an important reaction intermediate for both methanol partial oxidation and methanol decomposition. The results in **Figure 6.10** suggest that formate is formed from methoxy groups and that this process is fast. Formate decomposes into adsorbed CO very easily, as shown in the formate desorption study. We can, therefore, propose that the following step is a key one in methanol decomposition and oxidation.

$$CHO_s + O_s \rightarrow CO_2H_s \rightarrow CO_s + OH_s \qquad \textbf{Equation 6.2}$$

Once formate is formed, a variety of reaction pathways can occur that produce HCOOH, $CO_2$, or CO. Formate can form formic acid and desorb. Alternatively, it can decompose to CO or $CO_2$. The relative rates of these processes depend on the amount of oxygen present and the reaction temperature.

Formic acid was produced in large amounts on $Pt/Al_2O_3$ mainly when temperature was low, as seen in **Figure 6.9**. At higher temperatures, $CO_2$ and CO (especially CO) were formed. It is likely that higher temperatures cause more rapid decomposition of formate, not allowing it to desorb as formic acid.

The amount of oxygen also had a significant impact on formate and formic acid production. IR peaks for formate increased dramatically when oxygen was on the surface of $Pt/Al_2O_3$, as shown in **Figure 6.1**. This suggests that oxygen aids in the process of producing formate from methoxide. As shown in **Figure 6.11**, the amount of formic acid produced during catalytic partial oxidation decreases when $O_2$ concentration increases. This is most obvious when oxygen is completely removed from the feed at the end of the experiment: the formic acid production

increases dramatically. These results suggest that oxygen in some way inhibits production of formic acid, possibly by speeding up formate decomposition.

The reaction pathways responsible for $CO_2$ production are not obvious. There are two pathways that can be considered for $CO_2$ production. Some researchers conclude that $CO_2$ originates from formate decomposition [26,27]. The conclusions were made according to the experiments conducted under vacuum conditions at 160 K. It is also possible that $CO_2$ formation is due to the oxidation of adsorbed CO, since it is well known that CO can be oxidized into $CO_2$ at low temperatures on Pt [28]. Thus, $CO_2$ could be produced by direct decomposition of formate or through an indirect pathway through adsorbed CO, which forms from the decomposition of formate. Endo et al. [19] claimed that both reaction pathways proceed during the methanol oxidation on Pt (111) under ambient pressure conditions and at the temperatures below 550 K. However, they consider decomposition of formate as the major pathway for $CO_2$ production. In our study, the occurrence of the two pathways is also possible since formate is found to be the precursor for both $CO_2$ and CO production.

According to the results of methanol decomposition on $Al_2O_3$, $CO_2$ was formed by formate decomposition on the support, since it was noted in the gas phase long before CO was formed. It is more complicated on $Pt/Al_2O_3$. When formate species on $Pt/Al_2O_3$ were heated in the absence of $O_2$ (**Figure 6.4**), $CO_2$ was initially formed at low temperatures, with CO formation related to higher temperatures. Since oxygen was not present when $CO_2$ was produced, formate decomposition must be producing $CO_2$. When catalytic partial oxidation was run on $Pt/Al_2O_3$

127

(**Figure 6.11**), $CO_2$ and HCOOH had opposite trends with changing $O_2$ concentration in the feed of methanol partial oxidation, which implied that the source of the two could be same: formate.

Despite these indications that $CO_2$ could be formed from formate decomposition, we cannot rule out the possible role of CO oxidation. When catalytic partial oxidation of methanol was run at higher temperatures, CO selectivity increased while $CO_2$ selectivity decreased. This could indicate the faster desorption of CO, which would decrease the amount of $CO_2$ formed because the CO oxidation pathway would be diminished. It is possible that both formate decomposition and CO oxidation can form $CO_2$, and the relative importance of each change with temperature.

## 6.5    Conclusions

Dissociation adsorption of methanol occurs on both $Al_2O_3$ and $Pt/Al_2O_3$. Methoxy is one of the main species formed during dissociation. The presence of Pt decreases the temperatures at which $H_2$ and CO are produced through methanol decomposition. Formate is an important intermediate both in methanol decomposition and catalytic partial oxidation. Formate can decompose to form CO, $CO_2$, and $H_2$. Oxygen species play a key role in the formation of formate on the catalysts and also affects the product composition. In catalytic partial oxidation, methoxy forms first and is then converted to formate. Formate can desorb as formic acid, but is more readily converted to CO and $CO_2$ in the presence of oxygen. $CO_2$ could result directly from formate decomposition or could form from formate decomposition to CO followed by CO oxidation.

## 6.6 References

1 L.A. Espinosa, R.M. Lago, M.A. Pena, J.L.G. Fierro, Topics in Catal. 22 (2003) 245.

2 S. Velu, K. Suzuki, T. Osaki, Catal. Lett. 62 (1999) 159.

3 M.P. Zum Mallen, L. D. Schmidt, J. Catal. 161 (1996) 230.

4 B.E. Traxel, K.L. Hohn, Appl. Catal. A: general 244 (2003) 129.

5 S.J. Gentry, A.L. Jones, P.T. Walsh, J. Chem. Soc. Faraday Trans. I. 76 (1983) 2084.

6 C.N. Hodges, L.C. Roselaar, J. Appl. Chem. Biotechnol. 25 (1975) 609.

7 C. Cao, A. Bourane, J. Schlup, K.L. Hohn, Appl. Catal. A: General 344 (2008) 78

8 P.F. Rossi, G. Busca, V. Lorenzelli, J.of Phys. Chem. 149 (1986) 99.

9 G. Busca, Catal. Today, 27 (1996) 457.

10 C. Li, K. Domen, K. Maruya, T. Onishi, J. Catal. 125 (1990) 445.

11 G. Jacob, L. Williams, U. Graham, G.A. Thomas, D.E. Sparks, B.H. Davis, Appl. Catal. A: General 252 (2003) 107.

12 L. H. Little, *Infrared Spectra of Adsorbed Species*, Academic Press, London, New York, 1966.

13 P.G. Gopal, R.L. Schneider, K.L. Watters, J. Catal. 105 (1987) 366.

14 G.B. Deacon, R.J. Phillips, Coord.Chem. Rev. 33 (1980) 227.

15 A. Bourane, C. Cao, K.L. Hohn, Appl. Catal. A: General 302 (2006) 224.

16 C. Li, Y. Sakata, T. Arai, K. Domen, K. Maruya, T. Onish, J. Chem. Soc. Faraday Trans. I, 85 (1989) 1451.

17 T. Jin, Y. Zhou, G.J. Mains, J.M. White, J. Phys. Chem. 91 (1987) 5931.

18 A. Bourane, O.Dulaurent, D. Bianchi, J. Catal. 196 (2000)115.

19 M. Endo, T. Matsumoto, J. Kubota, K. Domen, and C. Hirose, J. Phys. Chem. B, 105 (2001) 1573.

20 O.V. Buyevskaya, D. Wolf, M. Baerns, Catal. Lett. 29 (1994) 249.

21 P. Ferreira-Aparicio, I. Rodríguez-Ramos, A. Guerrero-Ruiz, Appl. Catal. A: Gen. 148 (1997) 343.

22 B.A. Sexton, Surf. Sci. 102 (1981) 271.

23 B.A. Sexton, K.D. Rendulic, A.E. Hughes, Surf. Sci. 121 (1982) 181.

24 R.W. McCabe, D.F. McCeady, J. Phys. Chem. 90 (1986) 1428.

25 G.K. Chuah, N. Kruse, W.A. Schmit, J.H. Block, G. Abend, J. Catal. 119 (1989) 342.

26 M. Endo, T. Matsumoto, J. Kubota, K. Domen, and C. Hirose, J. Phys. Chem. B, 104 (2000) 4916.

27 M. Endo, T. Matsumoto, J. Kubota, K. Domen, and C. Hirose, Surf. Sci. 441 (1999) L931.

28 A. Wille, E. Fridel, Appl. Catal. B: Environmental 70(2007) 294.

# Chapter 7 Conclusions and future work recommended

## 7.1 Conclusions

This dissertation has studied the ignition process of methane catalytic partial oxidation and reaction pathways for methanol partial oxidation using in situ diffuse reflectance infrared spectroscopy and mass spectroscopy.

The ignition process of the partial oxidation of methane over $Pt/Al_2O_3$ catalysts has been investigated at atmospheric pressure. Contacting methane with the catalyst shows that the dissociative adsorption of methane, evidenced by the appearance of the linearly adsorbed CO species, is delayed to higher temperatures for an oxygen-covered surface compared to an oxygen-free surface. Carbonate species were progressively obtained on the surface before the ignition temperature when interacting $CH_4/O_2/He$ mixtures with the catalyst. They result from the interaction of produced carbon dioxide with the support. The temperature at which the carbonate species appears is lower for lower concentration of oxygen in the mixture. It has been shown that oxygen is mainly covering the surface until the ignition temperature. Competition between the two reactants is therefore assumed. It has been found that the state of platinum has a large effect on the ignition temperature, with the highest ignition temperature found for oxidized sample (platinum particle diameter, $D_{Pt}$ = 1.9~2.2 nm), the next highest for freshly reduced sample ($D_{Pt}$ = 1.7~1.9 nm), and the lowest on aged sample ($D_{Pt}$ = 4~5 nm). All of these results linked to microcalorimetry measurements and literature data suggest that the heat of adsorption of oxygen is a key factor for ignition of the surface reaction.

The ignition process of the partial oxidation of methane over $Rh/Al_2O_3$ catalysts has also been investigated. Different catalysts were studied: fresh, aged, sintered and oxidized catalysts. The ignition temperature when the $CH_4$ to $O_2$ ratio was two is lowest on reduced fresh catalysts. The ignition temperature decreased with an increase in oxygen concentration in the reactant mixture, which is the opposite trend previously noted for $Pt/Al_2O_3$. Methane activation was found to occur at different temperatures depending on the catalysts state. As the reactant mixture flowed over the catalyst and the temperature was raised towards the ignition temperature, the oxidation state of the catalyst changed and an oxidized rhodium state, $Rh^{n+}(1 \leq n \leq 3)$, progressively formed. In addition, a greater amount of $Rh^{n+}$ was found when the oxygen concentration in the feed was higher. From these results, it is hypothesized that ignition of methane CPO on $Rh/Al_2O_3$ is potentially related to the amount of the higher oxidation state Rh.

Different Rh sites play different roles in the heating process during methane activation. $Rh^0$ sites covered by $O_2$ are responsible for $C_2$ species formation at low temperatures while bare $Rh^0$ sites are preferred for CO production. $Rh^{n+}$ sites are also presumed active for $CH_4$ dissociation. They are then progressively reduced into lower oxidation state of Rh under $CH_4/He$ environment with increasing temperature.

Methanol CPO on $Pt/Al_2O_3$ catalysts was studied using in-situ diffuse reflectance infrared Fourier transform spectroscopy (DRIFTS). Methanol adsorption experiments were conducted on different catalyst states. Methoxy species, $CH_3O_s$ were formed during dissociative adsorption of methanol on the catalysts. More and more formate adspecies were formed with increasing

temperature under the methanol and helium mixture. The formate was probably formed from the reaction of methoxy species with oxygen species on the catalysts. Ignition of CPO was also studied, and it was found to occur at room temperature on both reduced and oxidized powder catalysts. Formate disappeared during this process, while CO species and $CO_2$ were detected in the products.

CPO of methanol was studied at different temperatures from 723 K to 973 K, and for methanol to oxygen mole ratios from 2 to 4. It was found that $CO_2$ productivity increased at lower temperatures and $H_2$ and CO had a higher selectivity at higher temperatures. Fuel lean conditions favored $H_2$ and HCOOH production. $CO_2$ increased when $O_2$ concentration increased in the reaction mixture. According to the results, it is suggested that formate was one of the important intermediates in the reaction pathway. Indirect formate decomposition is dominant for $CO_2$ production in the reactions at higher temperatures.

## 7.2 Future work

This work has mainly focused on catalyst state and reaction intermediates of CPO reaction at lower temperature and transient states. Future work may study catalyst states and reaction intermediates at high temperatures. According to the research experiences from this research, it was found that a good IR spectrum is not easy to obtain at high temperature under catalytic partial oxidation reaction. Two strategies can probably be used. One is conducting transient study at fixed temperatures. For example: $O_2$ can be pulsed onto catalyst at 773 K while the fuel such as methane or methanol is constantly flowing, or vice versa. Changes on the catalyst surface may be observed using IR and changes of reaction effluent can be detected using MS. The advantage of this study is that current experimental apparatus can be used without modification.

However, there is a possibility that no changes can be observed since surface reactions may be very fast.

Another strategy is to use a different IR technique, emission IR to study the reactions. Emission IR has significant advantages for in situ studies of CPO reaction because of the nature of the reaction at high temperatures, which may result in high emission signals.

The application of FT-IR emission spectroscopy has expanded considerably since the 1980's. A useful review was prepared by Sullivan and coworkers in 1992 [1]. Data were presented on CO chemisorption on $Pt/Al_2O_3$, NO-CO reaction on Pt and the oxidation of copper and ZSM-5. Spectra to frequencies as low as 500 $cm^{-1}$ were reported in several cases. Tobin and Richards reported on the molecule-substrate interaction in the case of the adsorption of CO on Pt(111) [2]. Data were available at frequencies as low as 425 $cm^{-1}$. FTIR emission studies for the adsorption of CO on $Rh/Al_2O_3$ and $Pt/Al_2O_3$ has been studied. Metal-carbon stretching frequencies below 500 $cm^{-1}$ were reported. The chemisorption of CO on Pt supported on Zeolite-Y has been investigated and the Metal-CO absorption was readily observed at 483 K [3]. Infrared spectra on these thin films prepared materials were obtained at frequencies as low as 400 $cm^{-1}$.

Despite the promise of using emission spectroscopy to study the CPO reactions, great challenges are existed. New reaction system needs to building up, this may require re-configuring the FIIR instrument so that the sample can act as the IR source. Previous IR experience is a necessity for the researchers to be able to obtain high quality spectra for the reaction. However, once the

techniques for using emission spectroscopy have been developed, the benefit for studying high temperature reactions will be significant.

## 7.3    References

1 D.H Sullivan, W.C. Conner, M.P. Harold, Appl. Spectroscopy, 46 (1992) 811

2 R.G. Tobin, P.L. Richards, Surf. Sci. 179 (1987) 387

3 M. Primet, P.E.O. Fouilloux, B. Imelik, J. Catal. 61 (1980) 553